TU Delft

Delft University of Technology

Application of poly(ε-caprolactone-b-ethylene oxide) micelles combined with ionizing radiation in cancer treatment

Liu, H.

Publication date
2021

Document Version
Final published version

Citation (APA)
Liu, H. (2021). *Application of poly(ε-caprolactone-b-ethylene oxide) micelles combined with ionizing radiation in cancer treatment*.

Important note
To cite this publication, please use the final published version (if applicable).
Please check the document version above.

Copyright
Other than for strictly personal use, it is not permitted to download, forward or distribute the text or part of it, without the consent of the author(s) and/or copyright holder(s), unless the work is under an open content license such as Creative Commons.

Takedown policy
Please contact us and provide details if you believe this document breaches copyrights.
We will remove access to the work immediately and investigate your claim.

This work is downloaded from Delft University of Technology.
For technical reasons the number of authors shown on this cover page is limited to a maximum of 10.

Application of poly(ε-caprolactone-b-ethylene oxide) micelles combined with ionizing radiation in cancer treatment

Huanhuan LIU

Application of poly(ε-caprolactone-b-ethylene oxide) micelles combined with ionizing radiation in cancer treatment

Dissertation

for the purpose of obtaining the degree of doctor
at Delft University of Technology
by the authority of the Rector Magnificus Prof.dr.ir. T.H.J.J. van der Hagen
chair of the Board for Doctorates
to be defended publicly on Friday 19th of November 2021 at 10:00 hour

by

Huanhuan LIU

Master of Engineering in Materials Science, Zhengzhou University, China
Born in Cangzhou city, China

This dissertation has been approved by the promotors:

Composition of the doctoral committee:

Rector Magnificus,	Chairman
Dr. R. Eelkema	Delft University of Technology, promotor
Dr. ir. A.G. Denkova	Delft University of Technology, promotor

Independent members:

Prof. dr. S.J. Picken	Delft University of Technology
Prof. dr. S. Heskamp	Radboud UMC
Dr. F. Nijsen	Radboud UMC
Dr. Y. Seimbille	Erasmus MC
Prof. dr. ir. J.R. van Ommen	Delft University of Technology, reserve member

Other member:

Prof. dr. H.Th. Wolterbeek	Delft University of Technology

Cover design Yu Zhang
Printed by Ridderprint | www.ridderprint.nl.
ISBN: 978-94-6384-266-2

Copyright © 2021 by Huanhuan Liu

All rights reserved. No part of the material protected by this copyright notice may be reproduced or utilized in any form or by any other means, electronic or mechanical, including photocopying, recording or by any information storage and retrieval system, without written permission from the author.

Printed in the Netherlands

Dedicated to my beloved grandparents

The research described in this thesis was performed at the Application of Radiation and Isotope section of the department of Radiation Science and Technology, Faculty of Applied Sciences, Delft University of Technology, the Netherlands. The Chinese Scholarship Council also partly financial supports this research.

CONTENTS

Chapter 1 Introduction 1

Chapter 2 Singlet oxygen sensor green is not a suitable probe for $^1O_2$ in the presence of ionizing radiation 21

Chapter 3 Ionizing radiation induced release from poly(ε-caprolactone-b-ethylene glycol) micelles.....47

Chapter 4 New, fast and simple method to radiolabel polymeric micelles used in drug delivery 77

Chapter 5 The mechanism of chelator free radiolabeling method for polymeric micelles explored using different block copolymers and radionuclides 99

Chapter 6 Exploring the potential of combined chemotherapy and radionuclide therapy by using poly(ε-caprolactone-b-ethylene oxide) micelles co-loaded with Paclitaxel and ^{177}Lu 131

Chapter 7 Conclusion.....155

Summary 161

Samenvatting.....165

List of publications 169

Acknowledgements.....171

Curriculum Vitae 175

Introduction

1

Introduction

1.1 Radiotherapy

Cancer is one of the major health threats globally, leading to around 9.8 million deaths in 2018.[1] Currently, surgery, radiotherapy and chemotherapy are the three main approaches applied in cancer treatment. Surgery is usually the first choice, provided that the tumor has not spread to other parts of the body and is easily accessible, while chemotherapy is essential in the treatment of malignant metastases. Radiotherapy is widely utilized for treating a variety of malignant tumors at the surface, as well as deep in the body.

Radiotherapy can be briefly categorized into external beam radiotherapy (EBRT), brachytherapy and radionuclide therapy, the first two are typically applied to localized tumors while the last is used to attack metastases. The widely-known EBRT makes use of external radiation sources such as X-rays, gamma-rays, and heavy particles, to irradiate the tumor sites.[2] In brachytherapy, radioactive sources are sealed and placed at or near the tumor site, so that the locally emitted radiation can kill tumor tissue while sparing healthy tissue. In radionuclide therapy, the radioisotopes are usually bound to targeting agents such as antibodies or small molecules, which are intravenously injected and accumulate at the tumor site due to an interaction between the targeting vectors and overexpressed tumor receptors.[3] Radioisotopes which can emit radiation having short range such as beta minus or alphas particles are typically applied. The different radiation sensitivities between normal tissue and tumor cells are the key factor for the success of all radiotherapy types, i.e. tumor tissue is more sensitive to ionizing radiation due to insufficient or slow DNA repair when compared to healthy tissue.

1.2 The interaction of radiation on matter

When radiation interacts with matter, an electron is typically kicked out from an orbital, resulting in ionization. The energy of the incident photons or particles gets dissipated when passing through a medium, and the rate of energy loss per unit length is defined as the linear energy transfer (LET). LET depends on the nature of the ionizing particles as well as the

nature of the medium.[4] Generally, high energy photons and electrons possess low LET, while alpha particles have high LET.[5, 6] Ionizing radiation can interact with matter directly or indirectly. An example of direct effect of ionizing radiation is illustrated in Figure.1.1 (a) by the interaction between electrons and medium. In the first stage, the ionization events appear at the spurs along the track, which would splash and interact with the nearby spurs and eventually merge together to form a homogeneous system.[4] For high LET particles, the spurs are much closer together and form clusters. Indirect effects of ionizing radiation are ascribed to reactions with radicals and different species produced by interaction of radiation with the medium.

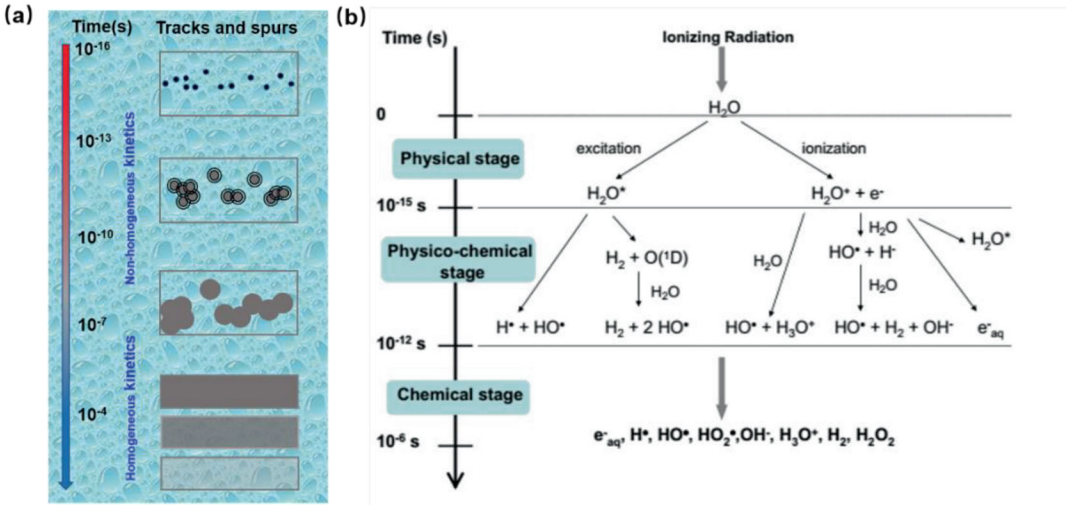

Figure 1.1. (a) Initial non-homogeneous spatial distribution of ionization events in spurs along the track, and evolution with time by diffusion and reaction leading to homogeneous distribution after $\approx 10^{-7}$s. (b) Main reactions occurring during the three stages of water radiolysis. Figure (a) and (b) are obtained from Ref [4] and Ref [7], respectively.

It is often quite hard to separately evaluate direct and indirect effects, especially when the reaction happens in the medium, for example, water. When water interacts with ionizing radiation, water radiolysis occurs. Water radiolysis can be separated into three stages (Figure.1.1(b)). In the first step, physical stage, the radiation directly interacts with the H_2O molecules which get excited to H_2O^* or ionized to $H_2O^{\bullet+}$, releasing electrons in the process. In the second stage, several reactions take place, such as ion-molecule reactions between $H_2O^{\bullet+}$ and H_2O, relaxation of the excited water molecules, solvation of electrons and so on, resulting in different transient species. In the last stage, the radicals diffuse and react with

each other or with other solvent molecules. Upon removal of the radiation sources, most of the radiolytic species will disappear with the exception of stable products such as H_2 and H_2O_2.[7] Though the transient reactive species will eventually disappear, they still can induce different chemical reactions during irradiation, for instance adducts between hydroxyl radicals ($^{\bullet}OH$) with halides and metal ions.[4]

1.3 DNA damage caused by ionizing radiation

The effects of ionizing radiation on tumors are also direct or indirect through formed radicals. Direct effects result from local deposition of energy to cell organelles and in particular DNA. The therapeutic outcome caused by direct effects is highly dependent on the type of ionizing radiation and the location of the radionuclide in the cell. External beam therapy and brachytherapy as well as radionuclide therapy using beta minus particles are less likely to induce direct damage. High LET particles such as α particles can directly cause clustered damage on the DNA and are more prone to lead to double-strand breaks (DSB) than low LET particles.[8, 9] DSB are much more difficult to repair than single strand breaks (SSB) and will therefore often lead to cell death. Some preclinical studies show that high LET radiation can overcome radiation resistance which is often observed in radiotherapy using low LET radiation.[10] Indirect effects are caused by the radiolytic species formed in water, such as different reactive oxygen species (ROS) which are very reactive and can damage the DNA molecules by chemical reactions.

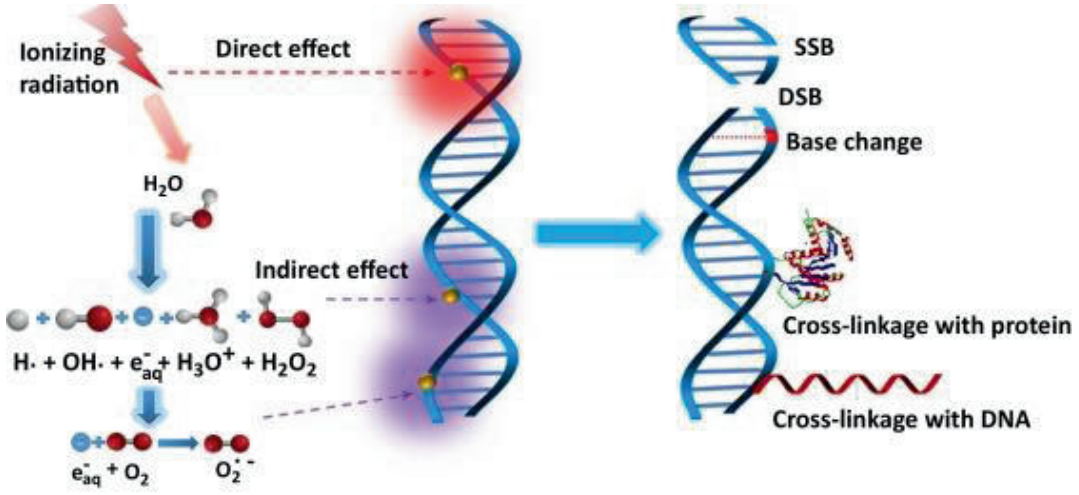

Figure 1.2. Schematic overview of the Mechanism of Ionizing Radiation (IR) in Radiotherapy. IR directly damages DNA (direct effect) and also affects the DNA by indirect effects in which IR leads to water radiolysis and the generation of reactive oxygen species (ROS). There are several types of DNA damage, such as single-strand breaks (SSBs), double-stranded breaks (DSBs), base damage, cross-linking of protein and so on. The figure is adapted from Ref. [11] with permission (copyright 2017, Elsevier).

1.4 Ionizing radiation as a trigger in other cancer therapies

Apart from being utilized as the direct source for cell damage, ionizing radiation can also be applied in an indirect way to trigger other in vivo reactions capable of damaging tumor cells. For instance, in the presence of scintillators, X-ray photons of high energy can be converted to photons of lower energy which are capable of activating photosensitizers used in photodynamic therapy. Interestingly, Cherenkov light, an accompanying phenomenon of ionizing radiation interaction with water (tissue), has been suggested to function as an internal light source for imaging or induction of photodynamic therapy.[12] In this section, more information is given on the different ways to apply ionizing radiation as the trigger for various cancer therapies.

1.4.1 X-ray/Gamma-ray-induced cancer treatment

The typical example for utilizing X-rays as a trigger is the so-called X-ray induced photodynamic therapy, in which high energy X-ray photons are converted to low energy

optical photons by interacting with scintillators.[13] The optical photons with low energy are then used to excite photosensitizers which are usually combined with the scintillators and in consequence generate singlet oxygen ($^1O_2$) that is capable of killing tumor cells.

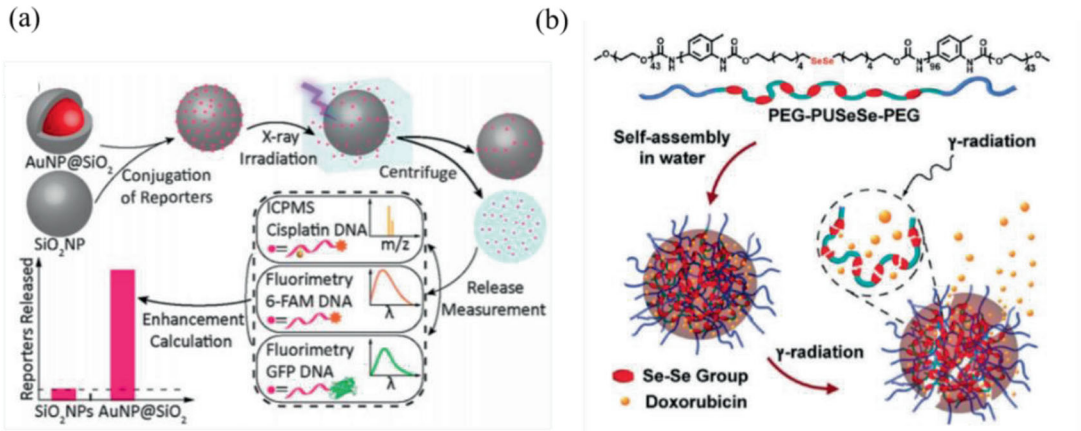

Figure 1.3. Overall design of reporters that are conjugated to the surface of SiO_2 NPs and AuNP@SiO_2 nanostructures; (b) Schematic illustration of the disassembly and drug release of the radiation-sensitive micelles under exposure to γ-radiation. Reproduction permission from Ref. [23] (copyright 2018, American Chemical Society) and Ref [24] (copyright 2011, American Chemical Society) are obtained for picture (a) and (b), respectively.

The concept of X-ray induced photodynamic therapy was first developed by Zhang et al. , who pointed out that ionizing radiation can generate light through scintillation and when combined with certain photosensitizers lead to cell death.[14] Two years later, Joly et al. synthesized a complex by LaF_3:Tb^{3+} and meso-tetra(4-carboxyphenyl) porphine (MTCP) and confirmed that the very reactive ROS, singlet oxygen, can be produced by exposing LaF_3:Tb^{3+}-MTCP to X-ray radiation.[15] Since then, the X-ray induced photodynamic therapy is drawing increasing attention. Various materials, such as silica coated $SrAl_2O_4$:Eu^{2+} (SAO) nanoparticles, silica coated $LiGa_5O_8$:Cr nanoparticles, special MOF (metal-organic framework) compounds and gold nanoclusters, have been studied and utilized to convert X-rays to optical photons and initiate in vivo photodynamic therapy.[16-19] Gamma-rays also act in a similar way, but much less studies can be found in the literature due to the higher energy used, usually in MeV range, which is much less likely to interact with nano-scintillator materials.[20]

Apart from being a light source for photodynamic therapy, the energetic photons can also be utilized as a trigger for controlled drug release. For achieving radiation-induced drug release, certain radiation-sensitive agents should be incorporated in the nanocarriers and induce sufficient structure damage once exposed to radiation.[21, 22] Su et al. developed a nanocarrier based on silica-covered gold nanoparticles, and conjugated several therapeutic substances on the surface of the nanoparticles by using DNA single strands as the linker responding to radiation (Figure 1.3(a)). When exposed to X-ray radiation, the locally accumulated reactive oxygen species generated by gold enhanced water-radiolysis , breaking the DNA strands and releasing the conjugated drugs to achieve local drug administration.[23] Ma et al. prepared radiation-sensitive block copolymers by introducing low energy (172 $kJ \cdot mol^{-1}$) selenium double bonds which are supposed to be easily broken under ionizing radiation (Figure 1.3(b)). These block polymers were used to form polymeric micelles for Dox delivery.[24] The loaded Dox was shown to be released from these micelles when exposed to gamma-ray radiation dose as low as 5 Gy, and apparent morphology changes could also be observed at 50Gy.

1.4.2 Cerenkov-induced photodynamic therapy

The Cerenkov phenomenon is electromagnetic radiation (light) that is produced when charged particles travel through a medium with speed faster than the speed of light in the medium (Figure 1.4).[25] Cerenkov light is typically observed in the core of nuclear reactors as strong blue light, but it is also seen in radiotherapy and diagnostic applications using radioisotopes capable of emitting high energy charged particles, e.g. ^{18}F, ^{64}Cu, ^{89}Zr. [26, 27] Recently, the Cerenkov phenomenon has drawn a lot of attention in cancer treatment because of the possibility to be applied as the internal light source in photodynamic therapy (PDT), overcoming the light penetration problem in tissue.[28, 29]

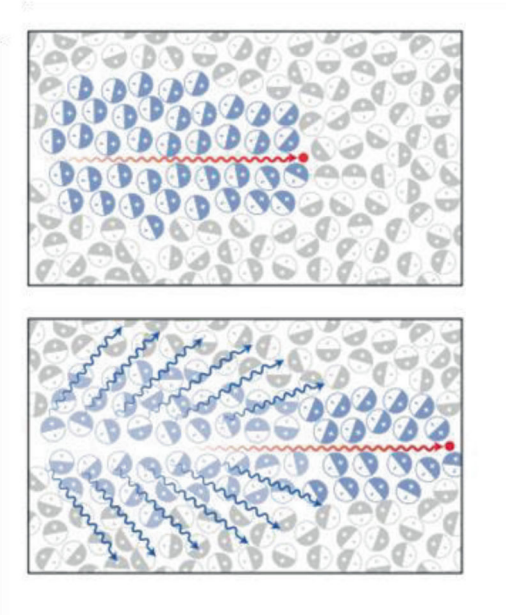

Figure 1.4. Top: A charged particle (red dot) travelling faster than light in a medium polarizes the medium. Bottom: As the medium returns to the ground state, photomagnetic radiation light is emitted in the forward direction. Reproduction permission (Copyright 2017, Nature Publishing Group) from Ref.[25] is obtained.

The first example of using Cerenkov as an internal light source for PDT was shown by Kotagiri et al. They used ^{64}Cu and ^{18}F as the radioactive source to induce Cerenkov light and TiO_2 nanoparticles as the photosensitizer together with a photoinitiator, titanocene (Tc). After being activated by the Cerenkov light, the TiO_2 NPs generated superoxide and hydroxyl radicals, efficiently killing tumor cells.[31] Since the spectrum of the emitted light by the Cerenkov phenomenon is very broad there are many different photosensitizers that could be applied. Kamkaew et al. applied mesoporous silica (HMSN-Ce6) nanoparticles loaded with chlorin e6 for Cerenkov-induced PDT. When combined with ^{89}Zr, a high energy beta plus emitter that can lead to Cerenkov phenomenon, the system exhibited quite superior therapeutic outcome in the treatment of 4T1 tumor-bearing mice. In contrast, mice treated by ^{89}Zr-HMSN or HMSN-Ce6 alone has much less effect on tumour growth.[28] However, the Cerenkov-induced PDT is still an issue of debate as researchers have shown that the produced Cerenkov light photons are far too little to induce any therapeutic effect and that most likely other phenomena are at work.[31]

1.5 Polymeric micelles applied in cancer treatment

1.5.1 Drug delivery systems based on polymeric micelles

Though chemotherapy is widely utilized in cancer treatment, it still faces some challenges. A large amount of anticancer chemotherapeutic drugs are hydrophobic, such as the Paclitaxel (PTX) and Docetaxel (DTX), and cannot form stable suspension in the bloodstream which leads to insufficient tumor accumulation. In addition, chemotherapeutic drugs often interact with different proteins in the bloodstream, which threatens the transportation of drugs in patients. This is why nano-carriers encapsulating drugs have been proposed as a way to improve the drug transportation and avoid unnecessary contact with substances in the bloodstream. Some nano-carriers have already been approved for clinical use, such as NK105 which refers to Paclitaxel encapsulated in certain type of polymer micelles.

The use of nano-carriers in chemotherapy has proven to decrease adverse side effects, although the treatment effectivity is comparable to conventional use of drugs. Different strategies have been developed to achieve targeted delivery of nano-carriers, including active-targeting and passive-targeting. Passive targeting is based on the Enhanced Permeability and Retention (EPR) effects caused by the leaky vascular structure and the lack of lymphatic drainage in tumor tissue. Active targeting uses targeting agents for tumor accumulation. However, this targeting method is not possible without the EPR effect but it can lead to longer residence time of the nano-carriers in the tumors. A variety of nanocarriers with different physiochemical properties, morphologies and functionalization possibilities have been developed among which polymeric micelles appear to be one of the most promising agents.

Polymeric micelles composed by amphiphilic block copolymers are widely researched in cancer treatment, and a few of them have already been applied in the clinic.[32, 33] The formation of micelles is based on the amphiphilic nature of block copolymers, that is, once being dispersed in aqueous solution, the hydrophobic segments will cluster together to decrease the contact with water, while the hydrophilic region would form a shell to surround the hydrophobic core. In this way the typical core-shell structure for micelles is obtained (as

shown in Figure.1.5). The hydrophobic core of the micelles is used to encapsulate hydrophobic anticancer reagents based on various interaction mechanisms and enhance drug accumulation at the tumor while reducing side effects. The hydrophilic corona plays an important role in protecting the nano-carriers from opsonization, leading to prolonged blood circulation time. The micelles can only be formed when the polymer concentration is higher than the so-called Critical Micelle Concentration (CMC). The polymeric micelles usually have a diameter below 100 nm, which can protect the drug delivery system from recognition by the reticuloendothelial system (RES) and have therefore better uptake by tumors. The accumulation of these micelles at the tumor site relies on the EPR effect. Though EPR effect is essential for tumor accumulation, it has been shown to vary dramatically per patient and cancer type.

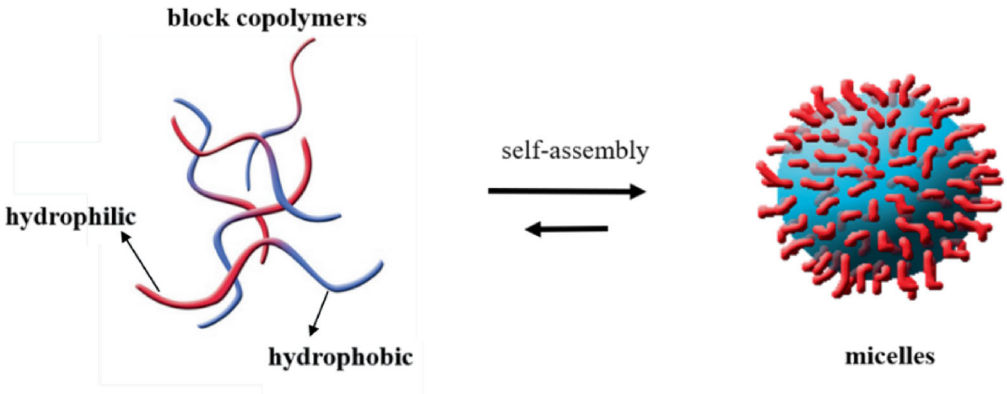

Figure 1.5. The formation of micelles by the self-assembly process of amphiphilic block-copolymers in aqueous solution

Apart from being simply utilized as drug carriers, a variety of functionalized micelles have also been developed as more precise and reliable drug delivery systems.[34] Usually, these functionalized micelles can respond to certain stimuli, such as pH, light and so on, and specifically release the encapsulated drugs at the tumor sites. For example, Cheng et al. developed the PCL-PEO micelles which have been functionalized with light sensitive molecules and have been used as carriers for Dox. The obtained nanocarriers exhibited rapid and complete drug release after being exposed to 254 nm UV light for 10 s.[35] Compared to light-sensitive micelles, radiation-sensitive nanocarriers have the great advantage with no limitations to penetration in tissue, as shown in the case of the diselenide-containing block copolymers.[24]

1.5.2 Biodegradable micelles

To be used in the clinic the polymeric micelles need to be biodegradable. Once degraded in vivo, nontoxic fragments should be excreted through metabolic processes preventing long-term accumulation in healthy tissue.[36] Currently, the FDA approved biodegradable polymers mainly consist of polyester containing molecules such as poly-caprolactone (PCL) and poly-lactic acid (PLA), which can de decomposed through hydrolysis or enzymatic processes. Some micelles composed of biodegradable polymers, such as poly(aspartic acid)(PAs), poly(glutamic acid) (PGlu), are even clinically applied as drug carriers in chemotherapy.[32, 37]

As a biodegradable and biocompatible material, PCL-PEO (poly(ε-caprolactone)-block-poly(ethylene oxide)) block copolymers with polyester bonds in the PCL segment have been extensively studied for clinical application. The formation of PCL-PEO block copolymer is based on the ring-opening polymerization between PEO and ε-caprolactone in the presence of catalyst, usually stannous octoate ($SnOct_2$).[38, 39] Varying experimental parameters of polymerization process, such as the molecular ratio between the PCL and PEO blocks, leads to synthesis of different PCL-PEO block copolymers.[40, 41] Functionalized PCL-PEO block copolymers can be synthesized by adding extra functionality during the ring-opening polymerization process.[35, 42] Similar to other polymeric micelles, the PCL-PEO based micelles either have been utilized as simple nanocarriers for hydrophobic drugs or as stimuli-response carriers for controlled drug release.[43-45]

1.6 Nuclear imaging technique for tracing the micellar systems in vivo

The increasing application of micelles in clinical studies requires a better understanding of the in vivo behavior of the micelles, such as pharmacokinetics and biodistribution. Therefore, tracing the micelles in vivo is of great importance. Some common imaging modalities that can be applied to study in vivo behavior are magnetic resonance imaging (MRI), X-ray computed tomography (CT), optical imaging and nuclear imaging techniques.[47] For tracing the micelles, various reagents were introduced to the micellar systems, for example,

Mn^{2+}, Ga^{3+} and superparamagnetic iron oxide nanoparticles for MRI imaging,[48, 49] some fluorescent probes with varying optical properties,[50, 51] gold nanoparticles for CT,[52, 53] and radioisotopes for nuclear imaging.[54]

Among these imaging techniques, nuclear imaging is widely utilized due to its non-invasive nature in collecting in vivo information with good accuracy and high spatial resolution. There are two techniques using radionuclides applied in imaging, i.e. single-photon emission computed tomography (SPECT) and positron emission tomography (PET). The former makes use of radioisotopes capable of emitting gamma-rays, such as ^{111}In, ^{131}I and ^{99m}Tc, while the latter relies on positron emitters, e.g. ^{18}F, ^{68}Ga and ^{89}Zr. To visualize in vivo behavior by SPECT or PET, the micelles should be radiolabeled with the radioisotopes. Therefore, a reliable and easy radiolabeling process is required for successful tracing of the micelles.

Outline of the thesis

The focus of this thesis is on the utilization of biodegradable drug nanocarriers combined with ionizing radiation in cancer treatment. Polymeric micelles based on PCL-PEO block copolymers were selected as the main platform for delivering various therapeutic substances due to their size, degradability and easy preparation. This thesis can roughly be divided into two main parts. In the first part we combined the external radiation beams with PCL-PEO micelles which are applied as a nanoplatform for chemotherapeutic drugs and photosensitizer and investigated the possibility that using the radiation power as a trigger for drug release from the micelles. In the second part, we focus more on the cooperation of radionuclides and PCL-PEO micelles. So far we developed a chelator-free method to radiolabel micelles for determining their in vivo behavior, as well as evaluated the possibility to combine chemotherapy with radionuclide therapy using the micelles as a nanoplatform. In both parts we attempted to unravel mechanisms behind the observed phenomena to be able to adjust the nano-carriers accordingly.

Chapter 2 focuses on the evaluation of the photochemical properties of the fluorescent probe Singlet Oxygen Sensor Green (SOSG), which is claimed to be specific for detecting singlet oxygen. The SOSG probe is commonly used to detect singlet oxygen and was also our probe of choice when investigating the interaction of the photosensitizer Ce6 and ionizing radiation. In this chapter we studied the photochemical performance of SOSG probe under ionizing radiation. The influence of various factors including radiation type and radiation dose on the fluorescence behavior of SOSG was studied.

Chapter 3 describes the synthesis of a radiation-sensitive drug delivery system (DDS) based on PCL-PEO micelles. We incorporated Chlorin-e6 (Ce6), a typical photosensitizer in photodynamic therapy, in the micelles and intended to use it as the photosensitizer to be excited by Cerenkov light generated by ionizing radiation. We evaluated the release performance of Ce6 and drugs loaded PCL-PEO micelles upon X-ray and γ-rays exposure and studied the mechanism behind the observed release.

In **Chapter 4**, we developed a chelator free method to radiolabel PCL-PEO micelles with ^{111}In. The ^{111}In radiolabeling efficiency and stability of various PCL-PEO micelles were evaluated and compared. SPECT/CT imaging of healthy mice was carried out to determine whether this radiolabeling method can be safely applied in vivo. Moreover, we also explored the possibility to radiolabel PCL-PEO micelles loaded with chemotherapeutic drugs and determined their radiolabeling efficiency and stability.

Chapter 5 explores the mechanism of interaction between micelles and different radioisotopes by studying the radiolabeling efficiency, stability and speciation of the different elements used. The CHEAQs software was applied to determine the speciation of the used metal ions as function of concentration and pH, and this was used to increase the stability of radiolabeling. Cryo-EM was also applied to get a better understanding of the radiolabeling mechanism.

In **chapter 6**, we used the PCL-PEO micelles to single load with Paclitaxel or ^{177}Lu and co-loaded with Paclitaxel and ^{177}Lu for chemotherapy, radionuclide therapy, and combined radionuclide-chemotherapy, respectively. In vitro experiments using U87 based tumor

spheroids were carried out to evaluate the spheroid uptake and distribution of the PCL-PEO micelles as well as the tumor killing efficiency of the single loaded and the co-loaded micelles.

Finally, **chapter 7** provides conclusions based on the understanding of the results.

References

[1] World Health Organization, 2021 March 3, Cancer. Retrieved from https://www.who.int/news-room/fact-sheets/detail/cancer

[2] S. Gianfaldoni, R. Gianfaldoni, U. Wollina, J. Lotti, G. Tchernev, T. Lotti, An Overview on Radiotherapy: From Its History to Its Current Applications in Dermatology, *Maced. J. Med. Sci*. **2017**, 5, 521-525.

[3] O.O. Peltek, A.R. Muslimov, M.V. Zyuzin, A.S. Timin, Current Outlook on Radionuclide Delivery Systems: from Design Consideration to Translation into Clinics, *J. Nanobiotechnology*. **2019**, 17, 90.

[4] J. Belloni, M. Mostafavi, T. Douki, M. Spotheim-Maurizot, Radiation chemistry - From basics to applications in material and life sciences, **2008**.

[5] G. Baldacchino, E. Brun, I. Denden, S. Bouhadoun, R. Roux, H. Khodja, C. Sicard-Roselli, Importance of Radiolytic Reactions During High-LET Irradiation Modalities: LET Effect, Role of O_2 and Radiosensitization by Nanoparticles, *Cancer Nano*. **2019**, 10, 3.

[6] S. Sanguanmith, J. Meesungnoen, Y. Muroya, M. Lin, Y. Katsumura, J.P. Jay-Gerin, On the Spur Lifetime and Its Temperature Dependence in the Low Linear Energy Transfer Radiolysis of Water, *Phys. Chem. Chem. Phys*. **2012**, 14, 16731-16736.

[7] S. Le Caër, Water Radiolysis: Influence of Oxide Surfaces on H_2 Production under Ionizing Radiation, *Water* **2011**, 3, 235-253.

[8] M. Niemantsverdriet, M.J. van Goethem, R. Bron, W. Hogewerf, S. Brandenburg, J.A. Langendijk, P. van Luijk, R.P. Coppes, High and Low LET Radiation Differentially induce Normal Tissue Damage Signals, *Int. J. Radiat. Oncol. Biol. Phys*. **2012**, 83, 1291-1297.

[9] A. Schipler, G. Iliakis, DNA Double-Strand-Break Complexity Levels and Their Possible Contributions to the Probability for Error-Prone Processing and Repair Pathway Choice, *Nucleic. Acids. Res.* **2013**, 41, 7589-7605.

[10] Y. Hirota, S. Masunaga, N. Kondo, S. Kawabata, H. Hirakawa, H. Yajima, A. Fujimori, K. Ono, T. Kuroiwa, S. Miyatake, High Linear-Energy-Transfer Radiation Can Overcome Radioresistance of Glioma Stem-Like Cells to Low Linear-Energy-Transfer Radiation, *J. Radiat. Res.* **2014**, 55. 75-83.

[11] H. Wang, X. Mu, H. He, X.D. Zhang, Cancer Radiosensitizers, Trends. *Pharmacol. Sci*. **2018**, 39, 24-48.

[12] B. Cline, I. Delahunty, J. Xie, Nanoparticles to Mediate X-Ray-Induced Photodynamic Therapy and Cherenkov Radiation Photodynamic Therapy, *Wiley Interdiscip. Rev. Nanomed. Nanobiotechnol*. **2019**, 11, e1541.

[13] W. Sun, Z. Zhou, G. Pratx, X. Chen, H. Chen, Nanoscintillator-Mediated X-Ray Induced Photodynamic Therapy for Deep-Seated Tumors: From Concept to Biomedical Applications, *Theranostics* **2020**, 10, 1296-1318.

[14] W. Chen, J. Zhang, Using Nanoparticles to Enable Simultaneous Radiation and Photodynamic Therapies for Cancer Treatment, *J. Nanosci. Nanotechnol*. **2006**, 6, 1159-1166.

[15] Y. Liu, W. Chen, S. Wang, A.G. Joly, Investigation of Water-Soluble x-Ray Luminescence Nanoparticles for Photodynamic Activation, *Appl. Phys. Lett*. **2008**, 92, 043901.

[16] W. Sun, L. Luo, Y. Feng, Y. Cai, Y. Zhuang, R.J. Xie, X. Chen, H. Chen, Aggregation-Induced Emission Gold Clustoluminogens for Enhanced Low-Dose X-ray-Induced Photodynamic Therapy, *Angew. Chem. Int. Ed. Engl*. **2020**, 59. 9914-9921.

[17] G. Lan, K. Ni, R. Xu, K. Lu, Z. Lin, C. Chan, W. Lin, Nanoscale Metal-Organic Layers for Deeply Penetrating X-ray-Induced Photodynamic Therapy, *Angew. Chem. Int. Ed. Engl.* **2017**, 56, 12102-12106.

[18] H. Chen, G.D. Wang, Y.J. Chuang, Z. Zhen, X. Chen, P. Biddinger, Z. Hao, F. Liu, B. Shen, Z. Pan, J. Xie, Nanoscintillator-Mediated X-Ray Inducible Photodynamic Therapy for In Vivo Cancer Treatment, *Nano Lett*. **2015**, 15, 2249-2256.

[19] H. Chen, X. Sun, G.D. Wang, K. Nagata, Z. Hao, A. Wang, Z. Li, J. Xie, B. Shen, $LiGa_5O_8$:Cr-Based Theranostic Nanoparticles for Imaging-Guided X-ray Induced Photodynamic Therapy of Deep-Seated Tumors, *Mater. Horiz*. **2017**, 4, 1092-1101.

[20] M.J. Wooseung Lee, Chiwoo Oh, Jin Yeong Choi and Hyung-Jun ImWooseung Lee et al., Preparation of Radiolabeled Europium loaded Nanoparticle for in vivo Imaging and Gamma Ray Induced Photodynamic Therapy, *J. Nucl. Med*. **2019**, 60 (supplement 1) 4

[21] W. Deng, W. Chen, S. Clement, A. Guller, Z. Zhao, A. Engel, E.M. Goldys, Controlled Gene and Drug Release from A Liposomal Delivery Platform Triggered by X-ray Radiation, *Nat. Commun.* **2018**, 9, 2713.

[22] F. Fan, S. Gao, S. Ji, Y. Fu, P. Zhang, H. Xu, Gamma Radiation-Responsive Side-Chain Tellurium-Containing Polymer for Cancer Therapy, *Mater. Chem. Front.* **2018**, 2,2109-2115.

[23] M. Su, K.G. Guggenheim, J. Lien, J.B. Siegel, T. Guo, X-ray-Mediated Release of Molecules and Engineered Proteins from Nanostructure Surfaces, *ACS Appl. Mater. Interfaces* **2018**, 10, 31860-31864.

[24] N. Ma, H. Xu, L. An, J. Li, Z. Sun, X. Zhang, Radiation-Sensitive Diselenide Block co-Polymer Micellar Aggregates: Toward the Combination of Radiotherapy and Chemotherapy, *Langmuir* **2011**, 27, 5874-5878.

[25] T.M. Shaffer, E.C. Pratt, J. Grimm, Utilizing the Power of Cerenkov Light with Nanotechnology, *Nat. Nanotechnol*. **2017**, 12, 106-117.

[26] A. Ruggiero, J.P. Holland, J.S. Lewis, J. Grimm, Cerenkov Luminescence Imaging of Medical Isotopes, *J. Nucl. Med*. **2010**, 51, 1123-1130.

[27] D. Thorek, R. Robertson, W.A. Bacchus, J. Hahn, J. Rothberg, B.J. Beattie, J. Grimm, Cerenkov Imaging - A New Modality for Molecular Imaging, *Am. J. Nucl. Med. Mol. Imaging* **2012**, 2, 163-173.

[28] A. Kamkaew, L. Cheng, S. Goel, H.F. Valdovinos, T.E. Barnhart, Z. Liu, W. Cai, Cerenkov Radiation Induced Photodynamic Therapy Using Chlorin e6-Loaded Hollow Mesoporous Silica Nanoparticles, *ACS Appl. Mater. Interfaces* **2016**, 8, 26630-26637.

[29] D. Duan, H. Liu, Y. Xu, Y. Han, M. Xu, Z. Zhang, Z. Liu, Activating TiO_2 Nanoparticles: Gallium-68 Serves as a High-Yield Photon Emitter for Cerenkov-Induced Photodynamic Therapy, *ACS Appl. Mater. Interfaces* **2018**, 10, 5278-5286.

[30] N. Kotagiri, G.P. Sudlow, W.J. Akers, S. Achilefu, Breaking the Depth Dependency of Phototherapy with Cerenkov Radiation and Low-Radiance-Responsive Nanophotosensitizers, *Nat. Nanotechnol*. **2015**, 10, 370-379.

[31] E.C. Pratt, T.M. Shaffer, Q. Zhang, C.M. Drain, J. Grimm, Nanoparticles as Multimodal Photon Transducers ofIonizing Radiation, *Nat. Nanotechnol*. **2018**, 13, 418-426.

[32] H. Cabral, K. Kataoka, Progress of Drug-Loaded Polymeric Micelles into Clinical Studies, *J. Control. Release* **2014**, 190, 465-476.

[33] A. Varela-Moreira, Y. Shi, M.H.A.M. Fens, T. Lammers, W.E. Hennink, R.M. Schiffelers, Clinical Application of Polymeric Micelles for the Treatment of Cancer, *Mater. Chem. Front.* **2017**, 1, 1485-1501.

[34] N. Bölgen, **2018**, Stimuli Responsive Polymeric Nanocarriers for Drug Delivery Applications, Volume 1, pp. 635-651, Woodhead Publishing Series in Biomaterials

[35] Y. Barenholz, Doxil(R)--the First FDA-Approved Nano-Drug: Lessons Learned, *J. Control. Release* **2012**, 160, 117-134.

[36] Q. Zhou, L. Zhang, T. Yang, H. Wu, Stimuli-Responsive Polymeric Micelles for Drug Delivery and Cancer Therapy, *Int. J. Nanomedicine* **2018**, 13, 2921-2942.

[37] C. C. Cheng, J. J. Huang, A. W. Lee, S. Y. Huang, C. Y. Huang, J. Y. Lai, Highly Effective Photocontrollable Drug Delivery Systems Based on Ultrasensitive Light-Responsive Self-Assembled Polymeric Micelles: An in Vitro Therapeutic Evaluation, *ACS Applied Bio. Materials* **2019**, 2, 2162-2170.

[38] M.A.R. Meier, S.N.H. Aerts, B.B.P. Staal, M. Rasa, U.S. Schubert, PEO-b-PCL Block Copolymers: Synthesis, Detailed Characterization, and Selected Micellar Drug Encapsulation Behavior, *Macromol. Rapid Commun*. **2005**, 26, 1918-1924.

[39] H.K. Cho, K.S. Cho, J.H. Cho, S.W. Choi, J.H. Kim, I.W. Cheong, Synthesis and Characterization of PEO-PCL-PEO Triblock Copolymers: Effects of the PCL Chain Length on the Physical Rroperty of W(1)/O/W(2) Multiple Emulsions, *Colloids Surf B Biointerfaces* **2008**, 65, 61-68.

[40] S.K. Patel, A. Lavasanifar, P. Choi, Molecular Dynamics Study of the Encapsulation Capability of A PCL-PEO Based Block Copolymer for Dydrophobic Drugs with Different Spatial Distributions of Dydrogen Bond Donors and Acceptors, *Biomaterials* **2010**, 31, 1780-1786.

[41] A. Ianiro, J. Patterson, Á. González García, M.M.J. van Rijt, M.M.R.M. Hendrix, N.A.J.M. Sommerdijk, I.K. Voets, A.C.C. Esteves, R. Tuinier, A Roadmap for Poly(ethylene oxide)-Block-Poly-ε-Caprolactone Self-Assembly in Water: Prediction, Synthesis, and Characterization, *J. Polym. Sci. Pol. Phys*. **2018**, 56, 330-339.

[42] J.G. Lebouille, L.F. Vleugels, A.A. Dias, F.A. Leermakers, M.A. Cohen Stuart, R. Tuinier, Controlled Block Copolymer Micelle Formation for Encapsulation of Hydrophobic Ingredients, *Eur. Phys. J. E*. **2013**, 36, 107.

[43] L. Zhang, Y. He, G. Ma, C. Song, H. Sun, Paclitaxel-Loaded Polymeric Micelles Based on Poly(varepsilon-caprolactone)-Poly(ethylene glycol)-Poly(varepsilon-caprolactone) Triblock Copolymers: In Vitro and In Vivo Evaluation, *Nanomedicine*, **2012**, 8, 925-934.

[44] A.L. Glover, S.M. Nikles, J.A. Nikles, C.S. Brazel, D.E. Nikles, Polymer Micelles with Crystalline Cores for Thermally Triggered Release, *Langmuir* **2012**, 28, 10653-10660.

[45] H. Liu, A.C. Laan, J. Plomp, S.R. Parnell, Y. Men, R.M. Dalgliesh, R. Eelkema, A.G. Denkova, Ionizing Radiation-Induced Release from Poly(ε-caprolactone-b-ethylene glycol) Micelles, *ACS Appl. Polym. Mater*. **2020**, 3, 968-975.

[46] S. Movassaghian, O.M. Merkel, V.P. Torchilin, Applications of Polymer Micelles for Imaging and Drug Delivery, *Wiley Interdiscip. Rev. Nanomed. Nanobiotechnol*. **2015**, 7, 691-707.

[47] Q. Yan, X. Dong, R. Xie, X. Xu, X. Wang, K. Zhang, J. Xia, J. Ling, F. Zhou, J. Sun, Preparation of Mn^{2+}@PolyDOPA-b-Bolysarcosine Micelle as MRI Contrast Agent with High Longitudinal Relaxivity, *J. Macromol. Sci. A* **2020**, 58, 175-181.

[48] B. Wu, K. Deng, S.T. Lu, C.J. Zhang, Y.W. Ao, H. Wang, H. Mei, C.X. Wang, H. Xu, B. Hu, S.W. Huang, Reduction-Active Fe_3O_4-Loaded Micelles with Aggregation- Enhanced MRI Contrast for Differential Diagnosis of Neroglioma, *Biomaterials* **2021**, 268, 120531.

[49] G. Yeroslavsky, M. Umezawa, K. Okubo, K. Nigoghossian, D. Thi Kim Dung, K. Miyata, M. Kamimura, K. Soga, Stabilization of Indocyanine Green Dye in Polymeric Micelles for NIR-II Fluorescence Imaging and Cancer Treatment, *Biomater. Sci*. **2020**, 8, 2245-2254.

[50] Q. Wang, D. Lei, F. Chen, Y. Chen, X. Luo, Tracing Difference: In Vitro and in Vivo Antitumor Property Comparison of pH-Sensitive Biomimetic Phosphorylcholine Micelles with Insensitive Micelles, *ACS Biomater. Sci. Eng*. **2019**, 5, 2258-2270.

[51] D. Xiong, X. Zhang, S. Peng, H. Gu, L. Zhang, Smart pH-Sensitive Micelles Based on Redox Degradable Polymers as DOX/GNPs Carriers for Controlled Drug Release and CT Imaging, *Colloids Surf. B Biointerfaces* **2018**, 163, 29-40.

[52] W. Lin, C. Yang, Z. Xue, Y. Huang, H. Luo, X. Zu, L. Zhang, G. Yi, Controlled Construction of Gold Nanoparticles in Situ from Beta-Cyclodextrin Based Unimolecular

Micelles for In Vitro Computed Tomography Imaging, *J. Colloid. Interface Sci*. **2018**, 528, 135-144.

[53] S. Shi, K. Shi, L. Tan, Y. Qu, G. Shen, B. Chu, S. Zhang, X. Su, X. Li, Y. Wei, Z. Qian, The Use of Cationic MPEG-PCL-g-PEI Micelles for Co-Delivery of Msurvivin T34A Gene and Doxorubicin, *Biomaterials* **2014**, 35, 4536-4547.

Singlet oxygen sensor green is not a suitable probe for $^1O_2$ in the presence of ionizing radiation

2

Adapted from: H.Liu, P.J.H.Carter, A.C.Laan, R. Eelkema, A.G. Denkova; Sci Rep, 2019, 9, 8393

Abstract

A great number of fluorescent probes have been developed for detecting singlet oxygen ($^1O_2$), which is considered to be one of the most effective reactive oxygen species (ROS), especially in clinical applications. The commercially available fluorescent probe Singlet Oxygen Sensor Green (SOSG) is widely used due to its reported high selectivity to $^1O_2$. In this study, we carried out systemic experiments to determine the activation of SOSG in the presence of ionizing radiation. The results show that the SOSG probe exhibits a pronounced fluorescence increase as a function of radiation dose delivered by gamma-rays as well as X-rays, in conditions where the formation of singlet oxygen is not expected. Furthermore, scavenger tests indicate that hydroxyl radicals may be involved directly or indirectly in the activation process of SOSG although the exact mechanism remains unknown.

Key words: SOSG, Ionizing radiation, ROS, Fluorescence, Sensors

Introduction

Reactive oxygen species (ROS) occur naturally in human cells and are known to play a role in various cancerous processes.[1] At the same time, a number of cancer therapies rely on the generation of ROS to induce cell death.[2] Among all ROS, singlet oxygen ($^1O_2$) is considered to be the most effective in killing tumour cells and has been widely used in photodynamic therapy (PDT).[3] To better understand the behaviour of photosensitizers generating ROS in PDT and consequently their biological effect, the detection of ROS, especially $^1O_2$, is of great importance. However, the short lifetime and the low concentration of $^1O_2$ tremendously complicate proper detection. Various approaches have been developed for the detection of $^1O_2$, including direct measurement of the $^1O_2$ luminescence at 1280 nm, electron spin resonance spectroscopy (ESR), fluorescent probes and others.[4-6] Fluorescent probes are widely employed due to their simplicity in utilization and high detection efficiency.[7] The commercially available probe Singlet Oxygen Sensor Green (SOSG) is currently the preferred choice for $^1O_2$ detection due to its claimed specific sensitivity to singlet oxygen.[8]

As shown in Figure 2.1, the SOSG molecule has two parts: a trapping moiety and a fluorophore.[9] The anthracene-derived trapping moiety, being an electron donor, quenches the luminescence of the fluorophore by photo-induced electron transfer. In an environment containing $^1O_2$, the trapping moiety will react with $^1O_2$ and form an endoperoxide anthracene moiety, which has a lower energy for the highest occupied molecular orbital (HOMO) than that of the fluorophore. Removing the quenching ability of the anthracene leads to fluorescence (FL) emission of the fluorophore under light excitation with a peak at around 530 nm. Despite the many advantages of SOSG, it was previously shown that this probe is not entirely reliable under certain conditions. The main drawback of SOSG is that, for instance when irradiated with UV light, its endoperoxide derivative acts as a photosensitizer itself, generating singlet oxygen which then induces even more fluorescence emission of SOSG.[9-11] Moreover, photo-bleaching of SOSG is observed even for short light exposure times.[9]

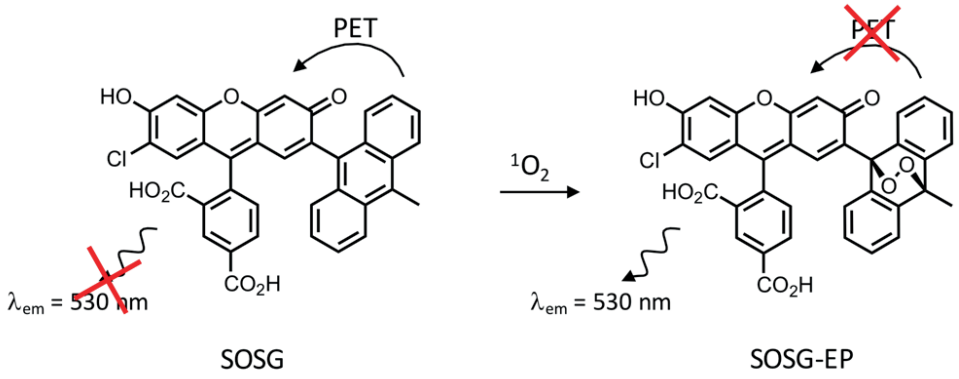

Figure 2.1. Chemical structure of SOSG and the formation of SOSG-EP upon interaction with $^1O_2$, leading to activation of fluorescence output

In photodynamic therapy, singlet oxygen is typically generated by light irradiation of a photosensitizer. Due to absorption and scattering effects of tissue, the penetration depth of light in living tissue can be very shallow, which limits further clinical application.[12] To overcome this challenge, one of the promising options is to combine PDT with radiotherapy. For example, nano scintillators conjugated to photosensitizers were developed which can convert ionizing radiation to light, producing ROS.[13-15] Very recently it was also suggested that radioactive isotopes (e.g. ^{18}F, ^{64}Cu) producing so-called Cerenkov light could function as internal light sources, which in combination with photosensitizers can be applied to induce tumour cell death.[3, 16] Moreover, in radiation-involved therapies, the generation of ROS is also an indirect strategy to reduce the growth of tumour cells. In these therapies, probes are also used to prove the generation of $^1O_2$.[17-19]

As far as we know, the influence of ionizing radiation on the photochemical behaviour of such probes has not been comprehensively evaluated. In this paper, the photochemical performance of SOSG was assessed when exposed to ionizing radiation under conditions similar to other studies.[13, 19] In this study we used gamma-rays (γ-rays) and X-rays, which are common types of ionizing radiation in external radiotherapy. After irradiation, the UV-vis absorption and fluorescence emission of SOSG were determined. We found that, under conditions that are unlikely to generate $^1O_2$, the SOSG probe shows an increasing fluorescence emission as the radiation dose is increased, without any detectable changes in

UV-vis spectrum. Furthermore, scavenger tests suggest that the generation of hydroxyl radicals may be related to the increase in fluorescence emission of SOSG.

Experimental details

2.1 Materials

Singlet Oxygen Sensor Green was purchased from Thermo Fisher; Chlorin-e6 ($C_{34}H_{36}N_4O_6$) was purchased from Bio-connect life sciences (Huissen, the Netherlands); Sodium azide, sodium acetate, ammonium molybdate ($(NH_4)_6Mo_7O_{24}•4H_2O$), potassium iodide (KI), sodium iodide (NaI) were obtained from Merck (Darmstadt, Germany); Methanol, hydrogen peroxide (H_2O_2, 30% (W/W)), acetic acid, Aminophenyl fluorescein solution (5 mM, in Dimethylformamide) (APF), 1,3-diphenylisobenzofuran (DPBF) and 9,10-antherachenediyl-bis(methylene) dimalonic acid (ABDA) were bought from Sigma Aldrich (Zwijndrecht, the Netherlands). Ethanol was bought from Brenntag (Zwijndrecht, The Netherlands). Dimethyl Sulfoxide (DMSO) was bought from Biosolve B. V. (Valkenswaard, The Netherlands). All chemicals were used without further treatment. Water used in these experiments was prepared with the in-house Milli-Q system from Merck Millipore.

2.2 Sample preparation

All samples were prepared in dim environment.

SOSG stock solution (10 μM): Typically, 100 μg of SOSG was dissolved in 33 μL of methanol, and then this yellow solution was added to 16.467 mL of MQ water. For preparing SOSG solutions with different concentrations, the volume of MQ water was changed as required. ABDA stock solution (2 mM): 1.64 mg of 9,10-anthracenediyl bis(methylene) dimalonic acid was dissolved in 2 mL of DMSO, then ultrasonicated for 10 min. DPBF stock solution (2 mM): 2.7 mg of 1,3-diphenylisobenzofuran was dissolved in 5 mL of DMSO and ultrasonicated for 10 min. Ce6 stock solution (10 μM): 1.79 mg of Ce6 was dissolved in 300 mL MQ water and ultrasonicated for 20 min to obtain a Ce6 solution. NaN_3 stock solution (21 mM): 6.825 mg of NaN_3 was dissolved in 5 mL of MQ water and ultrasonicated it for 10

min to obtain a transparent solution. NaN_3 solutions with the concentration of 4.2, 2.1, 1.05 and 0.21 mM were obtained by dilution of the NaN_3 stock. KI stock solutions (1 M): 2.656 g of KI was added to 16 mL of MQ water and ultrasonicated for 10 min. Ammonium molybdate($(NH_4)_6Mo_7O_{24}\bullet 4H_2O$) stock solution (5 mM): 98.9 mg of ($(NH_4)_6Mo_7O_{24}\bullet 4H_2O$) was dissolved in 16 mL of CH_3COONa / CH_3COOH buffer solution (1M) then ultrasonicated for 10 min.

SOSG sample (5 μM): 1 mL of SOSG solution was added to a glass vial (4 mL) wrapped tightly with aluminium foil, followed by the addition of 1mL MQ water. A SOSG (5 μM) + Ce6 (5 μM) solution: 1 mL of SOSG stock solution was added to a glass vial which was also tightly wrapped with aluminium foil, followed by the addition of 1 mL of Ce6 stock solution. DPBF sample: 0.1 mL of DPBF base was diluted by 2 mL of MQ water, achieving a final concentration of 0.1 mM. ABDA samples: 0.05 mL of ABDA base and 2 mL of MQ water was mixed well to form a mixture with the concentration of 0.05 mM. APF samples: 10 μL of the APF stock solution was mixed 10 mL of MQ water and formed a final APF sample with the concentration of 5 μM.

Samples for the scavenger tests: NaN_3 addition: 0.1 mL of NaN_3 solution with different concentrations were add to 2 mL of SOSG sample in a closed covered glass vials; Ethanol addition: expected amounts of ethanol were added to the SOSG samples (5 μM). Before radiation, all samples were thoroughly mixed.

N_2-saturated solutions were prepared by bubbling the samples with N_2 for 20 min.

2.3 Irradiation experiments

Gamma irradiation: A Cobalt 60 (^{60}Co) radioactive source (GC220, Nordion) was used for the gamma irradiations. The aluminium foil covered vials were placed in the centre of the source. The exposure periods were controlled to obtain irradiation doses of 1, 5, 10, 20 and 40 Gy; (The dose rates of 60Co was calculated using Fricke dosimetry corrected for the 2,778 day half-life of Cobalt-60).

X-ray irradiation: The X-ray irradiation was carried out using an X-ray source (Philips MCN 321 variable-energy X-ray tube) with a voltage of 320 kV and current of 3 mA, without filter. The samples were placed on a horizontal platform located 50 cm from the X-ray window (the dose rate was 1.36 Gy/min). The exposure doses were 5, 10, 15, 20 and 25 Gy.

UV (365 nm / 254 nm) irradiation: A commercial UV source (UVGL-58 handheld UV Lamp) was employed as the light source. The aluminium foil was first removed from the vials, followed by placing these vials in a dim box. Then the light source was turned on to irradiate these samples for fixed periods of time.

UV (400 nm) irradiation: A LED light connected to the FL spectrometer was employed as the light source. Samples were firstly transferred from vials to cuvettes, and then these cuvettes were placed in the sample tank, the light source was turned on (0.3~0.5 A and 0.3kV) to start the exposure.

Characterization

3.1 Instruments

Mass spectra of SOSG solutions were recorded using an ESI mass spectrometer (LCMS-2010A, Shimadzu). A UV-vis-NIR spectrophotometer (UV-6300PC, VWR) was used to measure the optical absorption of the prepared samples. A Cary Eclipse Fluorescence Spectrophotometer (Agilent technologies) was employed to characterize the fluorescence emission spectra of the samples. The emission peak for SOSG was located at 529 nm using a 504 nm excitation light. The slits of excitation and emission are 5 nm, if not be mentioned specially.

3.2 Evaluation the H_2O_2 production induced by ionizing radiation

The generation of H_2O_2 was detected by Ghormley's triiodide method:[20] the standard samples were prepared by diluting the H_2O_2 to obtain different concentrations; then 0.1 mL of the KI solution and 0.1 mL of the ammonium molybdate solution was added, and leaving it to react for 10 min, after which the UV intensity at 350 nm was measured.

Detection of H_2O_2 generation after ionizing radiation exposure: after the radiation treatment, 0.1 mL of the KI solution and 0.1 mL of the ammonium molybdate stock solution was immediately added to the samples, and the UV spectra was measured after reaction time of 10 min.

Results and Discussion

The effect of ionizing radiation on the photochemical properties of SOSG was studied systematically using two different external radiation sources, i.e., a cobalt-60 (^{60}Co) γ-ray source and an X-ray source. The fluorescence spectra of SOSG after exposure to gamma rays are presented in Figure 2.2(a), showing that the FL intensity of the SOSG solution increased with increasing radiation doses. Figure 2.2(b) shows the UV-vis absorption spectra of SOSG at the same irradiation conditions, where the maximum band at 507 nm belongs to the fluorescein moiety, while the large peak at 257 nm and the two smaller peaks at 374 and 394 nm correspond to the methylanthracene moiety.[9] No noticeable changes were observed in the UV-vis spectra as the radiation dose increases, suggesting that the structure of SOSG is not affected or the concentration of activated SOSG remains low. To check whether SOSG also reacts with ionizing photons of lower energy, we exposed the probe solutions to X-rays with a maximum energy of 320 keV and monitored the fluorescence spectra and UV-vis absorption at different doses. As shown in Figure 2.2(c), the X-ray exposure also induces fluorescence emission of the SOSG probe, and the FL intensity exhibits an upward trend with increasing radiation doses. In fact, the FL intensity increase is comparable to the raise observed when using the ^{60}Co source for the same radiation dose, showing that this process is most likely not dependent on the photon energy. The UV spectra of SOSG appear unchanged for all X-ray radiation doses (Figure 2.2(d)).

As a check we also exposed the SOSG samples to UV light sources using two different wavelengths (365 nm and 400 nm). These experiments show that the SOSG fluorescence intensity increases significantly as function of irradiation time (Figure S2.1), which is likely caused by the generation of $^1O_2$ in the presence of UV light. Meanwhile, in UV-vis the intensity of the peaks at 257, 507 and 394 nm decreases upon UV irradiation, caused by the formation of SOSG-EP.[10]

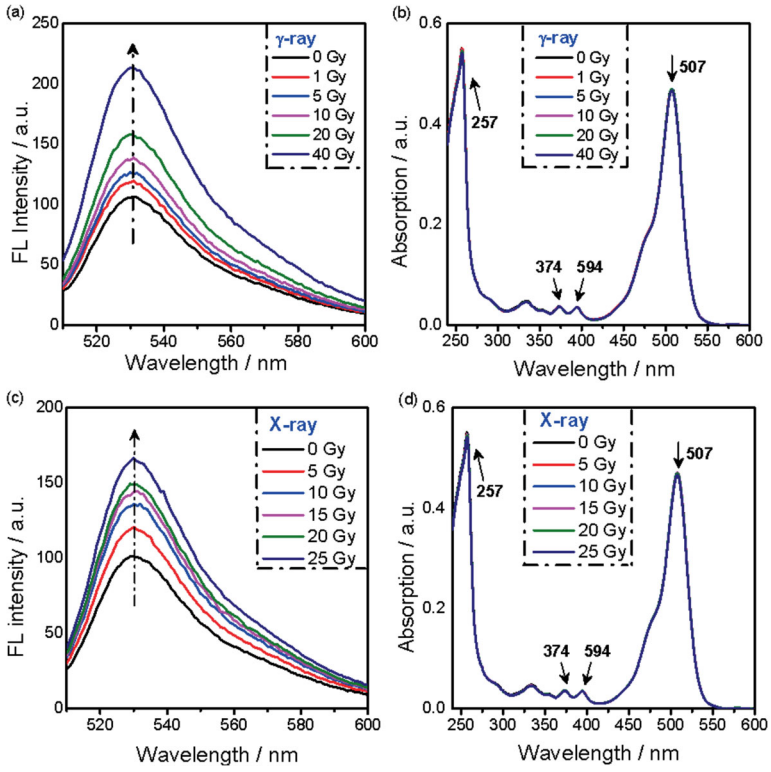

Figure 2.2. (a) Fluorescence spectra of SOSG solutions (5 µM) for varied radiation doses delivered by a ^{60}Co source (λex= 504 nm); (b) UV-vis absorption spectra of SOSG solutions (5 µM) for different radiation doses delivered by a ^{60}Co source; (c) Fluorescence spectra of SOSG solutions (5 µM) for different X-ray doses; (d) UV-vis absorption spectra of the SOSG solution (5 µM) for different X-ray doses

Ionizing radiation can have direct and indirect effects on the behavior of SOSG. In direct interaction, ionizing radiation can result in breaking of chemical bonds, changing the SOSG structure. Indirect effects result from the generation of reactive oxygen species in the aqueous solution which can react with SOSG, or influence the intermolecular electron transfer processes, resulting in the fluorescence emission of SOSG. According to the unchanged UV-vis spectra of the irradiated SOSG samples, chemical bonds are most likely not broken which is expected considering the nature of radiation (i.e. photons) and the low radiation dose (max 25 Gy). Therefore, we focused mostly on any possible indirect effects.

Figure 3.3 shows various photochemical processes that may take place in the aqueous SOSG solution induced by ionizing radiation, which may influence the photochemical performance of the SOSG probe. The ^{60}Co is a radioisotope that decays by beta minus emission, producing

in the process two energetic γ-rays of 1.17 MeV and 1.33 MeV.21 These photons can interact with water via the Compton effect, giving part of their energy to electrons. The energy of these photons is high enough to provide electrons with energies above the threshold for the production of Cerenkov radiation (261 keV in water).[22] It should be mentioned that Cerenkov light has a wide spectrum ranging from 250 to 800 nm with a maximum around 360 nm,[23-24] which overlaps with the absorption range of SOSG resulting in some probability of $^1O_2$ generation. Ionizing radiation also leads to the radiolysis of water which produces various reactive oxygen species, including OH•, $O_2^{-\bullet}$ and H_2O_2.[26] This means that both processes, i.e., the radiolysis of water and the Cerenkov induced singlet oxygen production by SOSG, can in theory generate ROS (Figure 2.3(a)). Similar to γ-rays, X-rays could also trigger the radiolysis of water, leading to a complex mixture of different reactive oxygen species. The X-rays that we used in this study have a maximum energy of 320 keV, however, the energy that could be transferred to the Compton electron is less than 180 keV, which is not sufficient to induce Cerenkov light (Figure 2.3(b)).

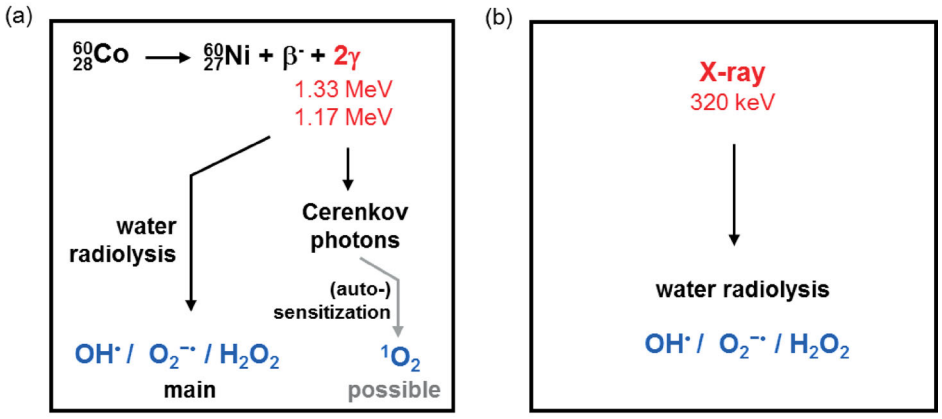

Figure 2.3. Possible reactive oxygen species generated under (a) gamma ray radiation and (b) X-ray (320 keV) radiation of aqueous SOSG solutions.

In order to determine what causes the increase in FL emission of SOSG when using ionizing radiation, we first measured the effect of SOSG concentrations on the fluorescence performance. As shown in Figure 2.4(a), there is no clear trend of the FL intensity when the concentration increases, implying the observed FL emission at a fixed radiation dose does not depend on [SOSG]. In another words, the radiation induced process in the solvent dominates the FL emission. Consequently, the influence of various reactive oxygen species on the SOSG fluorescence was measured. The addition of H_2O_2, a product of water radiolysis,

to the SOSG solution was found to lead to only a very slight increase in FL intensity at H_2O_2 concentrations much higher than those expected to be formed for this radiation dose (the H_2O_2 generation caused by radiolysis of water can be found in Figure S2.3). Considering the increasing FL intensity of SOSG probe under γ-ray and X-ray irradiation, H_2O_2 is unlikely to be the species responsible for the FL phenomenon.

Subsequently, we performed scavenger tests involving different ROS scavengers. First, we used NaN_3, an effective scavenger of $^1O_2$,[11] to check the effect of the possible singlet oxygen formation. According to the results shown in Figure 2.4(c), the FL intensity presents a negligible decrease at lower NaN_3 concentrations (i.e., 0.01, 0.05 and 0.1 mM), and then significantly increases when the concentration of NaN_3 increases to 0.2 mM and 1 mM. The low [NaN_3] experiments suggest a negligible contribution of singlet oxygen. The large FL intensity increase at high [NaN_3] may be ascribed to the interaction between SOSG and $N_3^{\bullet}$ radicals, a strong oxidant species generated by the reaction between N_3^- and OH•.[27] A large amount of hydroxyl radicals are formed under γ-ray radiation as shown in Figure S2.4. Therefore, NaN_3 is not considered to be a proper scavenger of $^1O_2$ for this study due the presence of hydroxyl radicals. In contrast, the introduction of small amounts of ethanol, a typical scavenger of hydroxyl radical (OH•),[28] leads to an evidently lower FL signal. Moreover, the FL signal exhibits a declining trend with the increasing addition of ethanol. Other common scavengers of OH•, i.e., NaI and methanol, also exhibit inhibition of the FL intensity of SOSG (Figure S2.6,7). The suppression of hydroxyl radicals during water radiolysis will also affect the formation of other radicals, which might interact with SOSG.[29] Therefore, it is not possible to state with certainty that the presence of OH• is the sole cause of the observed increase in FL intensity.

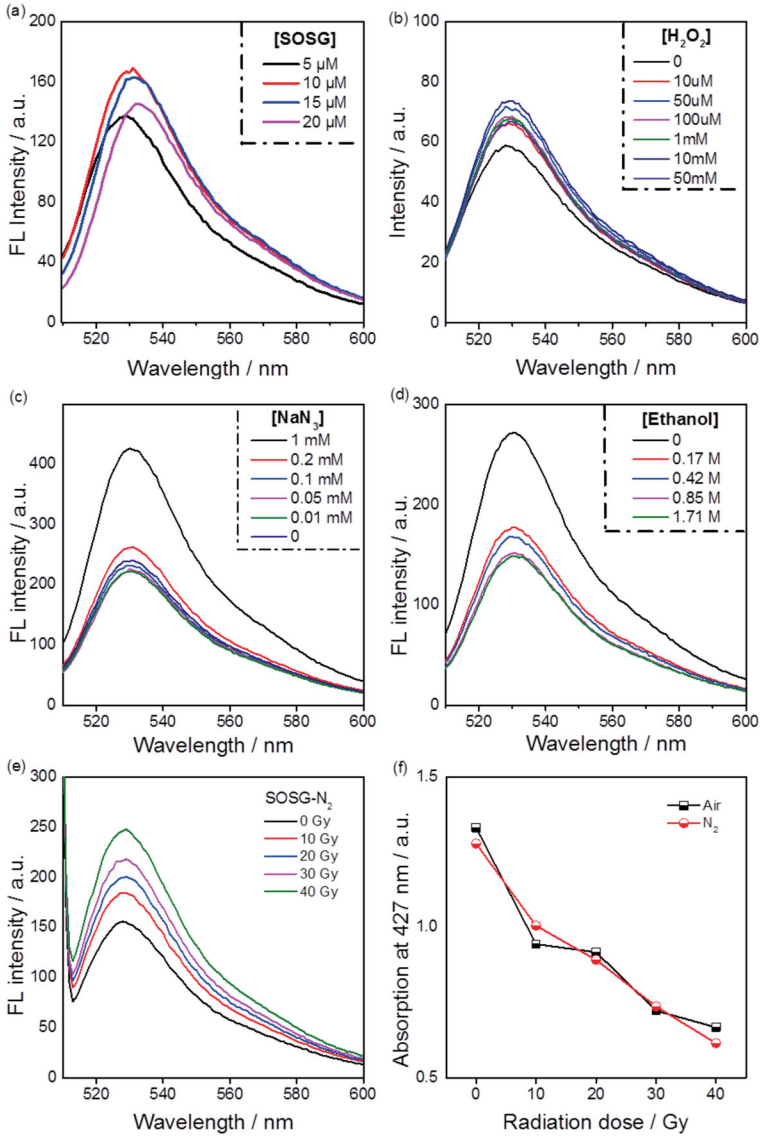

Figure 2.4. Fluorescence spectra (λex= 504 nm) of SOSG solutions (a) with varied SOSG concentrations, (b) reacted with H_2O_2 solutions with varied concentrations, (c) reacted with NaN_3 solutions with different concentrations and (d) in the addition of varied amount of ethanol under 20 Gy radiation dose from a ^{60}Co source; Fluorescence spectra of SOSG solutions (5 μM) (e) saturated with N_2 for varied radiation doses delivered by a ^{60}Co source; (e) The FL intensity determined at 529 nm of air-saturated and N_2-saturated SOSG solutions as function of radiation dose.

Since NaN_3 could not serve as a suitable scavenger of $^1O_2$, we carried out an indirect approach to evaluate the role of $^1O_2$ in these experiments by saturating the solutions with N_2. In N_2 saturated solutions, $^1O_2$ formation is impossible. As shown in Figure 2.4(e), the fluorescence of SOSG in a N_2-saturated aqueous solution shows an increasing signal as

function of radiation dose. Furthermore, comparing the FL intensity of SOSG solutions saturated with N_2 or normal air atmosphere (Figure S2.8) shows no significant difference, which strongly suggests that the fluorescence of SOSG in these experiments is not induced by singlet oxygen. Although γ-ray radiation delivered by ^{60}Co is able to generate Cerenkov light in the UV-Vis range, this light is likely not enough to activate the SOSG probe, in contrast to much higher intensity UV sources (365 nm, 400nm) that were used in our experiments.

In addition to the SOSG probe, we also checked the photochemical behavior of another two probes, i.e., DPBF (1,3-diphenylisobenzofuran) and ABDA (9,10-antherachenediyl-bis(methylene) dimalonic acid), which are widely used to detect the formation of $^1O_2$.[17, 30-33] As illustrated in Figure S2.9-10, both probes were activated in the presence of ionizing radiation. Comparison of the photochemical performance under different atmospheres (Figure S2.9(b) and S2.10(b)) again indicates that the activation processes are not caused by the formation of $^1O_2$.

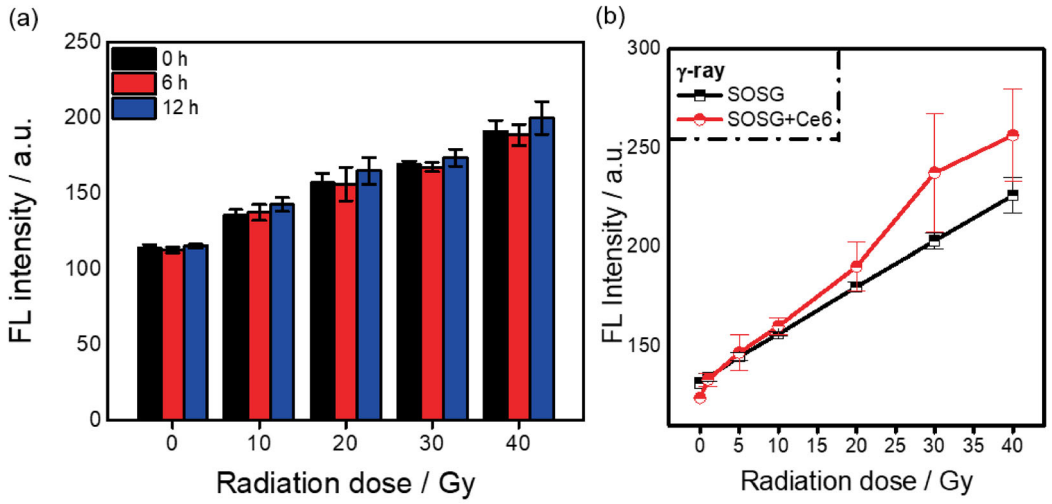

Figure 2.5. (a) Comparison of the fluorescence intensity at 529 nm for SOSG solutions (5 μM) at different time intervals after γ-ray irradiation of different radiation doses; (b) Comparison of the fluorescence intensity at 529 nm between pure SOSG solutions (5 μM) and SOSG solutions (5 μM) containing Ce6 (5 μM) (λex= 504 nm). (Error bars represent the standard deviation of at least 3 replicates).

In order to determine the long-term influence of ionizing radiation on the photochemical performance, we measured the fluorescence of SOSG at different time intervals after

exposure to various radiation doses. Figure 2.5(a) clearly indicates that the induced fluorescence is permanent which in turn implies that the molecular structure of SOSG might be affected. However, the measured mass spectra (Figure S2.2) show no noticeable change in molecular weight after exposure to ionizing radiation, when compared to original SOSG solutions. It is, nevertheless, possible that the amounts of SOSG that were affected were so small that they could not be properly detected, which hinders establishment of the mechanism leading to the observed phenomenon.

Additionally, since Cerenkov light is studied as a promising internal light source for photodynamic therapy,[3,21] we decided to study the activation of SOSG in the presence of the common photosensitizer chlorin-e6 (Ce6), which has been proven to be excited by exposure to Cerenkov light.[16] Ce6 is a typical photosensitizer that is known to be highly efficient in the generation of singlet oxygen and is widely used in photodynamic therapy. We exposed a simple SOSG solution and a SOSG solution mixed with Ce6 to gamma rays originating from the ^{60}Co source. Figure 2.5(b) shows that the FL intensity at 529 nm increases as a function of the gamma dose for both solutions. The FL values in the presence of Ce6 are somewhat higher than those in the pure SOSG solution at higher doses, although no firm conclusion can be drawn due to the large uncertainty of the measured FL intensity. Still, it is possible that at higher radiation doses Ce6 generates singlet oxygen through the Cerenkov effect. As a check we also exposed the same solutions to UV light sources of two different wavelengths (365 nm and 400 nm), showing that the SOSG fluorescence intensity increases significantly in the presence of Ce6 (Figure S2.11). Although there is some increase of FL intensity observed from the pure SOSG solution induced by the UV light sources, it is much smaller than the signal from the solution containing the photosensitizer. These results also support that the SOSG probe is very sensitive to singlet oxygen, under common experimental conditions.

Conclusions

In this paper, we studied the effect of ionizing radiation on the photochemical behavior of SOSG, showing that this probe becomes fluorescent when exposed to either γ-rays or X-rays. SOSG shows increased fluorescence intensity as function of radiation dose, which appears not to be related to singlet oxygen formation. Scavenger tests reveal that the suppression of hydroxyl radicals lead to a decrease in induced fluorescence intensity, which suggests that these species play some role in the activation of the SOSG probe in the presence of ionizing radiation. In contrast, when exposed to UV-light sources, SOSG is efficiently activated through the formation of the SOSG endoperoxide, caused by reaction with singlet oxygen. In addition, another two commercially available probes used for the detection of singlet oxygen, i.e. 1,3-diphenylisobenzofuran and 9,10-antherachenediyl-bis(methylene) dimalonic acid, were also evaluated under ionizing radiation conditions. These two probes appeared also to be activated by ionizing radiation. The exact mechanism leading to the activation of SOSG as well as the two other probes when exposed to ionizing radiation remains unclear but this study does clearly demonstrate that such probes should be cautiously used under such conditions.

References

[1]. G. Saravanakumar, J. Kim &W. J. Kim, Reactive Oxygen Species Responsive Drug Delivery Systems: Promises and Challenges, *Adv. Sci*. **2017**, 4, 1600124.

[2]. W. Fan, P. Huang & X. Chen, Overcoming the Achilles' Heel of Photodynamic Therapy. *Chem. Soc. Rev.* **2016**, 45, 6488-6519.

[3]. N. Kotagiri, G. P. Sudlow, W. J. Akers & S. Achilefu, Breaking the Depth Dependency of Phototherapy with Cerenkov Radiation and Low-radiance-responsive Nanophotosensitizers. *Nat. Nanotechnol.* **2015**, 10, 370-379.

[4]. A. Jimenez-Banzo, S. Nonell, J. Hofkens & C. Flors, Singlet Oxygen Photosensitization by EGFP and Its Chromophore HBDI. *Biophys. J.* **2008**, 94, 168-172.

[5]. E. Hideg, C. Spetea & I. Vass, Singlet Oxygen Production in Thylakoid Membranes during Photoinhibition as Detected by EPR Spectroscopy. *Photosynth. Res.* **1994**, 39, 191-199.

[6]. N. Hananya, O. Green, R. Blau, R. Satchi-Fainaro & D. Shabat, A Highly Efficient Chemiluminescence Probe for the Detection of Singlet Oxygen in Living Cells. *Angew. Chem. Int. Ed.* **2017**, 56, 11793-11796.

[7]. J. Takahashi & M. Misawa, Characterization of Reactive Oxygen Species Generated by Protoporphyrin IX under X-ray Irradiation. *Radiat. Phys. Chem.* **2009**, 78, 889-898.

[8]. G. Yang, X. Sun, J. Liu, L. Feng & Z. Liu, Light Responsive, Singlet Oxygen Triggered on Demand Drug Release from Photosensitizer-doped Mesoporous Silica Nanorods for Cancer Combination Therapy. *Adv. Funct. Mat.* **2016**, 26, 4722-4732 .

[9]. S. Kim, M. Fujitsuka &T. Majima, Photochemistry of Singlet Oxygen Sensor Green. *J. Phys. Chem. B* **2013**, 117, 13985-13992.

[10]. X. Ragas, A. Jimenez-Banzo, D. Sanchez-Garcia, X. Batllori & S. Nonell, Singlet Oxygen Photosensitisation by the Fluorescent Probe Singlet Oxygen Sensor Green®. *Chem. Commun*. **2009** , 2920-2922.

[11]. A. Gollmer et al., Singlet Oxygen Sensor Green®: Photochemical Behavior in Solution and in a Mammalian Cell. *Photochem. Photobiol*. **2011**, 87, 671-679.

[12]. A. M. Smith, M. C. Mancini & S. Nie, Second Window for In Vivo Imaging. *Nat. Nanotechnol*. **2009**, 4, 710-711.

[13]. S. Clement, W. Deng, E. Camilleri, B. C. Wilson & E. M. Goldys, X-ray Induced Singlet Oxygen Generation by Nanoparticle-Photosensitizer Conjugates for Photodynamic Therapy: Determination of Singlet Oxygen Quantum Yield. *Sci. Rep*. **2016**, 6, 19954 .

[14]. A. L. Bulin et al., X-Ray-Induced Singlet Oxygen Activation with Nanoscintillator-Coupled Porphyrins. *J. Phys. Chem. C* **2013**, 117, 21583-21589.

[15]. S. Clement, W. Chen, A. G. Anwer & E. M. Goldys, Verteprofin Conjugated to Gold Nanoparticles for Fluorescent Cellular Bioimaging and X-ray Mediated Photodynamic Therapy. *Microchimica. Acta*. **2017**, 184, 1765-1771.

[16]. A. Kamkaew et al., Cerenkov Radiation Induced Photodynamic Therapy Using Chlorin e6-Loaded Hollow Mesoporous Silica Nanoparticles. ACS Appl. Mater. Interfaces **2016**, 8, 26630-26637.

[17]. L. Chan et al., Sequentially Triggered Delivery System of Black Phosphorus Quantum Dots with Surface Charge-Switching Ability for Precise Tumor Radiosensitization. *ACS Nano* **2018**, 12, 12401-12415.

[18]. S. Clement, W. Chen, W. Deng & E. M. Goldys, X-Ray Radiation-Induced and Targeted Photodynamic Therapy with Folic Acid-Conjugated Biodegradable Nanoconstructs. *Int J Nanomedicine* **2018**, 13, 3553–3570.

[19]. W. Deng et al., Controlled Gene and Drug Release from a Liposomal Delivery Platform Triggered by X-Ray Radiation. *Nat. Commun*. **2018**, 9, 2713.

[20]. J. A. Ghormley & A. C. Stewart, Effects of γ-Radiation on Ice. *J Am Chem Soc* **1956**, 78, 2934-2939.

[21]. B. J. Parsons, Syntax of Referencing in Sterilisation of Biomaterials and Medical Devices, 56-70 (Elsevier Science, **2012**).

[22]. T. M. Shaffer, E. C. Pratt & J. Grimm, Utilizing the Power of Cerenkov Light with Nanotechnology. *Nat. Nanotechnol*. **2017**, 12, 106-117.

[23]. A. Hahn et al., Development of a Composite Large-Size SiPM (assembled matrix) Based Modular Detector Cluster for MAGIC. *Nucl. Instrum. Methods. Phys. Res. A* **2017**, 845, 89-92.

[24]. X. Ma, J. Wang & Z. Cheng, Cerenkov Radiation: A Multi-Functional Approach for Biological Sciences. *Front. Phys*. **2014**, 2, 4.

[25]. A. Bonardi, G. Pühlhofer, S. Hermanutz & A. Santangelo, A New Solution for Mirror Coating in γ-Ray Cherenkov Astronomy. *Exp. Astron*. **2014**, 38, 1-9.

[26]. O. Roth & J. A. LaVerne, Effect of pH on H_2O_2 Production in the Radiolysis of Water. *J. Phys. Chem. A* **2011**, 115, 700-708.

[27]. M. Bancirova, Sodium Azide as a Specific Quencher of Singlet Oxygen During Chemiluminescent Detection by Luminol and Cypridina Luciferin Analogues. *Luminescence* **2011**, 26, 685-688.

[28]. G. Fang, C. Liu, Y. Wang, D. D. Dionysiou & D. Zhou, Photogeneration of Reactive Oxygen Species from Biochar Suspension for Diethyl Phthalate Degradation. *Appl. Catal. B: Environ*. **2017**, 214, 34-45.

[29]. Bonnefont-Rousselot D, Gamma Radiolysis as A Tool to Study Lipoprotein Oxidation Mechanisms. *Biochimie*. **2004**, 86, 903-911.

[30]. H. Huang et al., Stable Black Phosphorus/Bi_2O_3 Heterostructures for Synergistic Cancer Radiotherapy. *Biomaterials* **2018**, 171, 12-22.

[31]. D. Duan et al., Activating TiO_2 Nanoparticles: Gallium-68 Serves as A High-Yield Photon Emitter for Cerenkov-Induced Photodynamic Therapy. *ACS Appl. Mater. Interfaces* **2018**, 10, 5278-5286.

[32]. D. Zhang et al., Tumor Microenvironment Activable Self-Assembled DNA Hybrids for pH and Redox Dual-Responsive Chemotherapy/PDT Treatment of Hepatocellular Carcinoma. *Adv. Sci*. **2017**, 4, 1600460.

[33]. M. E. Alea-Reyes et al., Amphiphilic Gemini Pyridinium-Mediated Incorporation of Zn(II)meso-Tetrakis(4-carboxyphenyl) Porphyrin into Water-Soluble Gold Nanoparticles for Photodynamic Therapy. *Colloids Surf. B Biointerfaces* **2017**, 158, 602-609.

Appendix

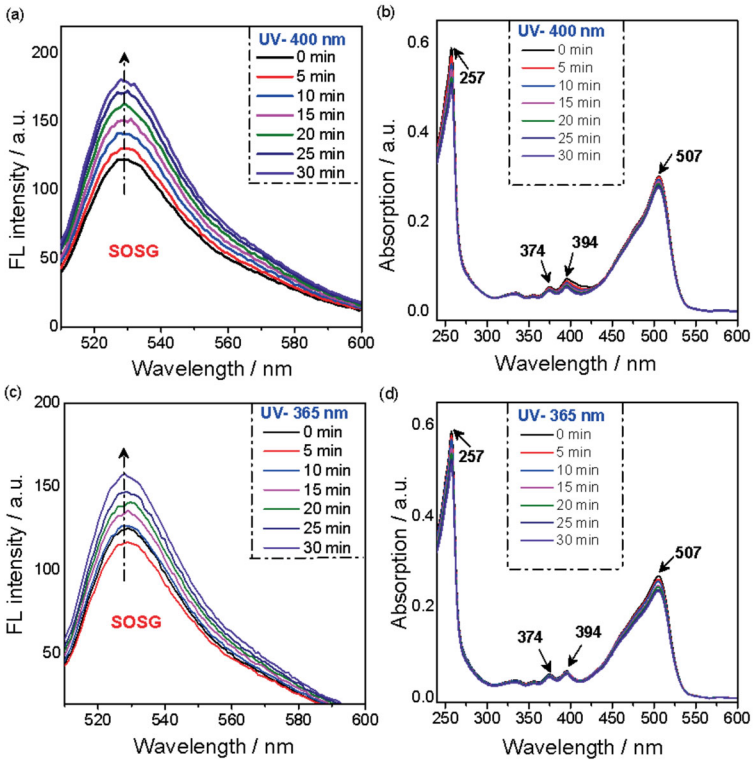

Figure S2.1. (a) Fluorescence spectra (λex= 504 nm) and (b) UV-vis spectra of SOSG solutions (5 μM) after irradiation with UV light at 400 nm; (c)Fluorescence spectra and (d) UV-vis spectra of SOSG solutions (5 μM) after irradiation with UV light at 365 nm.

The fluorescence emission in Figure S2.1(a,b) is predominantly due to the generation of singlet oxygen. In contrast to the UV-vis absorption spectra of SOSG irradiated by γ- and X-ray sources, the spectra of UV irradiated SOSG show noticeable decreasing absorption peaks (257, 365 nm and 400 nm). This effect is caused by endoperoxide (SOSG-EP) formation.[1] Meanwhile, the intensity of the 507 nm peak also shows a decreasing trend, which may be due to the photo bleaching of SOSG.

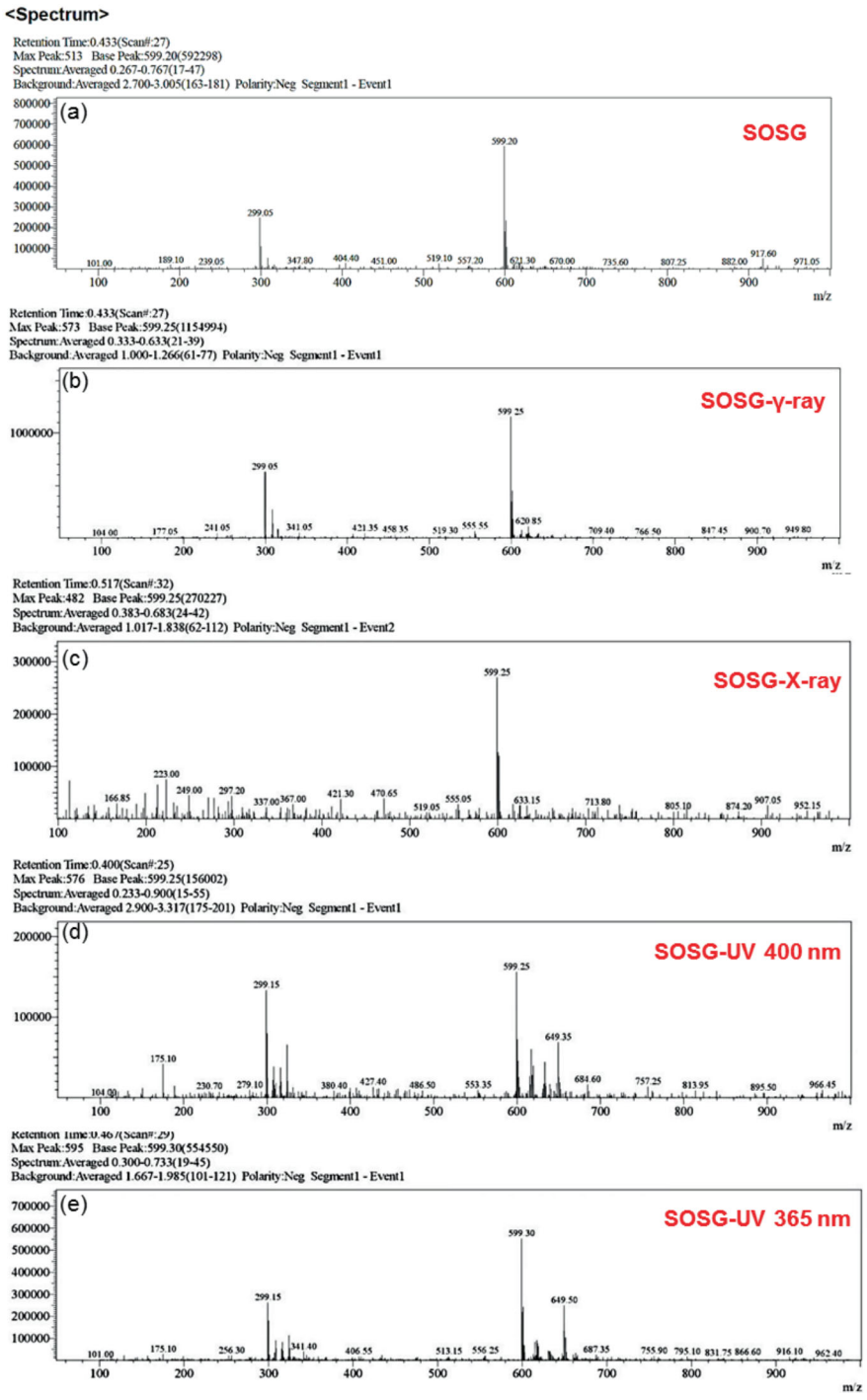

Figure S2.2. ESI Mass spectrum (negative mode) of (a) a SOSG solution; (b) a SOSG solution exposed to γ-ray radiation dose of 40 Gy; (c) a SOSG solution exposed to X-ray radiation dose of 20 Gy; (d) a SOSG solution exposed to 400 nm UV light for 50 min; (e) SOSG exposed to 365 nm UV light for 50 min. (concentration of the SOSG solution is 25 μM).

The mass spectra (ESI-MS) in Figure S2.2 show differences depending on the irradiation conditions. The spectra of SOSG solutions exposed to X- and γ-ray remain similar to that of the non-irradiated SOSG solution with a major peaks at m/z=599 and m/z=299, which correspond to the molecular structure of SOSG (mono-anion and di-anion respectively); spectra of SOSG exposed to UV sources (Figure S2.2(d,e)) exhibit a clear peak located at m/z=649, associated to the water adduct of SOSG-EP.[1]

Figure S2.3(a) shows the standard curve obtained through Ghormley's triiodide method, which achieves a linear relationship between UV intensity (350 nm) and H_2O_2 concentrations. Figure S2.3(b,c) show that the H_2O_2 concentration in aqueous solutions exposed to γ-ray radiation increases as function of radiation dose. According to the calibration line, the generation of H_2O_2 under 40 Gy is ~25.3 μM. Figure S2.3(d) demonstrates that the generation of H_2O_2 in pure water and in the SOSG solution is highly dependent on the radiation dose.

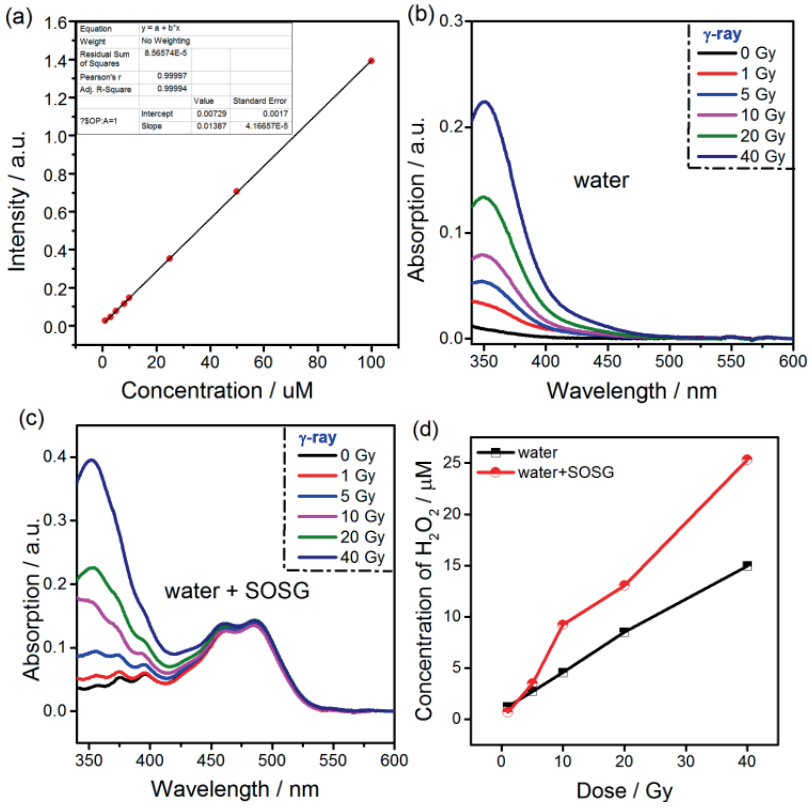

Figure S2.3. (a) Standard curve of H_2O_2 obtained through Ghormley's triiodide method; the UV spectrum for radiation exposed (b) water and (c) the SOSG solution (5 μM) by addition of KI and ADM solution; (d) The comparison of H_2O_2 generation in water and the SOSG solution (5 μM). (For detection of H_2O_2 concentration, the KI solutions and the ammonium molybdate stock solutions were added to water and the SOSG solutions used.)

APF (aminophenyl fluorescein) is a typical probe for the detection of hydroxyl radical. Figure S2.4 shows that even at a low dose, i.e., 1 Gy, ϒ-ray irradiation of aqueous solutions can induce the activation of this probe, indicating the generation of hydroxyl radicals.

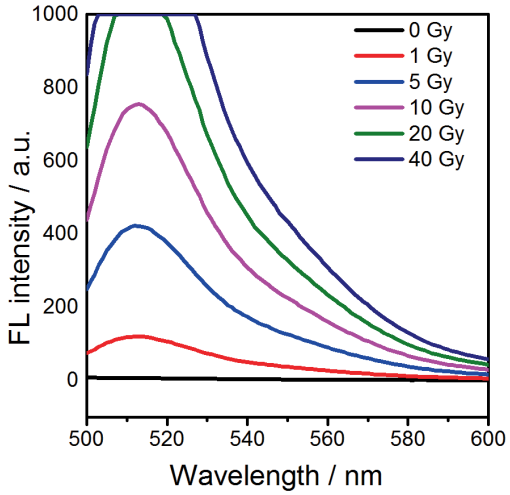

Figure S2.4. Fluorescence spectra (λ_{ex}= 480nm) of a 5μM APF aqueous solution as a function radiation dose delivered by ^{60}Co source.

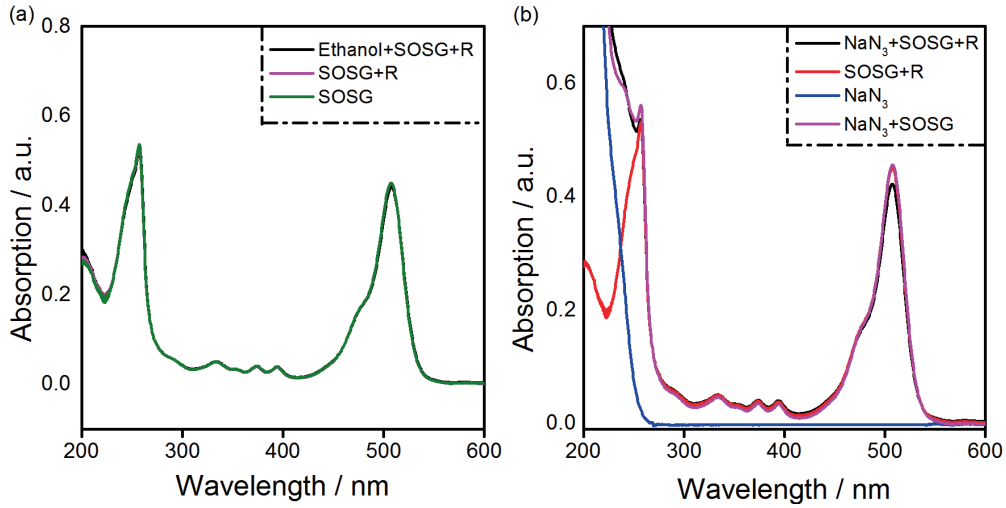

Figure S2.5. (a) UV-vis spectrum of SOSG solutions (5 μM) with the addition of ethanol(0.85 M) in the absence and presence of ionizing gamma radiation; (b) UV-vis spectrum of SOSG solutions with the addition of NaN_3 (1 mM)in the presence and absence of ionizing gamma radiation ('R' stands for a radiation exposure of 40 Gy from a ^{60}Co source.).

Figure S2.5 shows the UV-vis spectra of SOSG after irradiation experiments and the addition of various ROS scavengers. According to Figure S2.5(a), no structural changes were observed in SOSG molecules when exposed to 40 Gy of γ-ray radiation, in the presence or absence of EtOH. The introduction of NaN_3 also did not affect the structure of the SOSG molecule (Figure S2.5(b)). However, when exposed to radiation the mixture of NaN_3 and SOSG exhibited an evident decrease of the absorption at 507 nm which indicates a change of the fluorescein moiety, possibly due to reaction with $N_3^{\bullet}$ radicals.

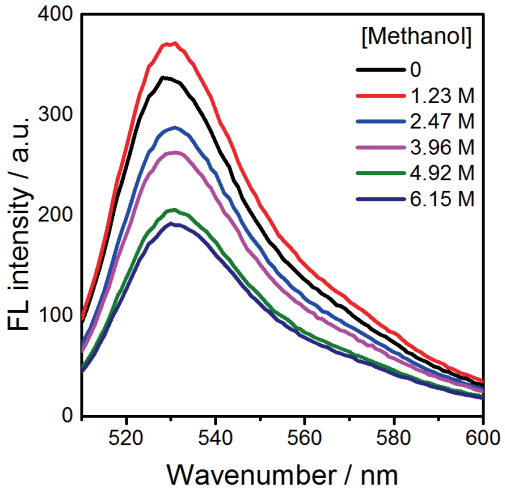

Figure S2.6. Fluorescence spectra (λ_{ex}= 504 nm) of SOSG solutions in the presence of different concentrations of methanol and when exposed to a radiation dose of 20 Gy delivered by a ^{60}Co source.

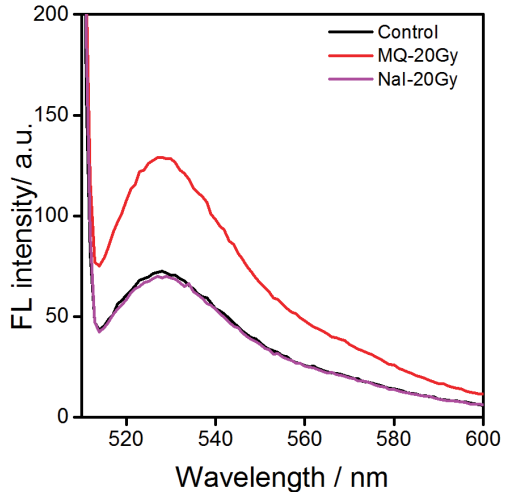

Figure S2.7. Fluorescence spectra (λ_{ex}= 504 nm) of SOSG solutions in the presence of NaI (50 mM) and when exposed to a radiation dose of 20 Gy delivered by a ^{60}Co source.

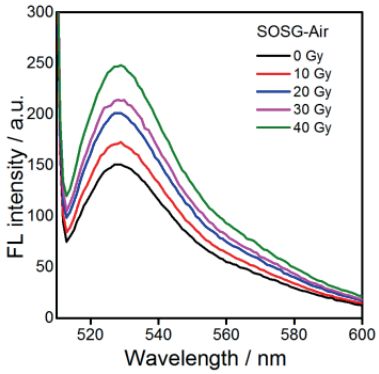

Figure S2.8. Fluorescence spectra (λ_{ex}= 504 nm) of SOSG solutions (5 μM) (e) saturated with N_2 for varied radiation doses delivered by a ^{60}Co source

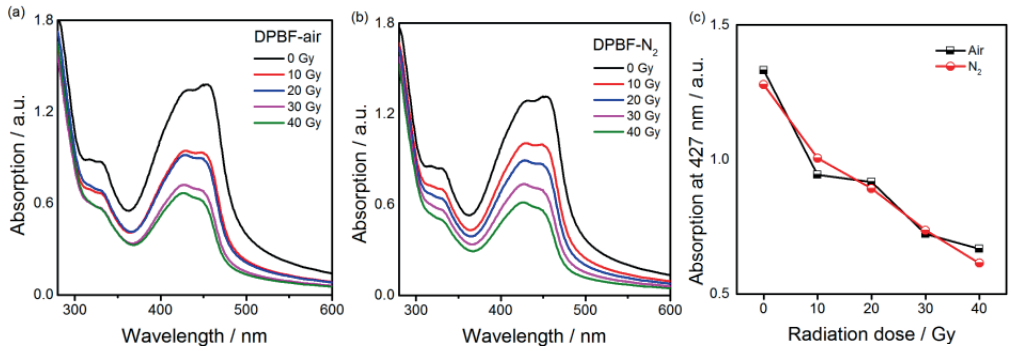

Figure S2.9. UV-vis spectra for DPBF solutions (100 μM) (a) saturated with air and (b) saturated with N_2 for varied radiation doses delivered by a ^{60}Co source; (c) The comparison of the intensity at 427nm between air-saturated SOSG solutions and N_2-saturated SOSG solutions after exposure to different gamma-ray doses.

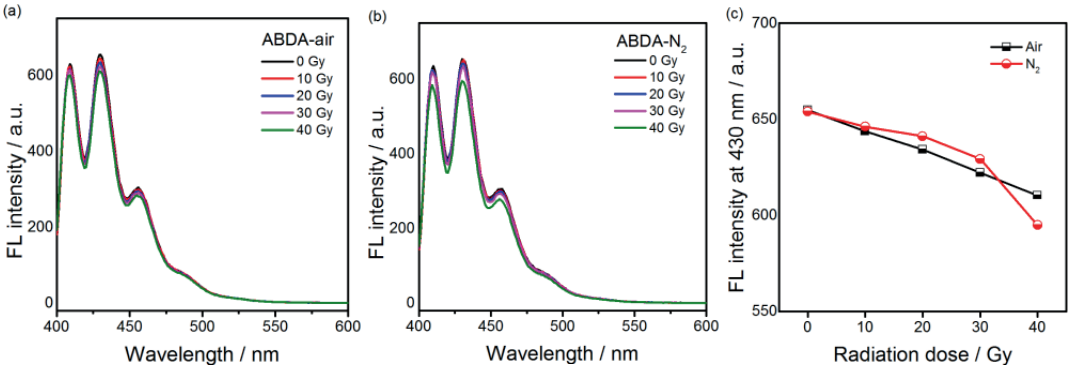

Figure S2.10. Fluorescence spectra (λ_{ex}= 380 nm) of ABDA solutions (50 μM) (a) saturated with air and (b) saturated with N_2 for varied radiation doses delivered by a ^{60}Co source; (c) The comparison for the FL intensity at 430 nm between air-saturated SOSG solutions and N_2-saturated SOSG solutions after exposure to different gamma-ray doses.

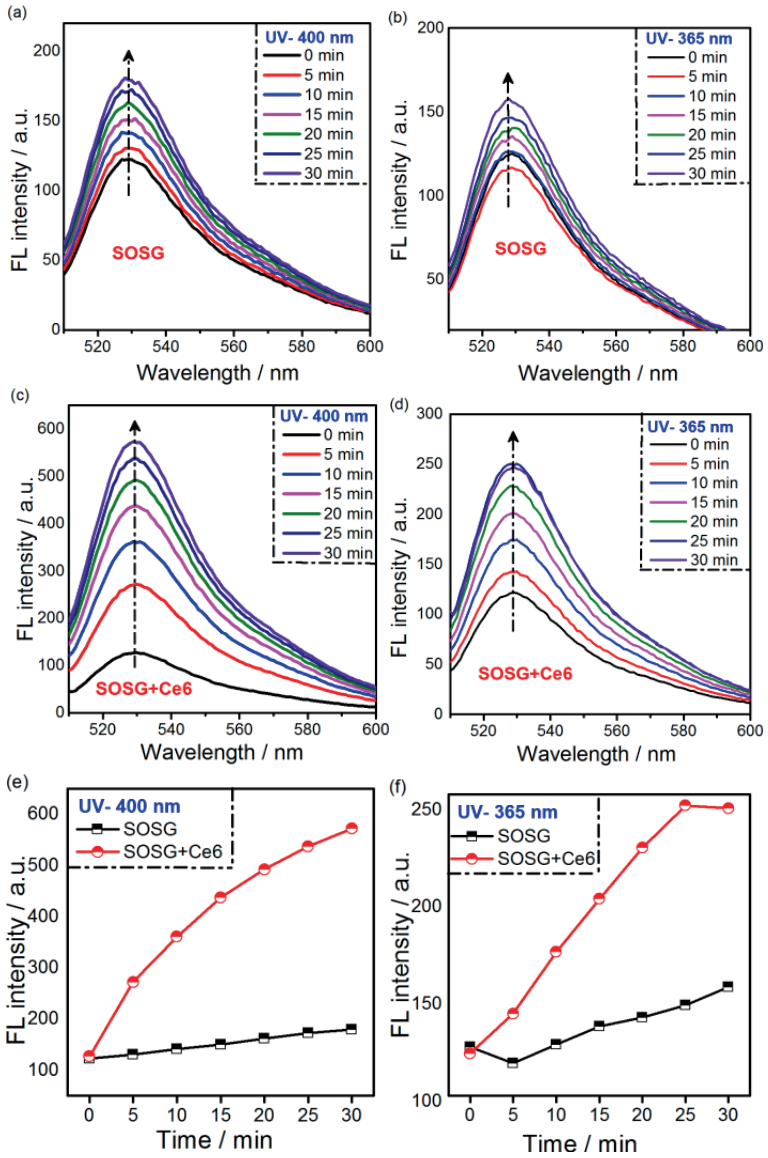

Figure S2.11. Fluorescence spectra (λ_{ex}= 504 nm) of SOSG solutions (5 μM) after irradiation with UV light at (a) 400 nm and (b) 365 nm; Fluorescence spectra of SOSG (5 μM)+Ce6 (5 μM) mixtures after irradiation with UV light at (c) 400 nm and (d) 365 nm; Comparison of the fluorescence intensity at ~530 nm between pure SOSG solutions (5 μM) and SOSG solutions (5 μM) containing Ce6 (5 μM) after irradiation with UV light at (e) 400 nm and (d) 365 nm.

Figure S2.11 show that both solutions, i.e. SOSG and SOSG+Ce6 have increased fluorescence intensity with increased UV irradiation time, which means that SOSG can act as a photosensitizer and produce singlet oxygen leading to increased fluorescence. The solution containing photosensitizer Ce6 renders much higher FL intensity than that for the pure SOSG system.

References

[1]. X. Ragas, A. Jimenez-Banzo, D. Sanchez-Garcia, X. Batllori & S. Nonell, Singlet Oxygen Photosensitisation by the Fluorescent Probe Singlet Oxygen Sensor Green®. *Chem. Commun*. **2009**, 2920-2922.

Ionizing radiation induced release from poly(ε-caprolactone-b-ethylene glycol) micelles

3

Adapted from: H.Liu, A.C. Laan, J. Plomp, S.R. Rarnell, Y. Men, R.M.Dalgliesh, R. Eelkema, A.G. Denkova; ACS Appl. Polym. Mater. 2021, 3, 2, 9

Abstract

Polymeric micelles, due to their easy preparation and versatile properties, have been widely applied as one of the most popular carriers for chemotherapeutic agents. Such micelles primarily prevent the leakage of drugs during transportation and thus protect healthy tissue. Controlled drug release, which releases the drugs at the site of interest using internal or external stimuli as triggers, can further improve the safety of the drug delivery process. In this paper we investigate whether ionizing radiation can be used to initiate release, focusing on using Cerenkov light as a possible trigger. For this purpose micelles composed of the degradable polymer poly(ε-caprolactone-b-ethylene glycol) (PCL-PEO) were first loaded with the photosensitizer chlorin e6 (Ce6) and subsequently exposed to gamma or X-ray radiation of varying radiation doses. The results reveal that Ce6 was released from the micelles under radiation regardless of the energy of incident photons, showing that Cerenkov light was not the driving force behind the observed release. SANS measurements showed that the volume fraction of the micelles containing Ce6 was reduced after exposure to radiation. This change in volume fraction suggests that the number of micelles was reduced which was probably responsible for the release of Ce6. The exact mechanism, however, remains unclear. Subsequently, the PCL-PEO micelles were loaded with Ce6 and one of the following drugs: doxorubicin (Dox), docetaxel (DTX) and paclitaxel (PTX). Under radiation exposure, Dox, which is quite stable in single-loaded micelles, shows an enhanced release profile in the presence of Ce6, while DTX and PTX remained in the micelles, regardless of the presence of Ce6.

Introduction

Cancer is one of the major causes of death in the developed world and new treatment strategies are continuously being pursued to increase the life expectancy of patients and to improve their life quality. In the case of metastasized tumours, chemotherapy is one of the most often-applied cancer treatments. Chemotherapy is indispensable in the clinic but it is still facing many challenges.[1] Two of the main problems of chemotherapy are: the hydrophobic nature of many anticancer drugs, such as paclitaxel and docetaxel, limits their solubility in blood and therefore their bioavailability; and the lack of targeting property that could lead to various adverse health effects.[2] Polymeric carriers have been proposed as a possible solution to both problems relying on the so-called EPR (enhanced permeability and retention) effect to limit toxicity to healthy tissue and to provide high loading capacity for hydrophobic substances.[3, 4] A few polymeric carriers have already been approved by the FDA for clinical application, among which poly (ε-caprolactone) containing vehicles are considered to be one of the best candidates due to their biodegradability.[5, 6] In addition to carriers for chemotherapeutic agents, micelles composed of this polymer have also been used in combined therapies such as photodynamic- and photothermal therapy.[7]

Toxicity to tissue can be further reduced if the delivery systems release the drugs primarily at the tumour site.[8] Various stimuli have been used to precisely discharge the active substances at the tumour, for example, pH, hypoxia and enzymes are commonly implemented as internal triggers [9-11] while heat and light are often applied as external stimuli.[12, 13] Light-responsive drug delivery systems have been widely studied due to the non-invasive nature of light,[14, 15] but suffer from the low penetration depth in tissue, which is limited to a few millimetres.[16]

In this respect ionizing radiation such as X-rays offers much better penetration possibilities and has been implemented as a trigger for release, although publications on this topic remain scarce. One example is the work of Deng et al. who has used liposomes and verteporfin to generate singlet oxygen under X-ray exposure, which in consequence destabilized the carriers and released their encapsulated cargo.[17] Other applications of ionizing radiation have been demonstrated by Xu's group who have developed a series of radiation-sensitive polymeric

carriers for controlled drug delivery.[18, 19] Apart from directly utilizing the energy of radiation, accompanying phenomena, such as the so-called Cerenkov light, can also work as an internal light stimulus but has so far not been implemented in drug release studies.[20, 21] Cerenkov light has a broad emission spectrum and it is emitted when charged particles pass through a medium with a speed greater than the speed of light in this medium.[22] Cerenkov light is typically observed when ionizing radiation interacts with water as well as tissues and has drawn increasing attention recently as an internal light source in photodynamic therapy.[20, 23]

Inspired by these studies we have designed PCL-PEO micellar systems containing a typical photosensitizer, i.e. Chlorin e6 (Ce6) and one of the following drugs: doxorubicin (Dox), paclitaxel (PTX) and docetaxel (DTX), which are commonly applied in chemotherapy. Initially we had intended to use Cerenkov light induced by radiation as an internal trigger to activate Chlorin e6 and destroy the micelles by simply exploiting the destructive character of reactive oxygen species (ROS) in particular singlet oxygen (as shown in Scheme 3.1). To investigate whether such a system can be used for triggered release we have performed a systematic study applying both X-rays and gamma rays (γ-ray), and varying the radiation dose. Drug release has been shown to occur but the mechanism behind these effects appears not to be related to Cerenkov light.

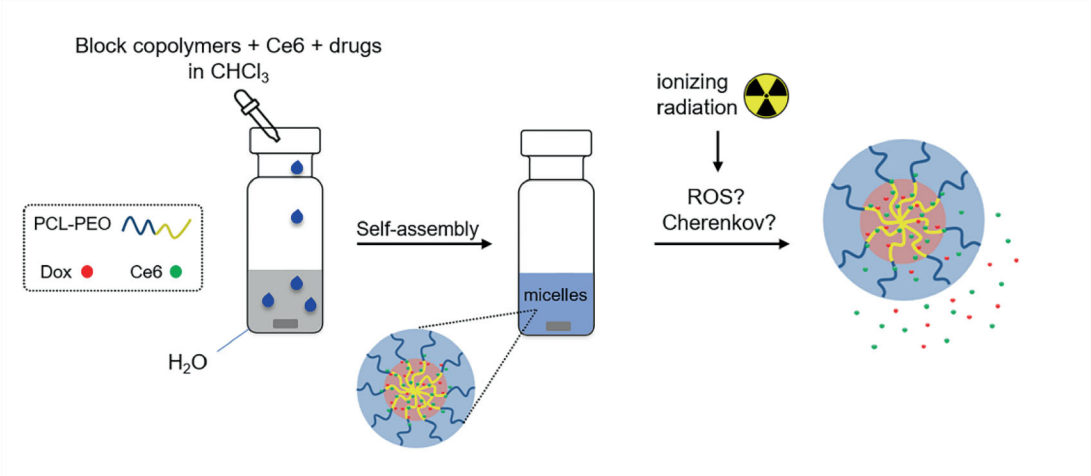

Scheme 3.1. The formation of Ce6&Dox-coloaded micelles and the drug release after being exposed to ionizing radiation.

Materials and methods

2.1 Materials

Poly (ε-caprolactone-b-ethylene glycol) block copolymer PCL-PEO (2800-2000) was purchased from Polymer source (Quebec, Canada). Chlorin e6 (Ce6) was bought from Frontier Scientific. Doxorubicin hydrochloride (Dox) was bought from VWR International BV. Docetaxel (DTX) was bought from Acros Organics. Chloroform, hydrogen peroxide (H_2O_2), triethylamine (TEA), paclitaxel (PTX) and sodium hypochlorite solution (NaClO) were bought from Sigma Aldrich (Zwijndrecht, the Netherlands). Ethanol (CH_3CH_2OH) was supplied by Brenntag (Zwijndrecht, the Netherlands). Iron (II) sulfate heptahydrate was purchased from Merck.

2.2 Synthesis

Preparation of micelles

The micelles were prepared according to our previous work.[24] Typically, 20 mg of block copolymer was dissolved in 0.2 mL of chloroform under sonication, followed by slowly dripping this solution into 2.3 mL of MQ water. The solution mixture was stirred overnight with the cap slightly open to evaporate the chloroform.

Preparation of Ce6-loaded micelles

Briefly, 20 mg of block copolymer was dissolved in 0.1 mL of chloroform, then 0.1 mL of 460 μM Ce6 solution (in chloroform) was added, the mixture was placed in an ultrasound water bath for several minutes and then slowly dripped into 2.3 mL of MQ water. The mixture was stirred overnight with the cap slightly open to evaporate the chloroform. Then the free Ce6 was removed by size exclusion chromatography (SEC, diameter 1 cm, length ~ 30 cm) filled with Sephadex G-25.

Preparation of Dox-loaded micelles

The 2 mg/mL Dox stock solution was obtained by dissolving 2 mg of Dox·HCl in 1 mL of chloroform, then 2 μL TEA was added to remove the HCl. The preparation process of Dox-loaded micelles was the same as that of the Ce6-loaded micelles described above.

Preparation of DTX-loaded micelles

The 10 mg/mL DTX stock solution was prepared by dissolving 5 mg of DTX in 0.5 mL of chloroform. The preparation process of DTX-loaded micelles was the same as the preparation of Ce6-loaded micelles.

Preparation of PTX-loaded micelles

The 5 mg/ mL PTX stock solution was prepared by dissolving 5 mg of PTX in 1 mL of chloroform. The PTX-loaded micelles were prepared in the same procedure as the Ce6-loaded micelles

Preparation of co-loaded micelles

The co-loaded micelles were prepared by dissolving 20 mg of PEO-PCL polymer in 0.1 mL of Ce6 stock solution and then adding 0.1 mL of the drug solution. After being fully mixed by sonication, the mixture was dripped into 2.3 mL of MQ water and stirred overnight to remove the organic solvent.

Characterization

3.1 Instruments

A dynamic light scattering apparatus was used to determine the hydrodynamic radius of the micelles. The dynamic light scatting instrument used in this study consisted of a JDS uniphase 633 nm 35 mW laser, an ALV sp 125 s/w 93 goniometer, a fibre detector and a Perkin Elmer photo counter. A UV-VIS-NIR spectrophotometer (UV-6300PC, VWR) was used to detect the absorbance spectra of Ce6 molecules. A Cary Eclipse fluorescence spectrophotometer (Agilent technologies) was also employed to characterize the fluorescence emission spectra of Dox-containing samples. A high-performance liquid chromatography (HPLC) was used to determine the loading efficiency of PTX and DTX. Cryogenic electron

microscope (Cyro-EM, Jeol JEM 1400) was used to determine the size and shape of the micelles. Differential scanning calorimetry (DSC) was carried out by TA instrument Q2000 with a temperature rate of 10 °C/min from -100 °C to 100 °C.

The samples for Small Angle Neutron Scattering (SANS) were prepared identically to all other samples but contained D_2O instead of H_2O to ensure sufficient contrast for the measurements. The SANS experiments were performed on the Larmor instrument at the ISIS pulsed neutron source in the UK. A 1 mm thick quartz cuvette containing the micelle solution in D_2O was used with a beam size of 8x6 mm. The temperature was maintained at 22 °C using a water bath. Larmor is a time of flight instrument with a fixed sample to detector distance of four meters which results in a momentum transfer (q) range of 0.003 - 0.7$Å^{-1}$. Data was reduced using the Mantid software.[25] These data were placed on an absolute scale (cm−1) using the scattering from a standard in accordance with established procedures.[26] The instrument produces an intensity plot radially integrated over constant q value to generate a typical SANS plot that reflects a density-density correlation function in reciprocal space. The data was fitted using the software SASView where we apply a core-shell-sphere model.[27,28]

3.2 Drug loading efficiency

The concentration of Ce6 was determined by measuring the light absorption intensity at 665 nm using a UV-VIS spectrophotometer. This wavelength was chosen rather than the 400 nm since it is not influenced by the light absorption spectra of the micelles. Due to the hydrophobic nature of Ce6, changes in the concentration of aqueous Ce6 solutions resulted in random shifts of the ~665 nm peak which could be clearly observed in the spectra. In contrast, when incorporated in micelles, the Ce6 665 nm peak is stable with only a 1-2 nm shift, which is hard to tell from the spectra. Regarding the difficulties in making a proper calibration line of Ce6 by UV-vis, we directly use the UV-vis intensity to represent the Ce6 concentration. The concentration of Dox was determined by the FL emission intensity at 590 nm which was excited at 488 nm wavelength. In the FL measurement, the slits for excitation and emission light are 10 nm. The loading efficiency of PTX and DTX was determined by

HPLC coupled to UV detector set at 227 nm. The mobile phase was a mixture of acetonitrile and aqueous formic acid solution (10 mM) having volume ratio of 45:55 respectively.
The loading efficiency (%) was calculated by the following equations:

LE(%) of Ce6 = (The absorbed light intensity (665nm)of final samples)/(The absorbed light intensity (665 nm) of samples before separation)×100%

LE(%) of drugs (Dox, DTX, PTX) = (The concentration of drugs in final samples)/(The initial drug concentration)×100%

3.3 Irradiation experiments

Gamma radiation: A Cobalt 60 (^{60}Co) radioactive source (GC220, Nordion) was used for the gamma irradiation. Samples were transferred to 4 mL glass vials which were covered with aluminum foil. These samples were placed inside the ^{60}Co source and irradiated for different periods resulting in doses ranging from 10 to 50 Gy.

In the case of the SANS experiments, irradiations were performed using a ^{137}Cs source, which emits gamma-rays with energy of 0.662 MeV, at Gray Laboratories, Department of Oncology, Cancer Research UK and Medical Research Council Oxford Institute for Radiation Oncology. Samples were transferred to 4 mL glass vials, which were covered with aluminum foil. These samples were placed inside the ^{137}Cs source and irradiated for different periods resulting in doses ranging from 10 to 50 Gy. The SANS measurements were performed 1.5 hours after irradiation.

X-ray radiation: The X-ray irradiation was carried out using an X-ray source (Philips MCN 321 variable-energy X-ray tube). The samples were placed on a horizontal platform located 50 cm from the X-ray window. The voltage for X-ray is 240 kV, and the current is 3 mA, achieving a dose rate of 0.64 Gy/min.

3.4 Reactions involving ROS

Different reactive oxygen species were prepared as described in a previous publication.[29] H_2O_2 was obtained by diluting a commercial H_2O_2 solution to a final concentration of 800 μM. $OH\cdot$ radicals were obtained by mixing H_2O_2 solution (800 μM) and Fe^{2+} aqueous solution (8000 μM) for half an hour. $^1O_2$ was obtained by mixing H_2O_2 solution (800 μM) and ClO^- aqueous solution (8000 μM). For determining the ROS effects on Ce6 release, 0.5 mL of Ce6-micelles samples was mixed with 0.5 mL of the above ROS solutions and reacted for half an hour.

3.5 Detection of Ce6 or drug release

The obtained irradiated samples were separated within 20 min by Amicon® Ultra-4 centrifugal filter (4000 rpm, 20 min) to remove the released photosensitizer and/or drugs. The non-irradiated control samples were treated in exactly the same way. Then UV-Vis, FL or HPLC were used to detect the substances remaining in the micelles as described above. For evaluating the retention ratio, the drugs or Ce6 amount in the non-irradiated samples after separation was regarded as the reference (i.e. 100%).

Results and Discussion

4.1 Ce6-loaded PCL-PEO micelles

The incorporation of Ce6 into the PCL-PEO (2800-2000) micelles was carried out during the self-assembly process and high loading efficiency was achieved (69.3 ± 10.6 %). The morphology of the Ce6 loaded micelles was determined by DLS and Cryo-EM. Figure 3.1(a) shows the obtained DLS data which reveals that most of the micelles have a hydrodynamic radius of ~16 nm. Two other peaks corresponding to larger sizes suggest that there are also larger species present. The Cryo-EM image (Figure 3.1(b)) shows that the Ce6 loaded micelles are primarily spherical and small but a few worm-like micelles are also visible. The peaks observed in the DLS data at larger diameters possibly correspond to these worm-like

micelles. The morphology of the empty micelles (Figure S3.1) and the ones loaded with Ce6 appear to be the same.

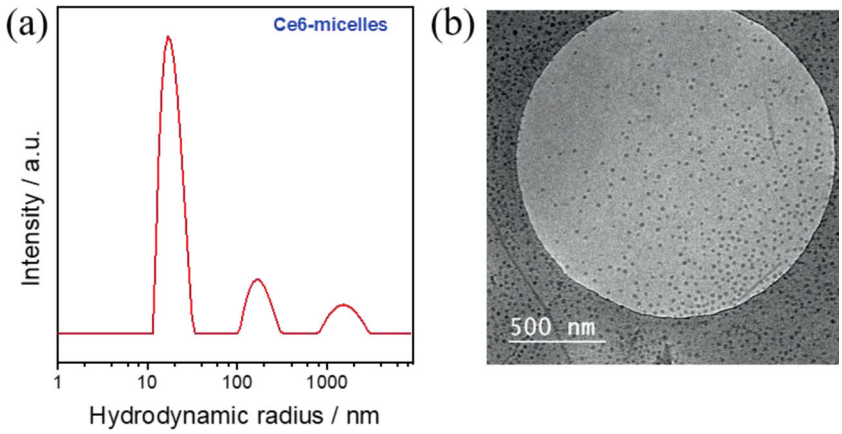

Figure 3.1. (a) The hydrodynamic radius of PCL-PEO micelles loaded with Ce6 as determined by DLS. (The polymer concentration was 0.14 mg/mL); (b) Cryo-EM images of the same micelles. The polymer concentration was 2.9 mg/mL and the initial Ce6 concentration was 20 μM)

To determine whether Cerenkov light can lead to release, we exposed the Ce6-loaded micelles to γ-rays (above the Cerenkov light energy threshold) and X-rays (below the Cerenkov light energy threshold) at different radiation doses. The release data shown in Figure 3.2 is obtained within 20 min after irradiation and indicates that the released amount goes up as the radiation dose increases. γ-rays lead to slightly higher release (48.5±3.5 % at 50 Gy) than X-rays (39.3±2.0 % at 50 Gy). Exposure of Ce6 stock solution (10 μM) to γ-radiation resulted in negligible change in the UV signals at 665 nm of the Ce6 molecules (Figure S3.2), revealing that Ce6 itself is not affected by the radiation exposure under these experimental conditions. Based on the DLS and SANS data (Figure S3.3-4), the morphology including size and shape of the empty PCL-PEO micelles also did not change when exposed to ionizing radiation. Moreover, according to the DSC result, the thermal properties of the irradiated micelles also show no difference when compared with the original sample (Figure S3.5).

The ^{60}Co source delivers γ-rays of two main energies (1.17 and 1.33 MeV) while the X-ray source that was used supplied X-rays with the maximum energy of 240 keV. The interaction mechanism of ionizing photons depends on their energy as well as on the Z number of the materials with which they interact. In this case, the Compton effect occurs in which photons

give part of their energy to an electron, a so-called Compton electron. The energy threshold for electrons to produce Cerenkov light is 261 keV in water,[22] which is above the value that the Compton electrons reach for the used X-ray energy. The γ-rays do have sufficient energy to create Compton electrons with energies above 261 keV and Cerenkov light is expected to be produced.

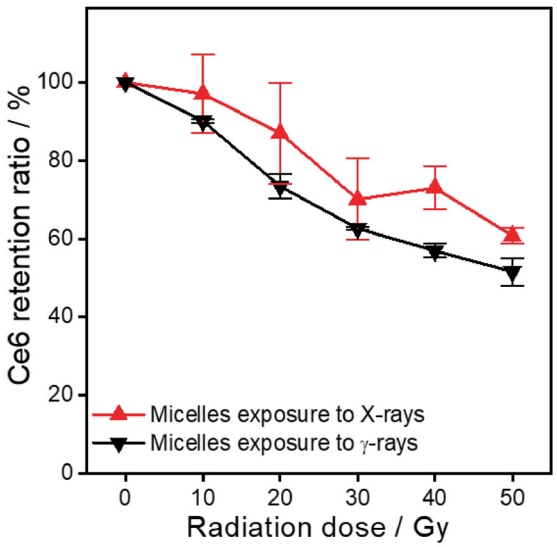

Figure 3.2. The Ce6 retention ratio in the micelles as a function of radiation dose for Ce6-loaded PCL-PEO micelles when exposed to γ-rays delivered by ^{60}Co source and X-rays of 240 kVp energy.

The fact that release is also observed when using X-rays reveals that release is caused by ionizing radiation rather than Cerenkov light. To determine whether the release might be associated to change of the self-assemblies we first investigated the morphology of the irradiated Ce6 loaded micelles by DLS and Cryo-EM.

According to the results discussed above, these radiation doses are not sufficient to lead to the destruction of PEO-PCL polymer which is in accordance with literature on similar systems where much higher doses (in the kGy range) have been shown to result in polymer damage.[30] Additionally, empty micelles exposed to radiation of 50 Gy have identical SANS patterns as well as intensity as the non-exposed ones (Figure S3.4). However, the SANS data in Figure 3.4 does show that the volume fraction of micelles containing Ce6 was

reduced after exposure to ionizing radiation, while the morphology of the micelles remained the same. The supporting information contains more details on the SANS fitting parameters.

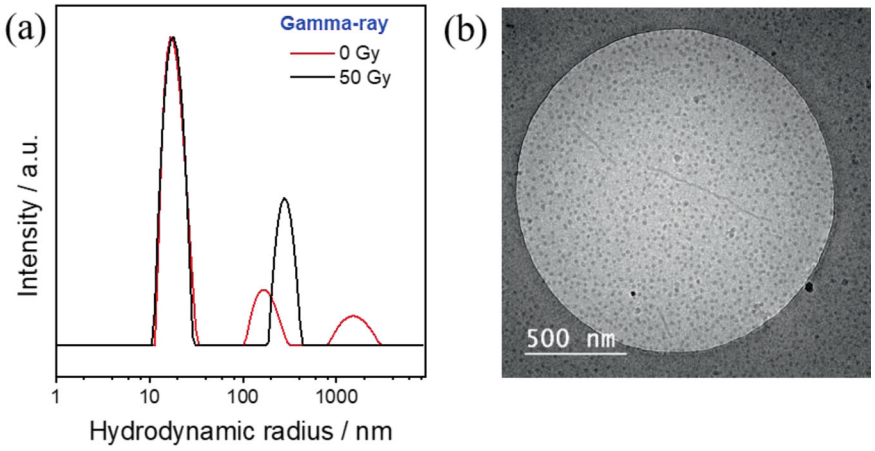

Figure 3.3. (a) The hydrodynamic radius obtained by DLS of Ce6 loaded PCL-PEO micelles before and after exposure to 50 Gy gamma-rays (b) Cryo-EM images of Ce6-loaded PCL-PEO micelles after exposure to 50 Gy delivered by gamma rays. The polymer concentrations were 0.14 and 2.9 mg/mL for DLS and Cryo-EM, respectively.

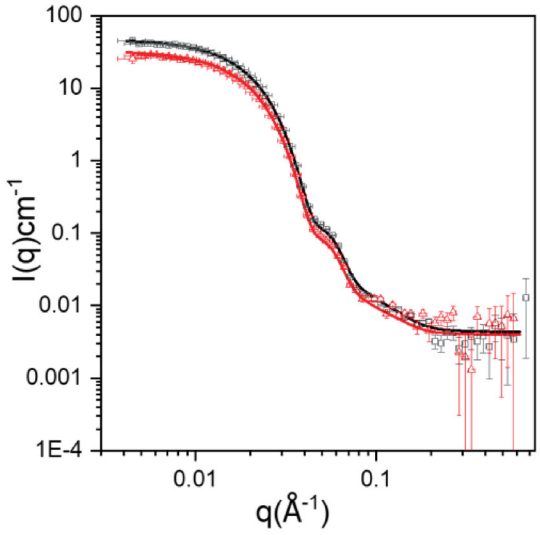

Figure 3.4. Figure Capture SANS curves obtained for micelles containing Ce6. Black square: Ce6-micelles; black line: the fitting curve for Ce6-micelles using a core shell model; red triangle: irradiated-Ce6-micelles, measured 1.5 hours after being irradiated by 50 Gy gamma-rays; red line: fitting curve using a core shell model of the irradiated Ce6-micelles.

Ionizing radiation can interact with matter directly, or indirectly through various radicals created by the radiolysis of water. Gamma rays have much less of a chance to directly damage

Ce6, since Ce6 is composed of light elements with low stopping power, which suggests that indirect effects may dominate the Ce6 release from micelles. To check this assumption we irradiated the micelles in a HEPES buffer which is a well-known radical scavenger.[31, 32] Figure 3.5 (a) shows that no Ce6 was released in HEPES while 48.6±3.2 % was released in water when the micelles were exposed to the same dose of radiation, i.e. 50 Gy, showing that radicals play the main role in the Ce6 release from the micelles.

The radiolysis of water is a complex phenomenon, which results in various radicals and chemical species among which OH radicals and hydrated electrons (e_{aq}^-) being some of the most reactive, and H_2O_2 is one of the most abundant and persistent. In order to determine whether OH radicals and H_2O_2 can play a role in the release, we exposed the micelles to these species obtained in a chemical way. The H_2O_2 solution was prepared by diluting commercial H_2O_2 solutions, to a concentration of 400 μM which is much higher than that generated under radiation treatment in our experiments.[33] The OH radicals were generated through a typical Fenton-reaction between H_2O_2 and Fe^{2+} ions.[34] As shown in Figure 3.5(b), the presence of H_2O_2 or OH radicals exhibited negligible influence onnik the release of Ce6. Although there are only very few reports on the presence of singlet oxygen purely due to the radiolysis of water,[35] we tried to eliminate singlet oxygen effects by using Argon-saturated samples, which decreased the possibility of $^1O_2$ generation. As shown in Figure 3.5(c), the micelles dispersed in Argon-saturated aqueous solution showed a similar release behavior compared to those in air-saturated water, i.e. around 65% of Ce6 was released from the micelles, indicating the $^1O_2$ was not the main cause for Ce6 release.

Besides the above-mentioned reactive oxygen species, hydrated electrons are another main product of the radiolysis of water. To evaluate the influence of hydrated electrons, we studied the release profiles of Ce6-loaded micelles in aqueous solution containing NO_3^- (20 mM), which is a typical scavenger of e_{aq}^-. Under these conditions, only 40.8 ± 6.3 % of Ce6 leaked out from the micelles after being exposed to 50 Gy gamma-rays, which is significantly less than that for samples dispersed in MQ water with 64.7 ± 0.8 % of the Ce6 being released. Note that the percentage of release differs somewhat per micelle batch hence the data shown in one single figure using the same batch of Ce6 loaded micelles.

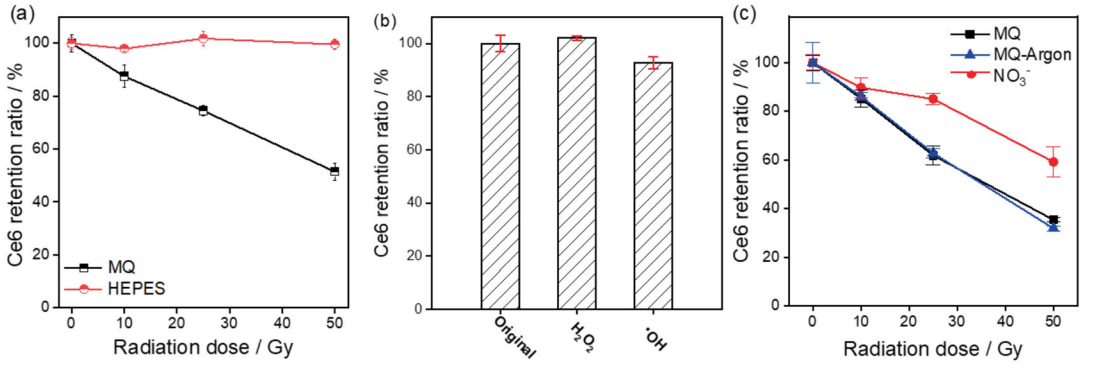

Figure 3.5. Release profiles of Ce6 from PCL-PEO micelles (a) in MQ and HEPES solution (1 mM) after gamma-ray exposure, (b) after reaction with H_2O_2 and OH for half an hour, (c) in argon saturated aqueous solution and NO_3^- aqueous solution (20 mM) after gamma exposure. Error bars represent the experimental uncertainties of at least 3 samples.

In previous experiments we observed that Ce6 could also be loaded into pre-formed micelles over a 24 hours period, which means the Ce6 can actively enter the micelles. Hence, after the radiation exposure, we immediately separated the released Ce6 molecules to avoid the re-loading process. In the experiments shown in Figure 3.2 and 3.5, the separation process has been managed within 20 mins (sample transportation) after radiation exposure. To check whether ionizing radiation can induce a sustained release of Ce6 from the micelles, we exposed such samples to gamma-rays of increasing radiation dose and separated the free Ce6 molecules after certain time intervals. Figure 3.6 shows that the immediate release after irradiation increases with the radiation dose, which is in agreement with the results in Figure 3.2. Moreover, the Ce6 retention in the samples remains relatively stable, although it is slightly increased after 2 days compared that at 0h. The residual Ce6 in irradiated samples is evidently less than that for non-irradiated samples, suggesting that the released Ce6 molecules are not likely to totally return to micelles under experimental conditions. Thus, irradiation gives a long-term change in the Ce6-micelle interaction.

We also carried out control experiments in which we separately irradiated either Ce6 or empty micelles and carried out again the synthesis process which showed that encapsulation efficiencies were nearly the same (Figure S3.7). Clearly, the release must be due to a change in interaction between Ce6 and the polymeric micelles occurring during irradiation. The exact mechanism however, remains unknown.

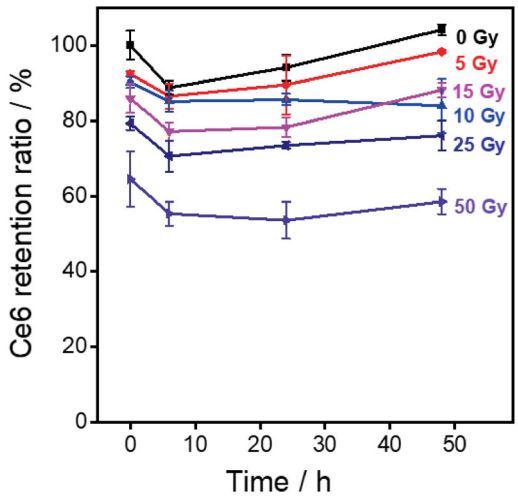

Figure 3.6. The retention of Ce6 in PCL-2800 micelles as function of time after exposure to γ-rays at different radiation doses. The polymer concentration was 2.9 mg/mL. The Ce6 retention ratio for samples at 0h was calculated using the light absorption intensity at 660 nm of the immediately separated samples after irradiation, and the average light absorption intensity of the non-irradiated samples was used as the reference for all samples

4.2 Drug-loaded PCL-PEO micelles

Although the mechanism of Ce6 release is not yet clear, we were interested in finding out whether such radiation-induced release was also observed for drugs with or without the presence of Ce6. For this purpose, we loaded the same micelles with different anticancer agents, i.e., Dox, PTX and DTX. The loading efficiencies of the drugs with or without the presence of Ce6 are summarised in Table 3.1, revealing that the more hydrophobic the drug is the higher loading efficiency (LE) it would achieve: i.e. the LE is 23.5 ± 3.5% for Dox, while it is 80.0 ± 14.2% and 95.8 ± 4.5% for DTX and PTX. Even though the efficiency differed in all cases, the morphology of the micelles appeared not to be affected for all samples (Figure S3.8). Interestingly, the LE(%) of Ce6 in these co-loaded samples shows quite different behavior. The LE of Ce6 significantly decreased to 33.8 ± 6.6% in the presence of Dox, while that for Ce6&DTX-micelles and Ce6&PTX-micelles was 57.6 ± 3.2% and 62.4 ± 8.1%. When compared to loading of Ce6 alone (69.3 ± 10.6%), the presence of PTX and DTX appeared not to be competing with Ce6 while Dox did.

Table 3.1. Summary of the loading efficiency of therapeutic drugs and Ce6 in micelles.

Sample	Drug loading/%	Ce6 loading/%
Dox-micelles	23.5±3.5*	--
Ce6&Dox-micelles	18.9±2.5	33.8±6.6
DTX-micelles	80.0±14.2	--
Ce6&DTX-micelles	61.7±9.3	57.6±3.2
PTX-micelles	95.8±4.5	--
Ce6&PTX-micelles	78.1±4.5	62.4±8.1
Ce6- micelles	--	69.3±10.6

* The error indicates standard deviation based on 3 measured samples.

Subsequently we exposed the Ce6&drug co-loaded and the Ce6 or drug single-loaded micelles to gamma radiation of different doses. The data summarized in Figure 3.7 (a,b,c) illustrates that there were more Ce6 molecules released from the co-loaded samples than in the case of the single Ce6-loaded micelles, which means the presence of the drugs somehow influences the interaction between Ce6 and the polymeric micelles. However, the release of drugs showed quite different behavior. The micelles only loaded with Dox, PTX and DTX had no evident drug release even when exposed to 50 Gy. In the case of the co-loaded micelles only Dox showed a significant release.

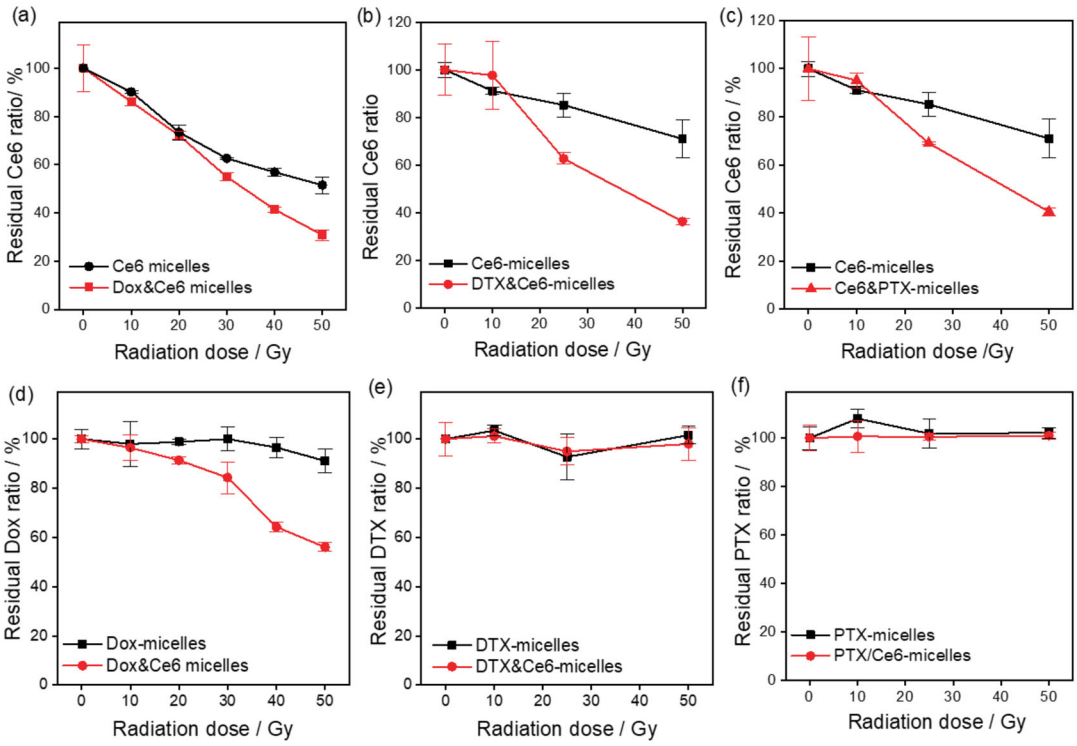

Figure 3.7. First row: the Ce6 retention of Ce6-micelles and co-loaded micelles with Ce6 and (a) Dox (b) DTX and (c) PTX; Second row: the release of the different drugs for single drug-loaded micelles and micelles co-loaded with Ce6 and (d) Dox, (e) DTX and (f) PTX under various γ-ray doses delivered by 60Co source.

To better understand the interaction between micelles and drugs, we freeze-dried all the samples and used differential scanning calorimetry (DSC) to detect changes in thermal behavior of the PCL-PEO micelles as result of the presence of drugs and Ce6. As shown in Table 3.2, the presence of Dox and Ce6 slightly decreases the melting temperature of PCL from 43.0 °C to 42.3 °C and 41.2 °C, while DTX and PTX increase the melting temperature of PCL to 44.6 °C and 45.8 °C respectively. In contrast, all drugs had a negligible influence on the melting behavior of the PEO. In terms of the crystallization temperature, the presence of the drugs had a larger influence on the PEO block and the crystallization temperature increased to 28.3 °C (Ce6), 29.6 °C (Dox), 37.8°C (DTX) and 37.6 °C (PTX) which was substantially higher than that of the empty micelles (26.0 °C). These results indicate that drugs stimulate the nucleation of PEO segments at higher temperature.[36]

The released energy during the crystallization process was calculated based on the DSC curve in Figure S3.10. As summarized in Table 3.2, the PCL and PEO segments for empty PCL-PEO micelles showed energy release of 67.7 and 119.5 J/g during the crystallization, which increased due to the addition of Dox and Ce6, while decreased due to the addition of DTX and PTX. However, Ce6 showed a smaller influence on the energy released during crystallization than the others, indicating less interaction between the Ce6 molecules and the micelles, which might be an explanation for the release of Ce6 under ionizing radiation. Moreover, the evident drop in loading efficiency of Ce6 in the presence of Dox implies that they are somehow synergistically working leading to a release of Dox along with Ce6.

Table 3.2. Summary of melting temperature, crystallization temperature and heat of fusion of the samples containing Ce6, Dox, PTX and DTX

Sample	T_m(PCL) °C	T_m(PEO) °C	T_c(PCL) °C	T_c(PEO) °C	$\triangle H_{f,s}$(PCL) $J.g^{-1}$	$\triangle H_{f,s}$(PEO) $J.g^{-1}$
PCL-PEO	43.0	52.1	19.5	26.0	67.7	119.5
Dox-micelles	42.3	52.1	19.8	28.3	93.6	144.1
Ce6-micelles	41.2	52.1	18.7	29.6	75.7	123.6
DTX-micelles	44.6	51.7	19.6	37.8	52.0	87.9
PTX-micelles	45.8	51.7	21.6	37.6	53.2	88.8

Conclusions

In this study we prepared block copolymer micelles that were loaded with Ce6 or co-loaded with Ce6 and drugs, and evaluated their radiation-induced release behavior. PCL-PEO micelles with a hydrodynamic radius of ~16 nm exhibited excellent encapsulation ability of Ce6 as well as DTX, PTX and Dox without any effect on the morphology of the micelles. Once exposed to ionizing radiation these micelles exhibited release of Ce6 as a function of dose by both gamma-rays and X-rays, which is possibly partly due to the interaction with hydrated electrons generated by water radiolysis. There was no significant difference in release after interacting with ionizing photons above and below the Cerenkov light threshold indicates that Cerenkov light was not part of the mechanism for the observed phenomenon. Moreover, the radiation used in these experimental conditions did not damage the Ce6 or the micelles, but rather induced a long-term change in the interaction between the Ce6 and micelles.

Micelles single-loaded with drugs, i.e. Dox, PTX and DTX, did not show drug release in the presence of radiation. In contrast, Dox exhibited an enhanced release profile upon exposure to radiation in the presence of Ce6, while PTX and DTX remained in the micelles. The DSC data revealed that the addition of Ce6 showed a small influence on the crystallization of PCL and PEO segment of the micelles, indicating a relatively loose interaction between Ce6 and PCL-PEO micelles. The radiation-induced release of Ce6 could be used to further trigger the release of other anticancer substances, i.e. Dox, which could be applied for controlled release using radiation as an external stimulus.

However, the full mechanism for radiation-induced drug release from PCL-PEO micelles remains unclear and requires further exploration. Currently, the radiation induced-release of Dox is only significant under high dose, i.e. 50 Gy, which could be utilized in some radiotherapy treatments, but more efforts are required to increase the radiation-sensitivity of the Ce6-drug micelles system for the clinical applications.

References

[1] Fan, W.; Tang, W.; Lau, J.; Shen, Z.; Xie, J.; Shi, J.; Chen, X., Breaking the Depth Dependence by Nanotechnology-Enhanced X-Ray-Excited Deep Cancer Theranostics. *Adv. Mater.* **2019**, 31 (12), e1806381.

[2] Perez-Herrero, E.; Fernandez-Medarde, A., Advanced targeted Therapies in Cancer: Drug Nanocarriers, the Future of Chemotherapy. *Eur. J. Pharm. Biopharm.* **2015**, 93, 52-79.

[3] Wei, G.; Wang, Y.; Huang, X.; Yang, G.; Zhao, J.; Zhou, S., Enhancing the Accumulation of Polymer Micelles by Selectively Dilating Tumor Blood Vessels with NO for Highly Effective Cancer Treatment. *Adv. Healthc. Mater.* **2018**, 7 (24), e1801094.

[4] Li, N.; Zhao, L.; Qi, L.; Li, Z.; Luan, Y., Polymer Assembly: Promising Carriers as co-delivery Systems for Cancer Therapy. *Prog. Polym. Sci.* **2016**, 58, 1-26.

[5] Bobo, D.; Robinson, K. J.; Islam, J.; Thurecht, K. J.; Corrie, S. R., Nanoparticle-Based Medicines: A Review of FDA-Approved Materials and Clinical Trials to Date. *Pharm. Res.* **2016**, 33 (10), 2373-87.

[6] Danafar, H.; Davaran, S.; Rostamizadeh, K.; Valizadeh, H.; Hamidi, M., Biodegradable m-PEG/PCL Core-Shell Micelles: Preparation and Characterization as a Sustained Release Formulation for Curcumin. *Adv. Pharm. Bull.* **2014**, 4 (Suppl 2), 501-10.

[7] Ren, S.; Cheng, X.; Chen, M.; Liu, C.; Zhao, P.; Huang, W.; He, J.; Zhou, Z.; Miao, L., Hypotoxic and Rapidly Metabolic PEG-PCL-C3-ICG Nanoparticles for Fluorescence-Guided Photothermal/Photodynamic Therapy against OSCC. *ACS Appl. Mater. Interfaces* **2017**, 9 (37), 31509-31518.

[8] Liu, J.; Yang, G.; Zhu, W.; Dong, Z.; Yang, Y.; Chao, Y.; Liu, Z., Light-Controlled Drug Release from Singlet-Oxygen Sensitive Nanoscale Coordination Polymers enabling Cancer Combination Therapy. *Biomaterials* **2017**, 146, 40-48.

[9] Wibowo, F. R.; Saputra, O. A.; Lestari, W. W.; Koketsu, M.; Mukti, R. R.; Martien, R., pH-Triggered Drug Release Controlled by Poly(Styrene Sulfonate) Growth Hollow Mesoporous Silica Nanoparticles. *ACS Omega* **2020**, 5 (8), 4261-4269.

[10] Kulkarni, P.; Haldar, M. K.; You, S.; Choi, Y.; Mallik, S., Hypoxia-Responsive Polymersomes for Drug Delivery to Hypoxic Pancreatic Cancer Cells. *Biomacromolecules* **2016**, 17 (8), 2507-13.

[11] Cao, Z.; Li, W.; Liu, R.; Li, X.; Li, H.; Liu, L.; Chen, Y.; Lv, C.; Liu, Y., pH- and Enzyme-Triggered Drug Release as an Important Process in the Design of Anti-Tumor Drug Delivery Systems. *Biomed. Pharmacother.* **2019**, 118, 109340.

[12] Jiang, K.; Zhang, L.; Hu, Q.; Zhang, Q.; Lin, W.; Cui, Y.; Yang, Y.; Qian, G., Thermal Stimuli-Triggered Drug Release from a Biocompatible Porous Metal-Organic Framework. *Chemistry* **2017**, 23 (42), 10215-10221.

[13] Jiang, S.; Wang, K.; Dai, Y.; Zhang, X.; Xia, F., Near‐Infrared Light‐Triggered Dual Drug Release Using Gold Nanorod‐Embedded Thermosensitive Nanogel‐Crosslinked Hydrogels. *Macromol. Mater. Eng*. **2019**, 304 (7), 1900087.

[14] Kim, K.; Lee, C. S.; Na, K., Light-Controlled Reactive Oxygen Species (ROS)-Producible Polymeric Micelles with Simultaneous Drug-Release Triggering and Endo/Lysosomal Escape. *Chem. Commun.* **2016**, 52 (13), 2839-42.

[15] Saravanakumar, G.; Lee, J.; Kim, J.; Kim, W. J., Visible Light-Induced Singlet Oxygen-Mediated Intracellular Disassembly of Polymeric Micelles Co-Loaded with a Photosensitizer and an Anticancer Drug for Enhanced Photodynamic Therapy. *Chem. Commun.* **2015**, 51 (49), 9995-8.

[16] Ash, C.; Dubec, M.; Donne, K.; Bashford, T., Effect of Wavelength and Beam Width on Penetration in Light-Tissue Interaction using Computational Methods. *Lasers Med. Sci*. **2017**, 32 (8), 1909-1918.

[17] Deng, W.; Chen, W.; Clement, S.; Guller, A.; Zhao, Z.; Engel, A.; Goldys, E. M., Controlled Gene and Drug Release from a Liposomal Delivery Platform Triggered by X-ray Radiation. *Nat. Commun.* **2018**, 9 (1), 2713.

[18] Ma, N.; Xu, H.; An, L.; Li, J.; Sun, Z.; Zhang, X., Radiation-Sensitive Diselenide Block Co-Polymer Micellar Aggregates: Toward the Combination of Radiotherapy and Chemotherapy. *Langmuir* **2011**, 27 (10), 5874-8.

[19] Cao, W.; Gu, Y.; Li, T.; Xu, H., Ultra-Sensitive ROS-Responsive Tellurium-Containing Polymers. *Chem. Commun.* **2015**, 51 (32), 7069-71.

[20] Duan, D.; Liu, H.; Xu, Y.; Han, Y.; Xu, M.; Zhang, Z.; Liu, Z., Activating TiO_2 Nanoparticles: Gallium-68 Serves as a High-Yield Photon Emitter for Cerenkov-Induced Photodynamic Therapy. *ACS Appl. Mater. Interfaces* **2018**, 10 (6), 5278-5286.

[21] Kamkaew, A.; Cheng, L.; Goel, S.; Valdovinos, H. F.; Barnhart, T. E.; Liu, Z.; Cai, W., Cerenkov Radiation Induced Photodynamic Therapy Using Chlorin e6-Loaded Hollow Mesoporous Silica Nanoparticles. *ACS Appl. Mater. Interfaces* **2016**, 8 (40), 26630-26637.

[22] Shaffer, T. M.; Pratt, E. C.; Grimm, J., Utilizing the Power of Cerenkov Light with Nanotechnology. *Nat. Nanotechnol*. **2017**, 12 (2), 106-117.

[23] Kotagiri, N.; Sudlow, G. P.; Akers, W. J.; Achilefu, S., Breaking the Depth Dependency of Phototherapy with Cerenkov Radiation and Low-Radiance-Responsive Nanophotosensitizers. *Nat. Nanotechnol*. **2015**, 10 (4), 370-9.

[24] Laan, A. C.; Santini, C.; Jennings, L.; de Jong, M.; Bernsen, M. R.; Denkova, A. G., Radiolabeling Polymeric Micelles for in Vivo Evaluation: a Novel, Fast, and Facile method. *EJNMMI Res.* **2016**, 6 (1), 12.

[25] Mantid, Manipulation and Analysis Toolkit for Instrument Data. **2013**. Mantid Project. http://dx.doi.org/10.5286/SOFTWARE/MANTID

[26] Wignall, G. D.; Bates, F. S., Absolute Calibration of Small-Angle Ueutron Scattering Data. *J. Appl. Crystallogr.* **1987**, 20 (1), 28-40.

[27] Guinier, A; Fournet G., Small-Angle Scattering of X-Rays, John Wiley and Sons, New York, (1955)

[28] M. Doucet, SasView Version 4.1.2, http://doi.org/10.5281/zenodo.825675.

[29] Duan, L. Y.; Wang, Y. J.; Liu, J. W.; Wang, Y. M.; Li, N.; Jiang, J. H., Tumor-Selective Catalytic Nanosystem for Activatable Theranostics. *Chem. Commun.* **2018**, 54 (59), 8214-8217

[30] Wang, G.; Hoornweg, A.; Wolterbeek, H. T.; Franken, L. E.; Mendes, E.; Denkova, A. G., Enhanced Retention of Encapsulated Ions in Cross-Linked Polymersomes. *J. Phys. Chem. B* **2015**, 119 (11), 4300-8.

[31] Hicks, M.; Gebicki, J. M., Rate Constants for Reaction of Hydroxyl Radicals with Tris, Tricine and Hepes buffers. *Febs. Lett*. **1986**, 199 (1), 92-94.

[32] Kirsch, M.; Lomonosova, E. E.; Korth, H. G.; Sustmann, R.; de Groot, H., Hydrogen Peroxide Formation by Reaction of Peroxynitrite with HEPES and Related Tertiary Amines. *J. Biol. Chem.* **1998**, 273 (21), 12716-24.

[33] Liu, H.; Carter, P. J. H.; Laan, A. C.; Eelkema, R.; Denkova, A. G., Singlet Oxygen Sensor Green is not a Suitable Probe for $^1O_2$ in the Presence of Ionizing Radiation. *Sci. Rep*. **2019**, 9 (1), 8393.

[34] Duan, L. Y.; Wang, Y. J.; Liu, J. W.; Wang, Y. M.; Li, N.; Jiang, J. H., Tumor-Selective Catalytic Nanosystem for Activatable Theranostics. *Chem. Commun.* **2018**, 54 (59), 8214-8217.

[35] Kraljić, V. A. S. I., Detection of Singlet Oxygen in Radiolysis of Aerated Queous Solutions. *Photochem. Photobiol*. **1978**, 28, 587-590.

[36] Yang, X.; Zhu, B.; Dong, T.; Pan, P.; Shuai, X.; Inoue, Y., Interactions between an Anticancer Drug and Polymeric Micelles Based on Biodegradable Polyesters. *Macromol. Biosci.* **2008**, 8 (12), 1116-25.

Appendix

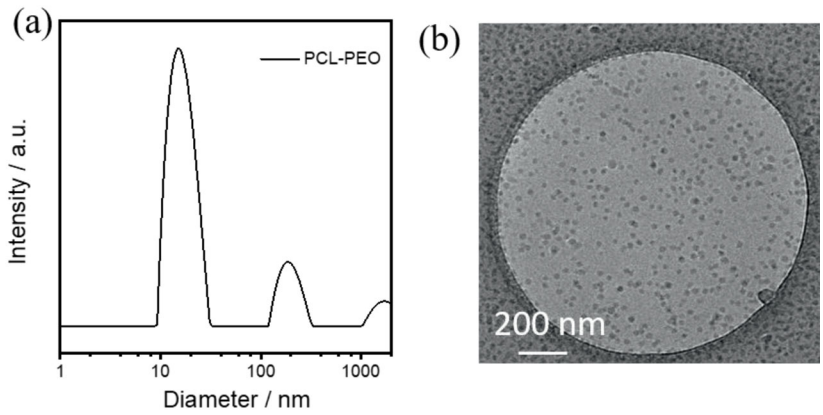

Figure S3.1. (a) The size distribution of PCL-PEO micelles as determined by DLS; (b) Cryo-EM images of PCL-PEO micelles. (The polymer concentration for DLS and Cryo-EM is 0.43 mg/mL and 8.7 mg/mL)

For measuring the stability of Ce6 when exposed to radiation, the samples were first exposed to gamma-rays of increasing radiation dose. To avoid possible measurement uncertainty due to Ce6 aggregation, the irradiated samples were mixed with THF by 1:1 volume ratio and then the UV-vis spectra were measured. The light absorption intensity at 665 nm was recorded to evaluate the stability of these samples. The UV-vis intensity at 665 nm of non-irradiated samples was used as the reference.

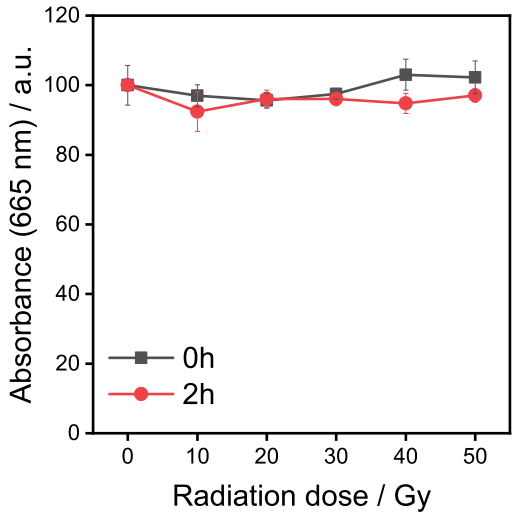

Figure S3.2. The absorption light intensity at 665 nm for Ce6 as function of the radiation dose and at different periods after irradiation. The concentration of Ce6 aqueous is 10 μM.

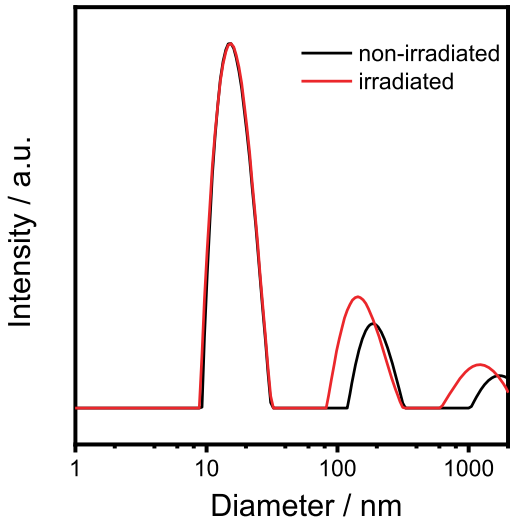

Figure S3.3. The size distribution of PCL-PEO micelles before and after being irradiated by 50Gy gamma-ray. The concentration of DLS samples is 0.43 mg/mL

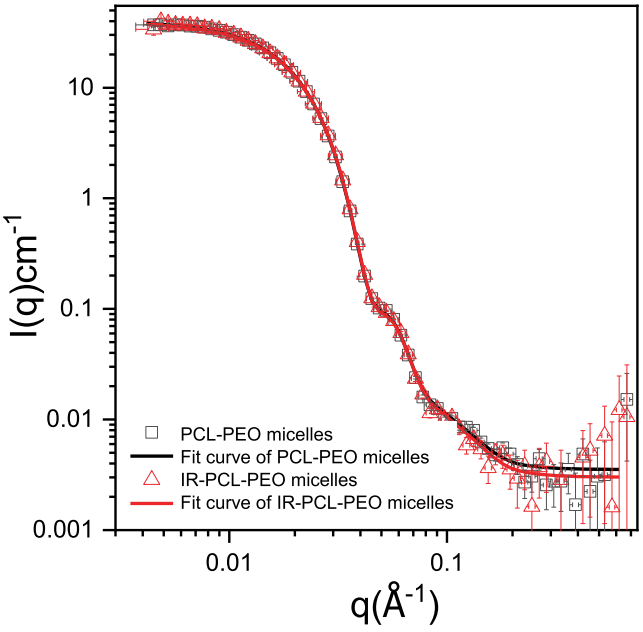

Figure S3.4. SANS intensity curve as a function of q for micelles composed of PCL-PEO before and after being irradiated by 50Gy gamma-rays (IR stands for irradiated samples).

SANS fit parameters for irradiated PEO-PCL micelles without Ce6

Q Range: min = 0.00416, max = 0.6713644687

Chi2/Npts = 37.541

scale = 0.0081185 +- 3.7411e-06

background = 0.003 1/cm

radius = 87 Ang

thickness = 40 Ang

sld_core = 1.49 1e-6/Ang^2

sld_shell = 5.51 1e-6/Ang^2

sld_solvent = 6.3 1e-6/Ang^2

radius.width = 0.17

thickness.width = 0.23

SANS fit parameters for irradiated PEO-PCL micelles without Ce6

Q Range: min = 0.00416, max = 0.6713644687

Chi2/Npts = 8.0146

scale = 0.008 +- 5.2913e-06

background = 0.0030155 +- 0.00024601 1/cm

radius = 87 Ang

thickness = 40 Ang

sld_core = 1.49 1e-6/Ang^2

sld_shell = 5.5 1e-6/Ang^2

sld_solvent = 6.3 1e-6/Ang^2

radius.width = 0.17

thickness.width = 0.23

SANS fit parameters for non-irradiated PEO-PCL micelles containing Ce6

Q Range: min = 0.00416, max = 0.6713644687

Chi2/Npts = 11.004

scale = 0.0084912 +- 4.5411e-06

background = 0.0043759 +- 0.0001291 1/cm

radius = 90.406 +- 0.02052 Ang

thickness = 40 +- 0.020622 Ang

sld_core = 1.49 1e-6/Ang^2

sld_shell = 5.5 1e-6/Ang^2

sld_solvent = 6.3 1e-6/Ang^2

radius.width = 0.17

thickness.width =0.23

SANS fit parameters for irradiated PEO-PCL micelles containing Ce6

Q Range: min = 0.00416, max = 0.6713644687

Chi2/Npts = 47.071

scale = 0.0059671 +- 7.6468e-06

background = 0.004 1/cm

radius = 90.4 Ang

thickness = 40 Ang

sld_core = 1.49 1e-6/Ang^2

sld_shell = 5.51 1e-6/Ang^2

sld_solvent = 6.31 1e-6/Ang^2

radius.width = 0.17

thickness.width = 0.23

SANS fit parameters for irradiated PEO-PCL micelles containing Ce6, 1 day later

Q Range: min = 0.00416, max = 0.6713644687

Chi2/Npts = 45.874

scale = 0.015487 +- 1.7245e-05

background = 0.004 1/cm

radius = 90.4 Ang

thickness = 40 Ang

sld_core = 1.49 1e-6/Ang^2

sld_shell = 5.51 1e-6/Ang^2

sld_solvent = 6.31 1e-6/Ang^2

radius.width = 0.17

thickness. width = 0.23

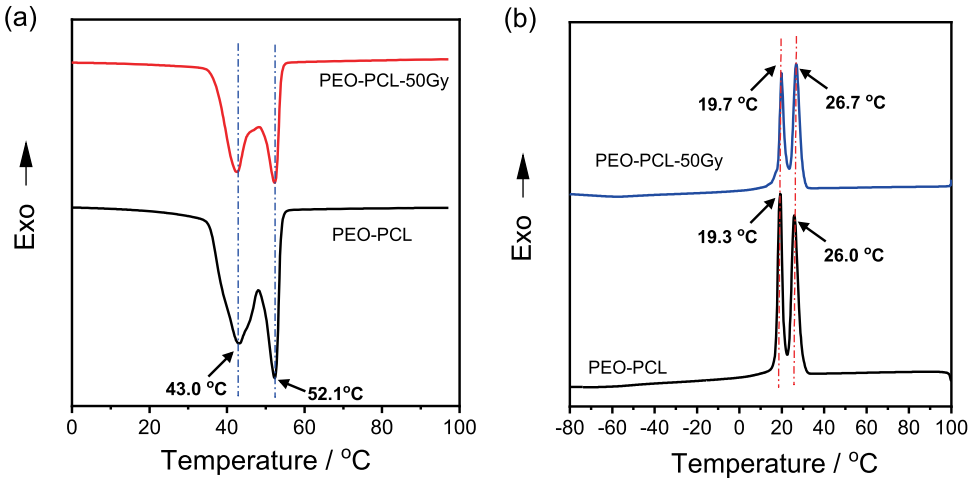

Figure S3.5. DSC curves of micelles composed of PCL-PEO before and after irradiated by 50 Gy gamma-rays (a) the first heating scan and (b) the first cooling scan.

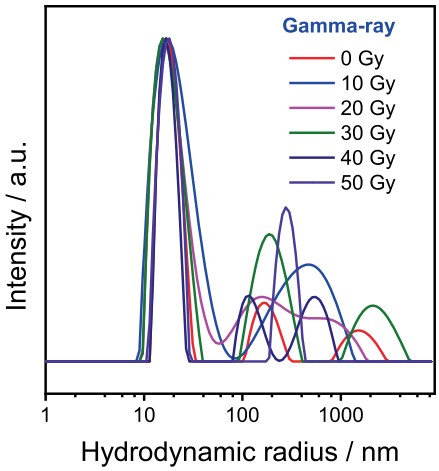

Figure S3.6. Size distribution of Ce6 loaded PCL-PEO micelles after exposure to increasing gamma radiation doses delivered by a ^{60}Co source.

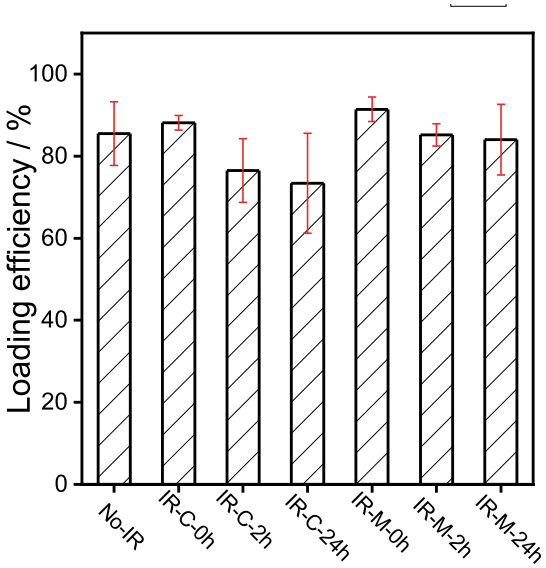

Figure S3.7. The loading efficiency of samples obtained by first irradiate Ce6/micelles and then mixed each part and allow to react for 24 hours. IR-C samples refers to gamma irradiated Ce6 aqueous solution (50 Gy) which was then mixed with the PCL-PEO micelles, while the IR-M samples refers to gamma irradiated PCL-PEO micelles (50Gy) which were then mixed with Ce6 solution. The concentration of micelles is 2.9 mg/mL, the concentration of Ce6 is 10 μM. The time 0/2/24 h means the waiting time before mixing Ce6 and micelles.

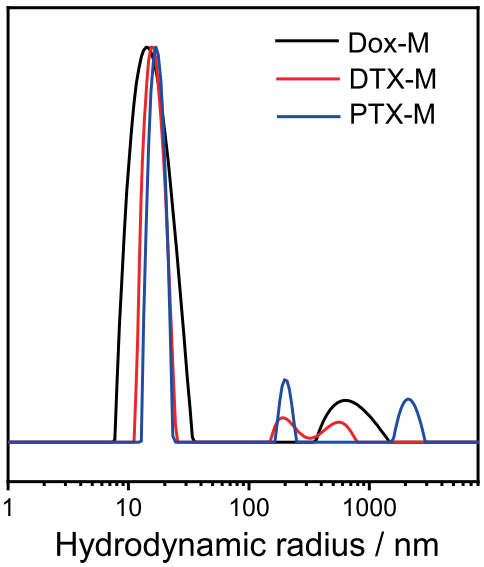

Figure S3.8. Size distribution of Dox-micelles, DTX-micelles and PTX-micelles. The polymer concentration is 0.14 mg/mL.

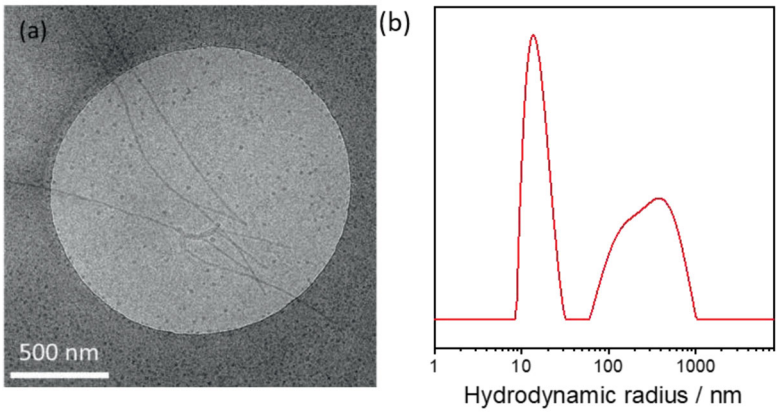

Figure S3.9. (a) Cryo-EM images and (b) size distribution of Dox&Ce6 co-loaded PCL-PEO micelles. The polymer concentration in the Cryo-EM and DLS experiments are respectively 2.9 mg/mL and 0.14 mg/mL.

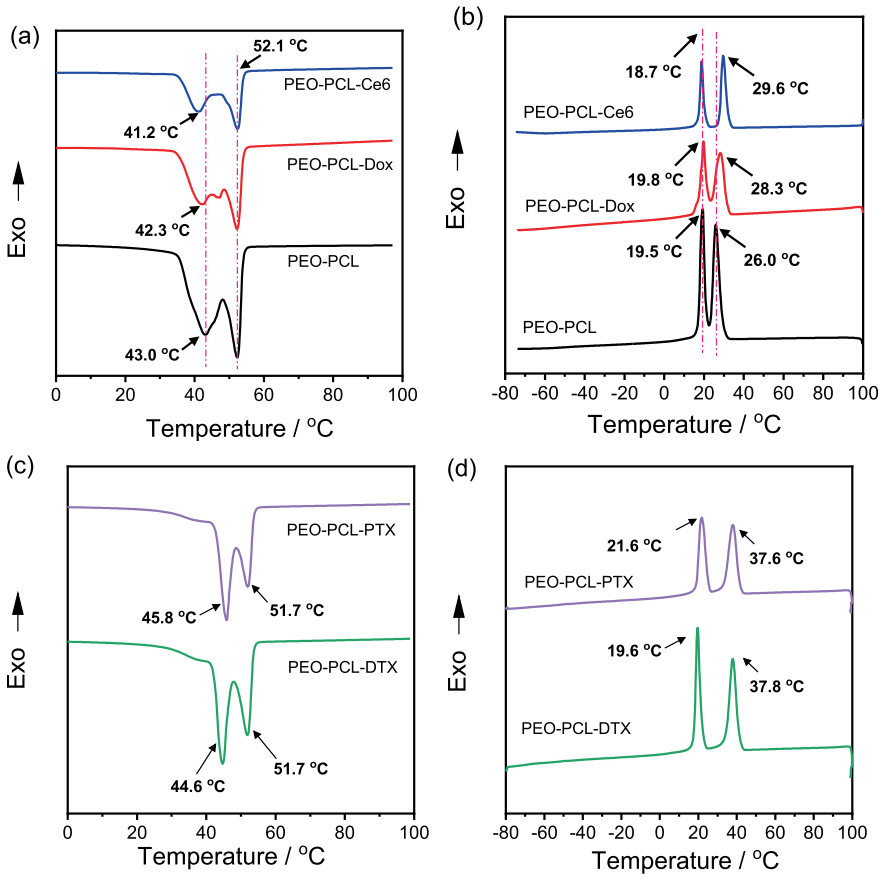

Figure S3.10. DSC curves of empty micelles and micelles loaded with Ce6, PTX , DTX and DOX recorded during (a,c) the first heating scan and (b,d) the first cooling scan.

New, fast and simple method to radiolabel polymeric micelles used in drug delivery

4

Abstract

Polymeric micelles are versatile nano-sized systems typically applied in drug delivery. The micelles assembled by block copolymers are composed of a hydrophobic core in which water-insoluble drugs can be encapsulated and a hydrophilic corona which helps to avoid the recognition by the immune system. Such delivery systems typically depend on the Enhanced Permeability and Retention (EPR) effect, which, unfortunately, is extremely heterogenous in patients. The possibility to determine the in vivo fate of micelles can help to achieve better therapeutic outcome. One of the most promising non-invasive imaging techniques that can be used to determine the in vivo behavior of micelles is SPECT (Single Photon Emission Computed Tomography). In order to use this technique, the micelles need to be radiolabeled. In this work, we present a novel and simple method for the radiolabeling of the core of polymeric micelles without affecting the inherent behavior of the nano-carriers. For this purpose we radiolabeled micelles composed by poly(ε-caprolactone-b-ethylene oxide) (PCL-PEO) with ^{111}In, a typical radionuclide used in SPECT studies. All PCL-PEO micelles exhibited very high ^{111}In radiolabeling efficiency (>80%). The same method was also used to radiolabel Paclitaxel (PTX)-loaded micelles composed of PCL-PEO, which showed that neither the radiolabeling efficiency nor the stability was affected by the presence of the drug. SPECT/CT pharmacokinetic study was performed to determine the stability of the radiolabeled micelles under in vivo conditions as well as the imaging potential of this radiolabeling method. As expected, the majority of the micelles were retained in the liver and no evident loss of ^{111}In (no bone uptake) was observed within 48 hours after administration. Finally, this radiolabeling method could also be applied to other medically relevant radionuclides (^{177}Lu and ^{89}Zr) and other polymeric micelles such as PLA-PEO (poly(lactic acid-b-ethylene oxide)).

Introduction

In the last two decades, nanotechnology has shown to have great potential in the field of medicine. A variety of nano-sized vehicles with different compositions, morphologies and properties have been developed primarily to ensure safer and more effective drug delivery process.[1] Among the different nano-carriers, polymer micelles have shown to be one of the most promising candidates in chemotherapy, leading to several formulations that are currently clinically applied. Micelles have a typical core-shell structure in which the hydrophobic core is used to encapsulate water-insoluble substances and the hydrophilic shell reduces interaction with blood plasma proteins.[2] The so-called enhanced permeability and retention effect (EPR) is believed to be one of the reasons for the accumulation of nano-carriers at the tumor site. For sufficient tumor accumulation, prolonged blood circulation is required. However, once being administered into the body, the plasma proteins in the blood stream will recognize the nanoparticles and form a protein corona on their surface, inducing their clearance by the mononuclear phagocyte system (MPS).[3] Therefore, poly(ethylene glycol)(PEG) is usually selected to increase the stealthiness of nano-carriers, i.e. to decrease contact with blood proteins and increase blood circulation time. Several studies have already demonstrated that the PEG shell of micelles is of great importance for the transportation of drugs to the tumor and that a slight change of the PEG surface, e.g. chain length and surface charge, can significantly influence the in vivo performance of micelles.[4, 5]

Besides the surficial properties of the nano-carriers, there are quite a few other factors that also affect the in vivo performance, such as composition, size and morphology.[6-8] For instance, small particles with a size less than 5.5 nm are easily excreted by the renal system,[9] while particles having larger size are cleared by the organs of MPS, such as the liver and spleen.[10] Despite these general trends, every formulation will have its own performance in vivo and differences between animal studies and final application in humans are unavoidable. Moreover, the EPR effect is heavily disputed in human patients mostly due to the very heterogenous behavior of micelles in vivo. Imaging techniques, such as single-photon emission computed tomography (SPECT) and Positron Emission Tomography (PET) are indispensable in the development of nano-formulations and can play also an essential role in

pre-determining the success of chemotherapy in patients receiving micellar formulations. SPECT and PET require diagnostic radionuclides that emit gammas and positrons, respectively. This in turns means that the micelles need to be radiolabeled. Generally, the conventional radiolabeling strategy for micelles is to conjugate a chelator molecule to the polymer chains composing the corona. The chelator then serves to coordinate the radioisotopes that are typically metals. [2, 11] However, the presence of chelators on the surface of the micelles may alter their inherent properties and influence the in vivo performance.[12, 13].

In this work, we present a facile, fast, and chelator-free method for radiolabeling the core of polymeric micelle. For this purpose, we selected poly(ε-caprolactone-b-ethylene oxide) (PCL-PEO) as the block copolymers to prepare micelles and ^{111}In as the radioisotope. The results showed that PCL-PEO micelles were capable of interacting with ^{111}In and leading to high radiolabeling efficiency. Moreover, chemotherapeutic drugs such as paclitaxel (PTX) could be enclosed together with the radioisotope without affecting the radiolabeling stability of the micelles. SPECT pharmacokinetic studies proved that this method can be safely applied in vivo. Finally, we also showed that this method can be applied to other polymeric systems, as well as other radioisotopes.

Materials and methods

2.1 Materials

Poly (ε-caprolactone-b-ethylene oxide) block copolymers including PCL-PEO (2800-2000, molecular weight), PCL-PEO (6500-5500), PCL-PEO (10500-5000) and PCL-PEO (13000-5000) were bought from Polymer Source (Quebec, Canada). Paclitaxel (PTX), Indium(III) chloride ($InCl_3$), 4-(2-hydroxyethyl)-1-piperazineethanesulfonic acid (HEPES), Sephadex G-25 resins and Sepharose 4B gels were bought from Sigma Aldrich (Zwijndrecht, the Netherlands). Diethylenetriaminepentaacetic acid (DTPA), Tropolone was bought from Merk. HCl and PBS buffer were purchased from VWR International BV. Fetal Bovine Serum(FBS) was purchased from Biowest (Amsterdam, the Netherlands). ^{111}In (Specific

activity was approximately 15.5 GBq/μg) in 0.01 M HCl solution was a kind gift from Erasmus Medical Centre (Rotterdam, the Netherlands).

2.2 Synthesis

2.2.1 Synthesis of polymeric micelles

The micelles were prepared by the solvent evaporation method described in our previous publication.[14] Typically, 0.2 mL of polymer stock solution (100 mg/mL, in chloroform) was added dropwise to 2.3 mL of MQ water and kept being stirred for overnight to remove organic solvent. The obtained micelles were denoted as PCL-2800, PCL-6500, PCL-10000 and PCL-13000. Tropolone containing micelles were also synthesized by the same procedure with a slight difference. That is, 5 μL of tropolone solution (20 mM, in 10 mM HEPES buffer with pH 7.4) was added to 2.3 mL MQ water before the addition of the polymer stock solution. The micelles containing tropolone were denoted as T-micelles, for example, T-PCL-2800 means PCL-2800 micelles in which tropolone was encapsulated.

2.2.2 Synthesis of PTX-loaded micelles

PTX-loaded micelles were prepared by adding PTX during the self-assembly process of the block copolymers. Briefly, 0.1 mL of PTX stock solution (5 mg/mL) was mixed with 0.1 mL of polymer stock solution (200 mg/mL, in chloroform) by sonication, then the mixture was added dropwise to 2.3 mL of MQ water and stirred overnight to remove the organic solvent. A filter with 220 nm cut-off was used to remove the large aggregates in the aqueous system, and size exclusion chromatograph (SEC) using a column (diameter 1 cm, length ~ 30 cm) filled with Sephadex G-25 was used to remove the unencapsulated PTX molecules. MQ water was used as the eluent, and every 1 mL of the eluent was collected as one fraction. The PTX-loaded micelles usually appeared between the 8^{th} to 11^{th} fractions, so four fractions were collected.

2.2.3 Radiolabeling with ^{111}In

The obtained micelles solution in water was filtered using a 220 nm cut-off syringe filter to remove possible large aggregates and mixed with HEPES buffer (20 mM, pH=7.4) in a volume ratio of 1: 1. Next, 50 kBq of ^{111}In (the volume was dependent on the elapsed time to compensate for decay and ranged from 5 to 13 μL) was added to 1 mL micelle solution which was subsequently stirred for 30 min. After the reaction, any free ^{111}In ions were removed by SEC. HEPES buffer (10 mM, pH=7.4) was used as the eluent. The radiolabeled samples usually appeared between the 8th to 12th fractions, so five fractions in a total volume of 5 mL were collected as the final radiolabeled sample.

To radiolabel the PTX-loaded micelles, a centrifuge filter tube was used to concentrate the PTX-loaded micelles solution (4 mL) to 1 mL and mixed it with HEPES buffer (20 mM, pH 7.4) in a volume ratio of 1:1. Then, the PTX-loaded micelles were radiolabeled with ^{111}In in the same way as the empty micelles.

2.2.4 Synthesis of In^{3+} loaded micelles

The ^{111}In radiolabeled In^{3+} stock solutions (13.87 mM) were prepared by adding 60 μL of ^{111}In stock solution (0.135 MBq) to 140 μL of non-radioactive indium solution (19.82 mM, in HCl aqueous solution, pH = 2) (change of the In^{3+} concentration change due to the presence of ^{111}In was neglected). In the meanwhile, non-radioactive In^{3+} stock solutions was prepared by adding 60 μL of HCl aqueous solution (pH=2) to 140 μL of Indium solution with a concentration of 19.82 mM. The loading process of In^{3+} ions was similar with that of ^{111}In radiolabeling, that is, 10 μL of the radiolabeled In^{3+} solution was added to 1 mL of the micelles in HEPES buffer (10 mM, pH = 7.4), stirred for half an hour and then removed the free In^{3+} ions by SEC. In this process, HCl solution (pH=2) was used as the eluent to make sure that indium ions did not precipitate during the separation.

Characterization

3.1 Instruments

A dynamic light scatting instrument (DLS) consisted of a JDS uniphase 633 nm 35 mW laser, an ALV sp 125 s/w 93 goniometer, a fibre detector and a Perkin Elmer photo counter and a

Cryogenic electron microscope (Cyro-EM, Jeol JEM 1400) were used to determine the morphology and size distribution of the micelles. A high performance liquid chromatography (HPLC, SPD-10A modal, Shimazu) was applied to determine the concentration of PTX. Automatic Gamma counter (Wallac WIZARD^2 2480, Perkin Elmer Technologies) was used to measure the counts of ^{111}In in all samples using the gamma peaks at 171 keV and 254 keV.

3.2 Radiolabeling/loading efficiency

The radiolabeling/loading efficiency was determined by Wallac:
The Radiolabeling efficiency (%) = (the counts of ^{111}In encapsulated in micelles / the counts of initially added ^{111}In) * 100%.

3.3 Stability test
In HEPES buffer (^{111}In radiolabeled micelles)
1 mL of the radiolabeled sample was separated by SEC at different time intervals, using HEPES buffer as the eluent.

Residual activity ratio = (The counts of ^{111}In measured in the micelles after SEC/ the total counts of ^{111}In before SEC separation) * 100%.

Challenging by DTPA
0.1 mL of DTPA solution (11 mM, in 10 mM HEPES buffer, pH=7.4) was added to 1 mL of the ^{111}In radiolabeled micelles. After being incubated for 24 hours, SEC was used to separate the ^{111}In-DTPA complex from the ^{111}In radiolabeled micelles. The micelles came out between fractions 8th to 12th fractions, while the DTPA eluted between the 14th and 18th fractions.

In FBS serum
0.5 mL of the obtained radiolabeled samples were mixed with 0.5 ml of serum and stored in an incubator at 37^{o}C. 24 hours later, the serum and micelle fractions were separated by Sepharose 4B gel column (diameter 1 cm, length 30 cm). HEPES buffer was applied as the eluent. The micelles appeared between the 8th to the 13th fraction, while serum came out

between the 17th to the 23rd fraction. Both micelle and serum fractions were collected, and the counts of ^{111}In in each sample was determined as explained previously.

3.4 In vivo biodistribution of ^{111}In radiolabeled micelles

The radiolabeled micelles for SPECT imaging were prepared by adding 80 MBq of ^{111}In to 1 mL of PCL-6500 micelles dispersed in HEPES buffer and incubating for 30 min. Subsequently, a PD10 column was utilized to remove any free ^{111}In ions using PBS buffer as the eluent. The fraction with the maximum counts was further used for the in vivo experiments.

All animal studies were performed in accordance with the Dutch Law on Animal Experimentation and all protocols were approved by the Animal Research Committee of the University Medical Center Utrecht. The in vivo biodistribution of micelles was carried out using a SPECT/CT scanner (VECTor^6/CT, MILabs B.V., The Netherlands). Three healthy C57BL/6 mice of 10 weeks old were used. For the animal studies, 200 μL of ^{111}In radiolabeled PCL-6500 micelles (~10 MBq, dispersed in PBS) was i.v. injected into the tail vein of the mice. SPECT/CT scans were carried out at 1h, 24h and 48 h post injection using a clustered pinhole collimator with 144 pinholes, 0.7mm each. The animals were anesthetized using a mixture of 2% isoflurane in air. VOI (Volume of interest) analysis using the software Pmod 4.2 was performed to quantitatively analyse the data.

Results and analysis

4.1 ^{111}In radiolabeled micelles

In previous research we showed that we can encapsulate radionuclides in PS-PEO (Poly(styrene-b-ethylene oxide)) micelles when using the ligand tropolone.[14] To check the role that tropolone can play, we performed the radiolabeling experiments with and without this ligand. Polymeric micelles with or without tropolone were prepared by the self-assembly of PCL-PEO block copolymers having different chain lengths. Figure 4.1 displays the DLS

data as well as Cryo-EM images of the different micelles. According to DLS data, the average hydrodynamic radius of PCL-2800, PCL-6500, PCL-10000 and PCL-13000 micelles was 16 nm, 39 nm, 54 nm and 65 nm, respectively. The presence of tropolone did not have influence on the hydrodynamic radius of PCL-2800 and PCL-13000 micelles, and a small decrease in size was observed for PCL-6500 and PCL-10000 micelles. The Cryo-EM images indicate that the polymers with shorter chain preferably form spherical small micelles. The longer chain polymers can form larger spherical structures that appear to be less dense than the micelles composed by the shorter chain polymers. In the samples containing the PCL-2800 micelles, worm-like structures were also observed (Figure 4.1(e)) which probably corresponded to the second larger peak found in the DLS data. To achieve a uniform micelles solution, we filtered the micelles solution by using the syringe filters with 220 nm cut-off.

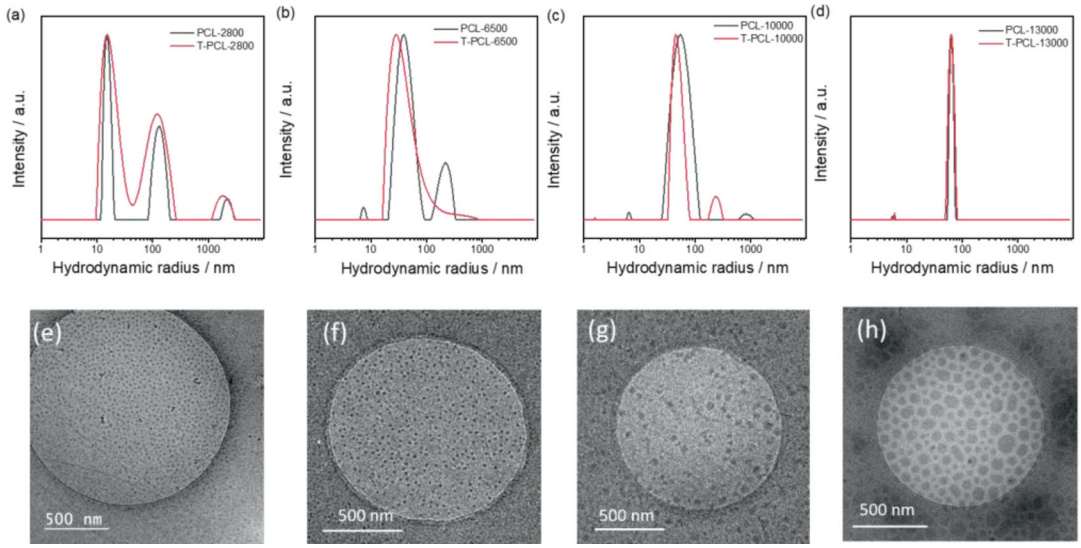

Figure 4.1. (a-d) The size distribution of the different polymer micelles as obtained by DLS; Cryo-EM images of (e) PCL-2800 (f) PCL-6500 (g) PCL-10000 and (h) PCL-13000 micelles. (The polymer concentration of the DLS samples was 0.43 mg/mL; the polymer concentration of the Cryo-EM samples was 8.3 mg/mL, the DLS and Cryo-EM analysis were performed before the samples were filtrated.)

The radioisotope ^{111}In is typically used in SPECT imaging due to its suitable gamma energies of 171.3 keV and 245.4 keV and convenient half-life ($t_{1/2}$=2.8 day).[14] In this work, we attempted to radiolabel the different PCL-PEO micelles by simply adding ^{111}In to the micelle solution. As shown in Figure 4.2(a), all micelles could be radiolabeled in this way yielding radiolabeling efficiency of 81.94 ± 1.59, 83.75 ± 1.49, 92.4 ± 2.41 and 90.66 ± 3.17% for

PCL-2800, PCL-6500, PCL-10000 and PCL-13000 micelles, respectively. The presence of tropolone was found to slightly increase the ^{111}In radiolabeling efficiency of the micelles assembled by the smaller block copolymers, i.e. PCL-2800 and PCL-6500, while no any effect could be observed for PCL-10000 and PCL-13000 micelles. The high ^{111}In radiolabeling efficiency of the PCL micelles without tropolone clearly demonstrated that the PCL-PEO micelles have different interaction with ^{111}In, than in the case of PS-PEO micelles which could not be radiolabeled with ^{111}In reaching high efficiency in the absence of tropolone.[14]

To further check the influence of tropolone on the radiolabeling process, the ^{111}In loss of the radiolabeled PCL-6500 and T-PCL-6500 just in buffered solution was measured and compared. As shown in Figure 4.2(b), there was no evident difference of ^{111}In retention between PCL-6500 micelles and T-PCL-6500 micelles with 88.29 ± 3.44% and 91.91± 2.15% of ^{111}In remaining in the PCL-6500 and T-PCL-6500 micelles on the 7th day after preparation. The results showed that tropolone did not influence the radiolabeling stability.

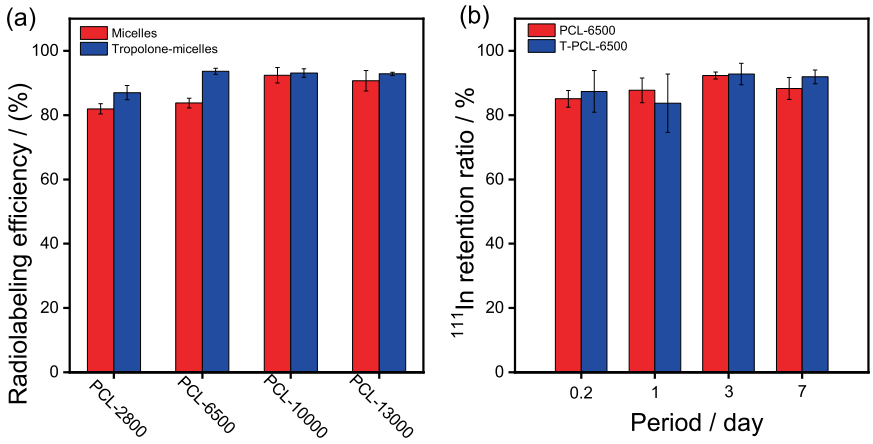

Figure 4.2. (a)The ^{111}In radiolabeling efficiency of PCL-PEO micelles with or without the presence of tropolone; (b) The comparison of radiolabeling stability between PCL-6500 and T-PCL-6500 micelles in HEPES buffer (The polymer concentration was 4.3 mg/mL(before filtration) in the radiolabeling process and 0.86 mg/mL in the stability experiment; 10 mM HEPES buffer of pH=7.4 was used in all samples.)

4.2 Interaction between In species and PCL-PEO micelles

The initial activity used in the previous experiments was 0.05 MBq that was equal to ~2.9×10^{-14} mol of indium ions, which was too little to help understanding the possible interaction between In species and the micelles. Therefore we increased the In^{3+} concentration by using non-radioactive In^{3+} ions to which tiny amounts of ^{111}In was added as a radiotracer. Although all micelles displayed high radiolabeling efficiency with ^{111}In, the loading performance using higher concentrations of In^{3+} differed (Table S4.1). The larger micelles, i.e. PCL-10000 and PCL-13000, could encapsulate more In^{3+} ions, particularly the PCL-10000 micelles which exhibited a loading efficiency of 50.78 ± 1.84%. By contrast, the PCL-2800 and PCL-6500 showed a loading efficiency of 3.91 ± 0.08% and 4.30 ± 0.10%, respectively. The higher capacity of the micelles composed with the larger polymers may also be due to the less dense structure of the micelles as well as the larger core. It is also plausible that the looser structure of the core allows the Indium ions to penetrate easier into the PCL-PEO micelles.

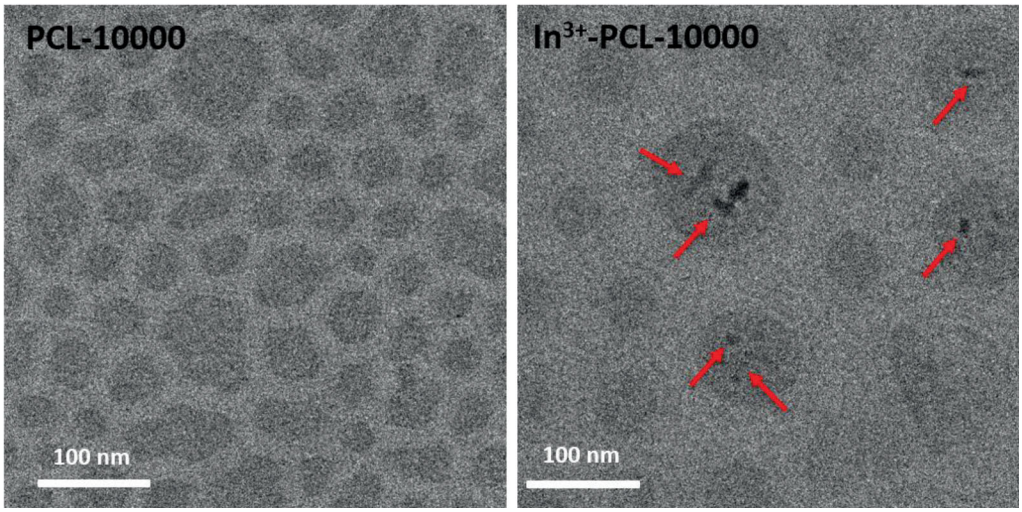

Figure 4.3. Cryo-EM of PCL-10000 micelles (left) and In^{3+}-PCL-10000 micelles (right). (For the micelles preparation: the concentration of polymers was 4.3 mg/mL in HEPES buffer and the initial In^{3+} concentration was 0.137 mM. For the Cryo-EM: the obtained samples needed to be concentrated to a solution with polymer concentration of around 8.7 mg/mL.)

To get a better understanding of the loading mechanism we used the Cryo-EM and non-radioactive In^{3+} ions (0.137 mM) to load PCL-10000 micelles. Figure 4.2 shows images of

the PCL-10000 micelles before and after addition of In^{3+} ions. Clear dark spots appeared in the core of the micelles after loading with In^{3+} ions which probably correspond to $In(OH)_3$ precipitates. The chemical speciation software CHEAQs confirmed that at that concentration $InOH_3$ precipitates are formed. It is, however, not clear whether $In(OH)_3$ precipitates were also formed at the concentrations of ^{111}In used in the radiolabeling experiments. Considering the high radiolabeling efficiency and stability of ^{111}In, we can speculate that also in this case ^{111}In precipitates in the core of the micelles.

4.3 Radiolabeling of PTX-loaded micelles with ^{111}In

PTX-loaded micelles were prepared by using three different PCL-PEO micelles. The amount of encapsulated PTX was determined by HPLC, showing that the drug encapsulation performance decreased with increasing size of the micelles, that is, 86.39 ± 6.28%, 75.72 ± 6.75% and 63.39 ± 7.29% of PTX molecules were encapsulated for respectively PCL-2800, PCL-6500 and PCL-10000 micelles. The morphology information of the PTX-loaded micelles was shown in Figure S4.2. Subsequently, ^{111}In was added to radiolabel the PTX-loaded micelles in the same way as for the empty micelles. The radiolabeling efficiency was found to decrease slightly (see Table 4.1) when compared to the empty micelles but it was sufficiently high.

Table 4.1. Drug loading efficiency and radiolabeling efficiency of co-loaded micelles.

Samples	PTX Loading efficiency (%)	^{111}In radiolabelling efficiency (%)
^{111}In&PTX-2800	86.39 ± 6.28*	73.73 ± 10.16
^{111}In&PTX-6500	75.72 ± 6.75	81.34 ± 5.23
^{111}In&PTX-10000	63.39 ± 7.29	82.39 ± 7.29

* The standard deviation is based on experimental uncertainty of three samples.

Tumors are known to be slightly acidic. Therefore, we determined the loss of ^{111}In at pH 5.2 and pH 7.4 using PBS buffer. As summarized in Figure 4.4(a), the three co-loaded samples exhibited excellent radiolabeling stability in PBS buffer with more than 80% of ^{111}In

remaining in the micelles after 1-day of incubation regardless of pH values. To further check the stability of the radiolabeled micelles, we used DTPA challenge and serum tests. [12, 14-16] DTPA is known to form thermodynamically stable complexes with ^{111}In and was therefore chosen as the challenging molecule. In this experiment, we added 0.1 mL of DTPA solution (11 mM, in HEPEs) to 1 mL of the micelle solution and created harsh environment, in which the number of DTPA molecules was much higher than ^{111}In ions in the micelles. The co-loaded micelles displayed good stability in the presence of DTPA, with more than 80% of the encapsulated ^{111}In remaining inside the micelles, regardless of the block copolymer used. The serum tests showed ^{111}In&PTX-2800 and ^{111}In&PTX-6500 had an ^{111}In retention higher than 80%. The ^{111}In&PTX-10000 sample appeared to be unstable in serum solution and some large precipitations were visible at the bottom of the vial after 24 hour of incubation. In fact, only ~42% of ^{111}In that remained encapsulated in the intact PCL-10000 nano-carriers after 24 hours (Fig. 4.4(b)). However, in these experiments we could not determine whether ^{111}In appeared in the serum fraction due to weak interaction between ^{111}In and micelles or due to interaction between serum proteins with the micelles.

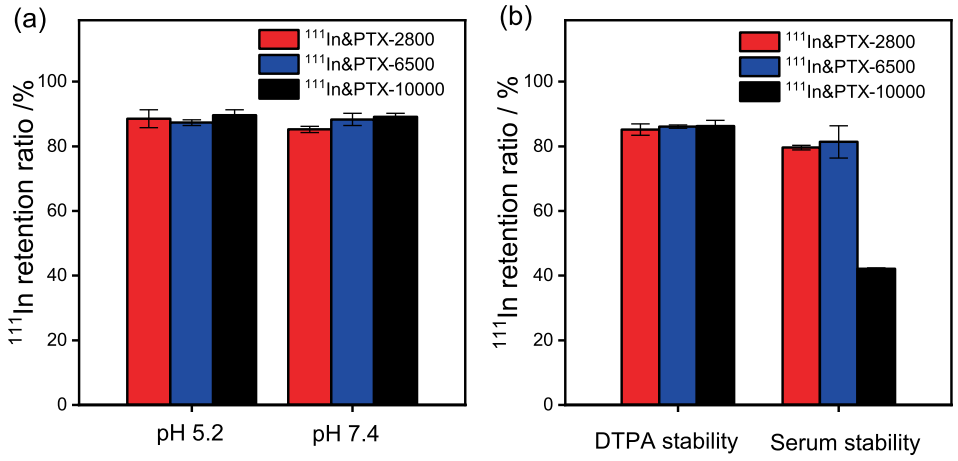

Figure 4.4. The radiolabeling stability ^{111}In&PTX co-loaded micelles after 24 hours of incubation (a) in PBS buffer having different pH values and (b) under DTPA challenge and in serum (polymer concentration was 0.22 mg/mL for samples dispersed in PBS and in serum and 0.43 mg/mL for DTPA challenge.)

The influence of serum on the smaller micelles was much less and more than 80% of the activity remained inside the micelles. We also compared the radiolabeling stability between

PCL-6500 and PTX-loaded PCL-6500 micelles. As summarized in Figure S4.3, the radiolabeling stability of PTX-loaded micelles was comparable with that of the empty PCL-6500, indicating the presence of PTX did not have significant influence on the interaction between ^{111}In and micelles.

4.4 In vivo tests

In order to check the stability of radiolabeling as well as the imaging potential of the radiolabeled micelles we performed pharmacokinetic studies using PCL-6500 micelles. It has to be noted that the purpose of this study was not to determine the best properties for in vivo delivery but to check the safety and utilization potential of this radiolabeling method. This is why we have chosen healthy mice for the in vivo studies. We radiolabeled the PCL-6500 micelles with ^{111}In, and achieved ~66 MBq of ^{111}In encapsulated by the micelles when given an initial activity of 80 MBq. The ^{111}In retention in the micelles was found to be around 93% after being incubated at 37^{o}C for 4 hours.

The SPECT/CT results are shown in Figure 4.5. The results reveal that the majority of activity appeared in the liver after 1 h post-injection and that a small amount of ^{111}In was found in the spleen. At the same time, activity was also measured in the heart showing that the micelles were still circulating in the blood stream. For micelles and nano-carriers of this size, liver and spleen uptake is expected since they are the typical organs of the mononuclear phagocyte system. [12, 17, 18] The VOI (Volume Of Interest) analysis (software Pmod 4.2) was utilized as the tool to quantitively analyze the activity distribution in different organs.[19, 20] The results showed that 56.38 ± 6.17% of the activity ended in the liver, 1.09 ± 0.78% activity was detected at the spleen, and 1.12 ± 0.27 % of the activity was found in the heart after 1h p.i.. There was almost no activity could be observed in the heart at 24 h p.i., indicating that the micelles no longer circulated in the blood stream. In the meanwhile, 55.35 ± 4.22% and 1.85 ± 0.38% of the activity was detected in the liver and the spleen. At 48 h p.i., the similar activity values were measured in liver and spleen (54.06 ± 3.84% and 1.96 ± 0.76% respectively) showing the ^{111}In did not leak out. The SPECT images confirmed that the radiolabeled micelles are stable in vivo.

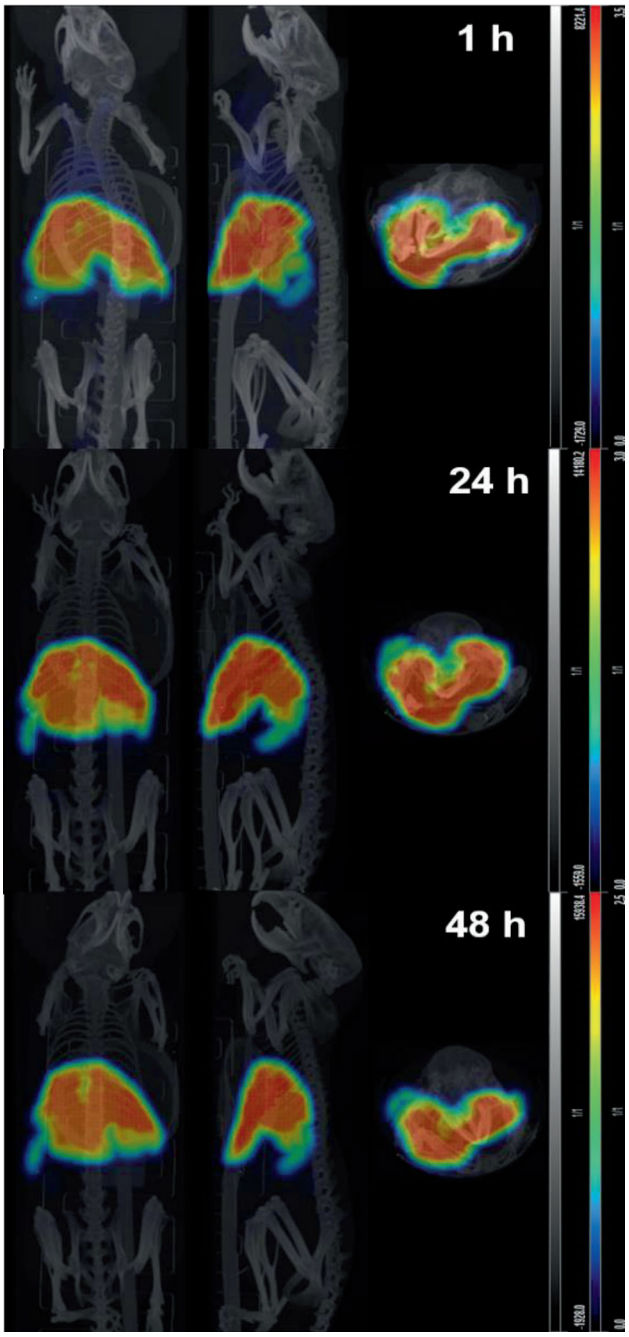

Figure 4.5. SPECT/CT images of ^{111}In radiolabeled PCL-6500 micelles in healthy mice measured at 1 hour, 24 h and 48 h post injection (The polymer concentration of the micelle solution in PBS was 4.3 mg/mL, the initially administered activity was around 10 MBq).

4.5 Extended application of the chelator-free radiolabeling

Apart from ^{111}In, we also used other isotopes including ^{177}Lu and ^{89}Zr to radiolabel the PCL-PEO micelles and achieved high radiolabeling efficiency with 94.21± 0.54 % for ^{177}Lu and 84.75 ± 1.83% for ^{89}Zr. In addition, we also explored the same method to radiolabel PLA-PEO (poly(lactide-b-ethylene oxide) PLA-PEO(10500-5000)) with ^{111}In. In this case a radiolabeling efficiency of 69.7 ± 3.28% and radiolabeling stability of 79.26 ± 11.57% after challenge with DTPA for 24 hours were achieved. These results demonstrate that this method is promising for other polymeric micelles as well as other clinically relevant radionuclides.

Conclusions

In this chapter we demonstrated a fast, easy and chelator-free method to radiolabel PCL-PEO micelles as well as PTX-loaded PCL-PEO micelles. All PCL-PEO micelles, i.e. PCL-2800, PCL-6500, PCL-10000 and PCL-13000, exhibited excellent radiolabeling efficiency with ^{111}In. Also, the presence of PTX located in the hydrophobic core appeared not to influence the radiolabeling process. The Cryo-EM images indicated that the In species can somehow pass through the PEO shell and precipitate in the hydrophobic core. The small micelles showed good radiolabeling stability in the presence of both DTPA and serum, while the larger micelles, i.e. PCL-10000, were much less stable in serum possibly due to their less dense structure. The SPECT/CT in vivo tests revealed that the blood circulation of PCL-6500 micelles was longer than 1 h and the majority of the micelles were retained in the liver and spleen without an evident loss of ^{111}In. Our results showed that this radiolabeling method is very promising due to its simplicity and the possibility to be applied to various polymeric micelles and radionuclides of interest.

Reference

[1] L. Salvioni, M.A. Rizzuto, J.A. Bertolini, L. Pandolfi, M. Colombo, D. Prosperi, Thirty Years of Cancer Nanomedicine: Success, Frustration, and Hope, *Cancers (Basel)*. **2019**, 11.

[2] C.M.R. Oda, R.S. Fernandes, S.C. de Araujo Lopes, M.C. de Oliveira, V.N. Cardoso, D.M. Santos, A.M. de Castro Pimenta, A. Malachias, R. Paniago, D.M. Townsend, P.M. Colletti, D. Rubello, R.J. Alves, A.L.B. de Barros, E.A. Leite, Synthesis, Characterization and Radiolabeling of Polymeric Nano-Micelles as A Platform for Tumor Delivering, *Biomed Pharmacother*. **2017**, 89, 268-275.

[3] J. Guo, H. Hong, G. Chen, S. Shi, Q. Zheng, Y. Zhang, C.P. Theuer, T.E. Barnhart, W. Cai, S. Gong, Image-Guided and Tumor-Targeted Drug Delivery with Radiolabeled Unimolecular Micelles, *Biomaterials*. **2013**, 34, 8323-8332.

[4] K. Xiao, Y. Li, J. Luo, J.S. Lee, W. Xiao, A.M. Gonik, R.G. Agarwal, K.S. Lam, The Effect of Surface Charge on In Vivo Biodistribution of PEG-Oligocholic Acid Based Micellar Nanoparticles, *Biomaterials*. **2011**, 32, 3435-3446.

[5] H. Gao, J. Liu, C. Yang, T. Cheng, L. Chu, H. Xu, A. Meng, S. Fan, L. Shi, J. Liu, The Impact of PEGylation Patterns on the In Vivo Biodistribution of Mixed Shell Micelles, *Int J Nanomedicine*. 2013, 8, 4229-4246.

[6] S.A. Kollenda, J. Klose, T. Knuschke, V. Sokolova, J. Schmitz, M. Staniszewska, P.F. Costa, K. Herrmann, A.M. Westendorf, W.P. Fendler, M. Epple, In Vivo Biodistribution of Calcium Phosphate Nanoparticles after Intravascular, Intramuscular, Intratumoral, and Soft Tissue Administration in Mice Investigated by Small Animal PET/CT, *Acta Biomater*. **2020**, 109, 244-253.

[7] A.L. Bailly, F. Correard, A. Popov, G. Tselikov, F. Chaspoul, R. Appay, A. Al-Kattan, A.V. Kabashin, D. Braguer, M.A. Esteve, In Vivo Evaluation of Safety, Biodistribution and Pharmacokinetics of Laser-Synthesized Gold Nanoparticles, *Sci Rep*. **2019**, 9 12890.

[8] M.J. Ernsting, M. Murakami, A. Roy, S.D. Li, Factors Controlling the Pharmacokinetics, Biodistribution and Intratumoral Penetration of Nanoparticles, *J Control Release*. **2013**, 172, 782-794.

[9] H.S. Choi, W. Liu, P. Misra, E. Tanaka, J.P. Zimmer, B. Itty Ipe, M.G. Bawendi, J.V. Frangioni, Renal Clearance of Quantum Dots, *Nat Biotechnol*. **2007**, 25, 1165-1170.

[10] E. Blanco, H. Shen, M. Ferrari, Principles of Nanoparticle Design for Overcoming Biological Barriers to Drug Delivery, *Nat Biotechnol*. **2015**, 33, 941-951.

[11] D. Psimadas, H. Oliveira, J. Thevenot, S. Lecommandoux, P. Bouziotis, A.D. Varvarigou, P. Georgoulias, G. Loudos, Polymeric Micelles and Vesicles: Biological Behavior Evaluation using Radiolabeling Techniques, *Pharm Dev Technol*. **2014**, 19, 189-193.

[12] L. Cheng, S. Shen, D. Jiang, Q. Jin, P.A. Ellison, E.B. Ehlerding, S. Goel, G. Song, P. Huang, T.E. Barnhart, Z. Liu, W. Cai, Chelator-Free Labeling of Metal Oxide Nanostructures with Zirconium-89 for Positron Emission Tomography Imaging, *ACS Nano*. **2017**, 11, 12193-12201.

[13] S. Goel, F. Chen, E.B. Ehlerding, W. Cai, Intrinsically Radiolabeled Nanoparticles: An Emerging Paradigm, *Small*. **2014**, 10, 3825-3830.

[14] A.C. Laan, C. Santini, L. Jennings, M. de Jong, M.R. Bernsen, A.G. Denkova, Radiolabeling Polymeric Micelles for In Vivo Evaluation: A Novel, Fast, and Facile method, *EJNMMI Res*. **2016**, 6, 12.

[15] G. Wang, R.M. de Kruijff, D. Abou, N. Ramos, E. Mendes, L.E. Franken, H.T. Wolterbeek, A.G. Denkova, Pharmacokinetics of Polymersomes Composed of Poly(Butadiene-Ethylene Oxide); Healthy versus Tumor-Bearing Mice, *J Biomed Nanotechnol*. **2016**, 12, 320-328.

[16] T.M. Shaffer, M.A. Wall, S. Harmsen, V.A. Longo, C.M. Drain, M.F. Kircher, J. Grimm, Silica Nanoparticles as Substrates for Chelator-Free Labeling of Oxophilic Radioisotopes, *Nano Lett*. **2015**, 15, 864-868.

[17] V. Kumar, V. Mundra, Y. Peng, Y. Wang, C. Tan, R.I. Mahato, Pharmacokinetics and Biodistribution of Polymeric Micelles Containing miRNA and Small-Molecule Drug in Orthotopic Pancreatic Tumor-Bearing mice, *Theranostics*. **2018**, 8, 4033-4049.

[18] L. Tian, X. Yi, Z. Dong, J. Xu, C. Liang, Y. Chao, Y. Wang, K. Yang, Z. Liu, Calcium Bisphosphonate Nanoparticles with Chelator-Free Radiolabeling to Deplete Tumor-Associated Macrophages for Enhanced Cancer Radioisotope Therapy, *ACS Nano*. **2018**, 12, 11541-11551.

[19] M. Cachovan, A.H. Vija, J. Hornegger, T. Kuwert, Quantification of ^{99m}Tc-DPD Concentration in the Lumbar Spine with SPECT/CT, *EJNMMI Res*, **2013**, 3, 45.

[20] K. McLarty, B. Cornelissen, Z. Cai, D.A. Scollard, D.L. Costantini, S.J. Done, R.M. Reilly, Micro-SPECT/CT with ^{111}In-DTPA-Pertuzumab Sensitively Detects Trastuzumab-Mediated HER2 Downregulation and Tumor Response in Athymic Mice Bearing MDA-MB-361 Human Breast Cancer Xenografts, *J Nucl Med*. **2009**, 50, 1340-1348.

Appendix

The loading of the different PCL-PEO micelles varied when higher In concentration was used: the PCL-10000 micelles exhibited the highest loading with a loading efficiency (LE) up to 50.78 ± 1.84%, which was followed by PCL-13000 micelles with a LE of 15%. The LE of the smaller micelles was comparable, with 3.9% for PCL-2800 and 4.3% for PCL-6500. If converting all the encapsulated In^{3+} ions to ^{111}In ions, the max ^{111}In loading capacity of PCL-10000 micelles that could be reached was 28.23 GBq/mg. For this calculations, specific activity of ^{111}In of 15.5GBq/µg was used.

Table S1. Indium loading efficiency of the obtained PCL-PEO micelles.

Samples	Loading efficiency (%)
PCL-2800	3.91 ± 0.08*
PCL-6500	4.30 ± 0.10
PCL-10000	50.78 ± 1.84
PCL-13000	15.02 ± 0.78

* The standard deviation is based on three samples

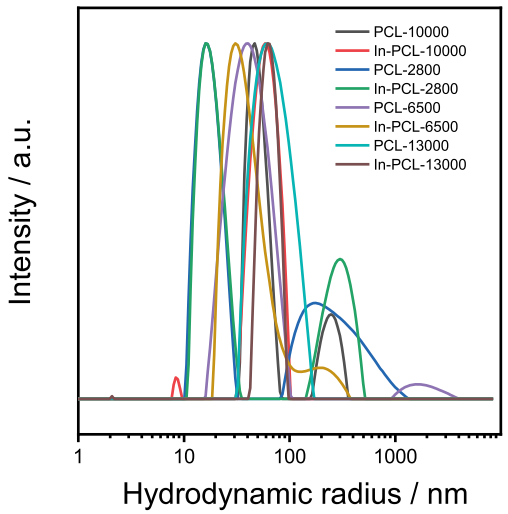

Figure S4.1. The size distribution of PCL-PEO block copolymer with different chain length in the presence and absence of In.

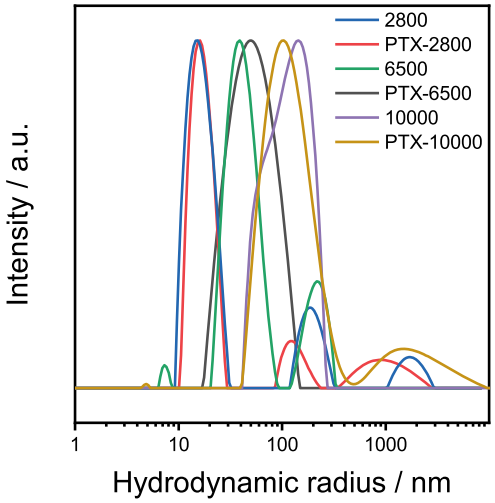

Figure S4.2. The size distribution of PTX-loaded micelles with the drug to polymer mass ratio of 0.5:20. (Polymer concentration: 0.435 mg/mL).

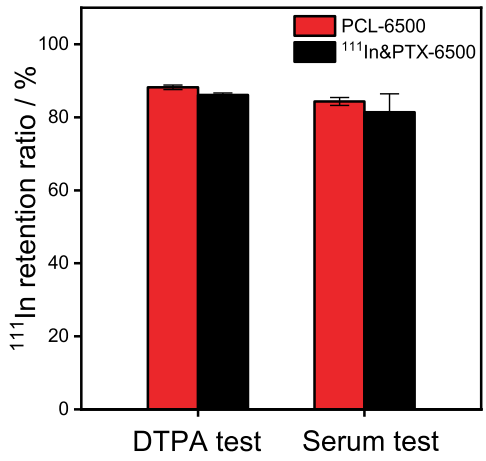

Figure S4.3. Evaluation of the ^{111}In radiolabeling stability of micelles with/without the presence of PTX under challenging of DTPA solution (1mM, in 10 mM HEPES buffer with pH 7.4) for 24 h and in serum for 24 h. (polymer concentration: ~0.79 mg/mL for DTPA challenging and ~0.44 mg/mL for serum test).

5

The mechanism of chelator free radiolabeling method for polymeric micelles explored using different block copolymers and radionuclides

Abstract

Polymeric micelles are increasingly used in the clinic, primarily in chemotherapy. To evaluate the potential for clinical applications knowledge on the biodistribution and pharmacokinetics of these micelles is essential. Nuclear imaging technique such as single-photon emission computed tomography (SPECT) and (positron emission tomography) PET can provide clinically relevant information and are also indispensable in the development of new formulations. To apply these techniques to micelles, a radiolabeling process is required. Recently, we have developed a chelator free method for radiolabeling of polymeric micelles. In this work we investigated the radiolabeling mechanism by performing experiments with different polymeric micelles and different metal ions. Furthermore, we also employed Cryo-EM and FT-IR to study the radiolabeling process. The results suggested that the radiolabeling of polymeric micelles was highly dependent on the interaction between the metal ions and the block copolymers composing the core of the micelles. The stability of the radiolabeled micelles depended on whether a solid precipitate was formed in the micelle core. In this study we showed a successful radiolabeling of PCL-PEO based micelles with ^{111}In, ^{177}Lu and ^{89}Zr. Moreover, by performing loading experiments with other metals having radioisotopes of clinical relevance, we demonstrated that this radiolabeling method can be applied to various other radioisotopes.

Introduction

Polymeric micelles have been widely used for delivering various therapeutic agents in cancer treatment and in particular in chemotherapy. [1-3] The main advantages of these micelles are the high encapsulation efficiency of water-insoluble anti-cancer drugs, the versatile functionalization possibilities, and their accumulation at the tumour due to the enhanced permeability and retention (EPR) effect. Due to these properties various formulations have achieved clinical translation.[4] Nevertheless, the biodistribution and especially tumour uptake of polymeric micelles seem to vary between tumour types but also among patients even having the same disease. A way to personalize treatment using polymeric carriers or simply help to predict efficacy based on tumour uptake, is using non-invasive imaging techniques, such as Single Photon Emission Computed Tomography (SPECT) and Positron Emission Tomography (PET). These techniques are commonly applied in drug development and offer also great opportunities to determine the in vivo fate of drug delivery systems. Both techniques detect gamma radiation directly or indirectly emitted by radioisotopes to determine the spatial distribution of radiolabeled compounds. Besides the clinical relevance of SPECT and PET, they are also indispensable in pre-clinical evaluation of nano-carries. [5, 6]

In order to use either PET or SPECT, the micelles need to be radiolabeled. Radiolabeling of micelles is typically done by the conjugation of a chelator to the outer surface of the micelles. The chelator is used to stably coordinate the radioisotopes needed for SPECT or PET. There are two main radiolabeling strategies, i.e. the conjugation of the chelator-radioisotope complex to the already prepared micelles[6, 7] or linking the chelator molecules to the block copolymers followed by their self-assembly and addition of the radioisotopes.[5, 8] Both methods have been successfully applied to radiolabel micelles. However, the conjugation of chelator molecules to the outer surface of the micelles may affect the inherent pharmacokinetics of the nano-carriers. Moreover, it requires an additional synthesis step which increases the complexity of the formulation.[9] Thus, radiolabeling methods without the presence of chelators are desirable.[10]

In previous research we have shown that we can radiolabel PCL-PEO (poly(ε-caprolactone-b-ethylene oxide)) micelles with ^{111}In in the absence of a chelator. The radiolabeling method is fast, easy and the loss of radiolabel is negligible. In this work, we examined the mechanism behind this radiolabeling method in order to provide a general approach for the radiolabeling of polymeric micelles with various radioisotopes. For this purpose we studied the radiolabeling efficiency and stability using different block copolymers (poly(ε-caprolactone-b-ethylene oxide), poly(lactide-b-ethylene oxide), poly(styrene-b-ethylene oxide) and poly(butadiene-b-ethylene oxide)) as well as different radioisotopes (^{111}In, ^{177}Lu and ^{89}Zr). Moreover, we employed FT-IR and Cryo-EM to further elucidate the mechanism behind this radiolabeling method. To broaden the application of this approach, we also tested the loading capacity of the PCL-PEO micelles with other metal ions, including Ho^{3+} and Y^{3+}, which both have clinically applied radioisotopes.

Materials and methods

2.1 Materials

The block copolymers poly(ε-caprolactone-b-ethylene oxide) (including PCL-PEO (6500-5500) and PCL-PEO (10000-5000)), poly(lactide-b-ethylene oxide) (PLA-PEO (10500-5000)), poly(styrene-b-ethylene oxide) (PS-PEO (9500-18000)) and poly(butadiene-b-ethylene oxide) (PBd-PEO (5500-5000)) were bought from Polymer Source (Quebec, Canada). Indium chloride ($InCl_3$), Holmium chloride hexahydrate ($HoCl_3.6H_2O$), Lutetium chloride ($LuCl_3$), 4-(2-hydroxyethyl)-1-piperazineethanesulfonic acid (HEPES), Sephadex G-25 resins and Sepharose 4B gels were bought from Sigma Aldrich (Zwijndrecht, the Netherlands). Zirconium chloride ($ZrCl_4$) was purchased from Alfa Aesar. Yttrium chloride hexahydrate ($YCl_3.6H_2O$) was purchased from Ventron GMBH (Karlsruhe, Germany). HCl, acetonitrile were purchased from Central warehouse L&M. ^{111}In and ^{177}Lu (in 0.01 M HCl solution, the specific activity was 15.5GBq/μg and 0.5GBq/μg for ^{111}In and ^{177}Lu, respectively) were kindly provided by Erasmus Medical Centre (Rotterdam, the Netherlands). ^{89}Zr (in 1M oxalic acid, the specific activity was 8.1~15.4 GBq/μmol) was bought from PerkinElmer® (Groningen, the Netherlands).

2.2 Synthesis

2.2.1 Synthesis of polymeric micelles

The micelles were synthesized by the solvent evaporation method.[7] Briefly, polymer stock solutions were prepared by dissolving PCL-6500, PCL-10000, PBd or PS block copolymer (20 mg) in chloroform (0.2 mL). Then the mixture was added dropwise to 2.3 mL of MQ water and kept stirred overnight to remove organic solvent. The PLA-PEO micelles were synthesized in a slightly different way: PLA-PEO (20 mg) polymer was dissolved in acetonitrile (1.0 mL) and sonicated for 20 min to fully dissolve the polymer powder. Then, the mixture was added to MQ water (4.0 mL) followed by stirring overnight to remove the acetonitrile. After synthesis, the obtained micelles were filtered through filters (220 nm cut-off for the two PCL micelles, 400 nm cut-off for all other micelles) to remove large aggregates.

The micelles composed of PCL-PEO (6500-5500), PCL-PEO (10000-5000), PLA-PEO (10500-5000), PBd-PEO (5500-5000) and PS-PEO (9500-18000) were denoted as PCL-6500, PCL-10000, PLA, PBd and PS micelles respectively.

2.2.2 Radiolabeling with radioisotopes

^{111}In

Before radiolabeling the micelles, HEPES buffer (20 mM, pH = 7.4) was added to the aqueous micelle solution in a volume ratio 1:1. Consequently, 50 kBq of ^{111}In (the volume was dependent on the activity of the stock solution and ranged between 5 to13 µL) was added to 1.0 mL of micelle solution. After 30 min reaction time, size exclusion chromatography (SEC) using in house prepared Sephadex G-25 columns was applied to remove the free ^{111}In from the radiolabeled micelles. HEPES buffer (10 mM, pH = 7.4) was used as the eluent and every 1 mL of the eluent was collected as one fraction. The ^{111}In radiolabeled samples eluted in the 8th to 12th mL fraction. Therefore, a total of 5 mL radiolabeled sample was typically collected.

^{177}Lu

^{177}Lu radiolabeled samples were prepared in the exact same way as the ^{111}In samples, i.e. 50 kBq of ^{177}Lu was used to radiolabel each PCL-PEO micelle sample.

^{89}Zr

The as-purchased ^{89}Zr was dissolved in oxalic acid (1M). Before radiolabeling of the micelles, 2 MBq of ^{89}Zr was stirred in 0.2 mL of HCl solution (pH=2) for at least 4 hours. Then 50 kBq of ^{89}Zr was added to 1.0 mL of micelle solution and stirred for 1 hour, followed by removal of the free ^{89}Zr ions by SEC.

2.2.3 Synthesis of In^{3+} loaded micelles

In^{3+} solution (19.82 mM) was prepared by dissolving $InCl_3$ (2.85 mg) in an HCl solution (0.65 mL, pH = 2). To radiolabel the In^{3+} solution, 60 μL of ^{111}In stock solution (equal to 0.135 MBq at the time of the experiment) was added to non-radioactive indium solution (140 μL) to achieve a final In^{3+} concentration of 13.87 mM. For the loading process, 10 μL of the radiolabeled In^{3+} solution was added to 1.0 mL of the micelles in HEPES buffer (10 mM, pH = 7.4), stirred for 30 mins followed by the removal of free In^{3+} ions by SEC. In this process, HCl solution (pH = 2) was used as the eluent to avoid possible indium precipitation which might elute in the same fraction as the micelles.

2.2.4 Synthesis of micelles loaded with other metal ions

Other metal ion solutions were prepared by dissolving metal chlorides, including $LuCl_3$, $ZrCl_4$, $HoCl_3$ and YCl_3, in HCl solution (pH = 2) under ultrasound to achieve a finial concentration of 10 mM. Then 10 μL of the metal chloride solutions were added to 1.0 mL of PCL-10000 micelles solution in HEPES buffer (10 mM, pH = 7.4) and stirred for 1 hour. Finally, SEC was applied to remove the free metal ions by using HCl solution (pH = 2) as the eluent.

Characterization

3.1 Instruments

Dynamic light scatting (DLS) instrument consisting of a JDS uniphase 633 nm 35 mW laser, an ALV sp 125 s/w 93 goniometer, a fibre detector and a Perkin Elmer photo counter was utilized to obtain the size distributions of the obtained micelles. A cryogenic electron microscope (Cryo-EM) (Jeol JEM 1400) was used to observe the morphology of the micelles and the loading mechanism. A Fourier-transform infrared spectroscopy (FT-IR) (NicoletTM 6700) was used to determine possible interaction between the metal ions and polymer composing the micelles. The spectra were recorded in the range from 4000-400 cm^{-1} with a resolution of 4 cm^{-1}. The automatic Gamma counter (Wallac WIZARD2 2480, Perkin Elmer Technologies) was used to determine the radioactivity of all radiolabeled micelles. An ICP-OES apparatus was applied to detect the loading efficiency of the non-radioactive metals.

3.2 Radiolabeling/Loading efficiency

3.2.1 Radiolabeling efficiency

The formula used to calculate the radiolabeling efficiency (RE) of the micelles was as follow:

RE (%)= (Measured Counts of $^{111}In/^{177}Lu/^{89}Zr$ encapsulated in micelles) / (Measured counts of initially added activity)×100%

3.2.2 Loading efficiency of metal ions

An ICP-OES facility was applied to determine the loading efficiency of the metal ions without activity. To prepare samples for ICP-OES, 1 mL of the metal-loaded PCL-PEO micelles was mixed with 1 mL aqua regia which was followed by ultrasonication (50^{o}C, 4 h) to destroy the micellar structure and dissolve the encapsulated metal ions. Then, MQ water (5.0 mL) was added to prepare the final samples for measurement.

3.3 Stability test

Stability test with DTPA

0.1 mL of DTPA solution (11 mM, in 10 mM HEPES buffer, pH=7.4) was added to 1 mL of the $^{111}In/^{177}Lu/^{89}Zr$ radiolabeled PCL micelles (10 mM HEPES buffer, pH = 7.4). After being incubated for 1 day, the mixture was passed through a SEC column to separate the free radionuclide-DTPA complex (14^{th} – 17^{th} fractions) and the radiolabeled micelles (8^{th} – 12^{th} fractions). The radioactivity left in micelles was measured using the Wallac gamma counter.

The stability test in FBS serum

The radiolabeled samples (0.5 mL) were mixed with the same volume of serum and stored in an incubator at 37°C. After one day of incubation, the mixture was separated by a column (diameter 1 cm, length 30 cm) packed with Sepharose 4B gel and HEPES buffer was applied as the eluent. Similar as the separation with SEC, every 1 mL of the eluent was collected as one fraction. The micelle appeared at fraction 8^{th} to 13^{th}, while the FBS appeared around 17^{th} to 22^{nd} fractions. The activity in each part was measured by the Wallac gamma counter.

Results and analysis

4.1 ^{111}In radiolabeled micelles

We prepared five different micelles, namely PCL-6500, PCL-10000, PLA, PBd, and PS micelles, by the solvent evaporation method. The morphology information of these different micelles were shown in Figure S5.1. Then, we radiolabeled the obtained micelles with ^{111}In by the chelator-free method. As shown in Figure 5.1(a), the PCL-10000 micelles exhibited the highest radiolabeling efficiency (RE) with 92.4 ± 2.41% of ^{111}In encapsulated in the micelles, followed by PCL-6500 micelles with a RE of 83.75 ± 1.49%. The RE of PLA micelles, PBd-micelles, and PS-micelles were respectively 69.7 ± 3.28 %, 56.5 ± 6.80% and 16.1± 2.55%.

The DTPA chelation test is a typical method to evaluate the stability of radiolabeled compounds, in which the free or weakly bonded radioisotopes are taken over by DTPA due to the high stability constant of DTPA complexes with various metals (hence metallic radioisotopes).[11] The representative curve for radiation distribution in each eluent fractions for different micelles was shown in Figure S5.3. As summarized in Figure 5.1(b), there were 7.28± 1.35%, 8.83 ± 0.21%, and 12.88± 1.52% of ^{111}In was released from the PCL-6500, PCL-10000 and PLA micelles, while around 80% of ^{111}In was removed from PBd and PS micelles in a timeframe of 24 hours. This test clearly showed that the PCL and PLA micelles had superior ^{111}In radiolabeling stability compared to that of PBd and PS micelles.

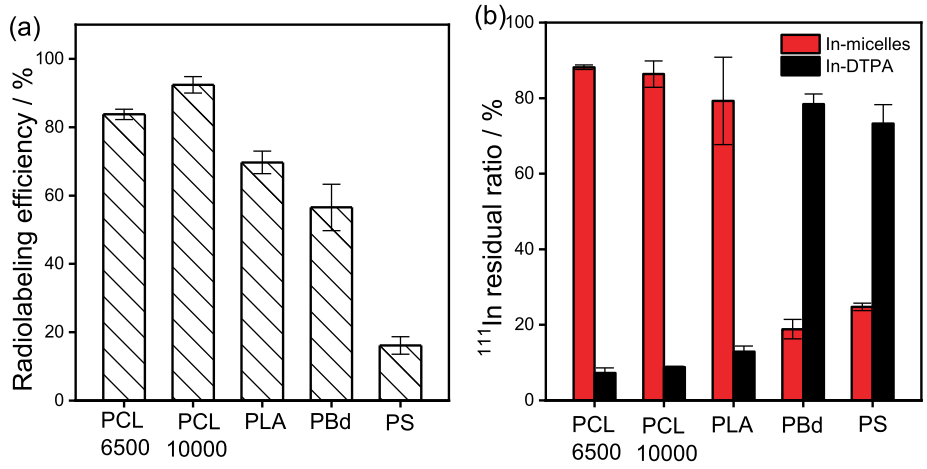

Figure 5.1. (a) The ^{111}In radiolabeling efficiency of micelles composed of different polymers; (b) the ^{111}In radiolabeling stability of micelles challenged with DTPA for 24h (DTPA concentration: 1mM, in 10 mM HEPES buffer with pH = 7.4; polymer concentration: ~0.79 mg/mL for PCL/PBd/ PS micelles and ~0.45 mg/mL for PLA micelles).

4.2 Loading of micelles with non-radioactive Indium

To further check the interaction between In^{3+} ions and PCL-PEO micelles, we measured the loading efficiency of In as function of time by using In^{3+} ions and small amounts of ^{111}In as a radiotracer. Here, we used SEC to separate the free In^{3+} ions from micelles fraction after being reacted for 2, 10 and 30 minutes. The results (Figure S5.4(a)) showed that 8.36 ± 2.99% of In^{3+} ions were already in the micelles after 2 minutes of interaction, which evidently

increased to 30.90 ± 7.04 % for samples reacting for 10 min. Prolonging the reaction period to 30 min, led to 50.78 ± 1.84 % of In^{3+} ions encapsulated in the micelles. These results revealed that the loading of In^{3+} ions by PCL-PEO micelles is a time-dependent process.

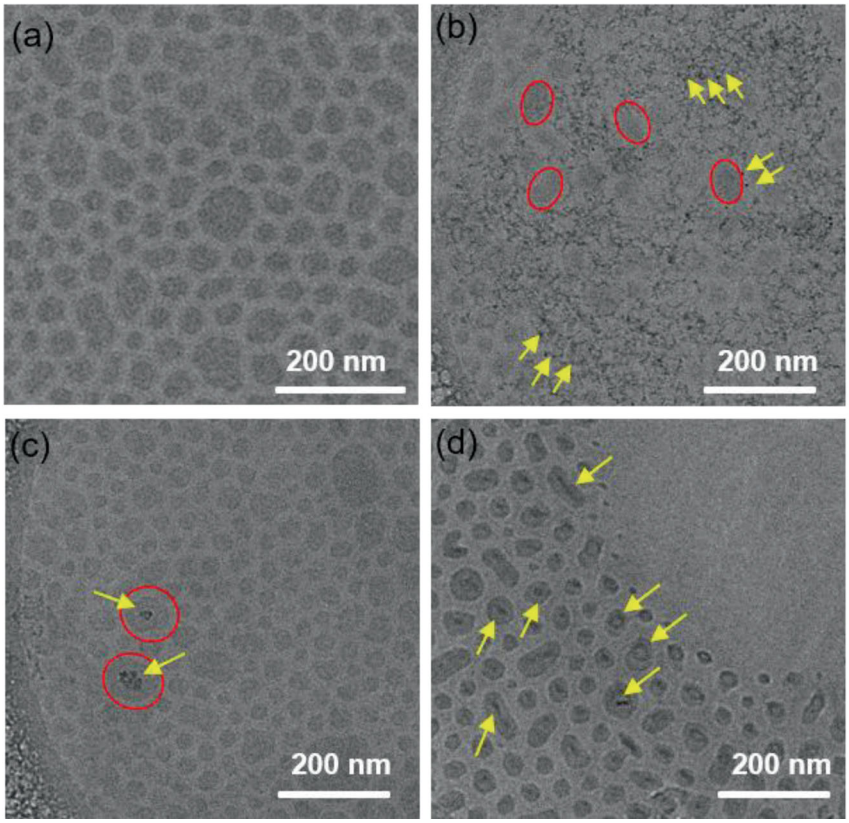

Figure 5.2. Cryo-EM of (a) empty PCL-10000 micelles, and mixture of In^{3+} species and PCL-10000 micelles obtained after reacting for (b) 2 min, (c) 10 min and (d) 30min. (The concentration of the polymer was 4.3 mg/mL in HEPES buffer and the initial In^{3+} concentration was 0.137 mM in HCl aqueous solution, pH = 2.)

Cryo-EM was applied to observe the process of metal ions encapsulation at different time points using PCL-10000 micelles and In^{3+} ions. The samples of Cryo-EM were prepared by immediately freezing the micelles-indium mixture after a reaction period of 2, 10, or 30 min, without separation of the free Indium ions. As shown in Figure 5.2(b-d), the introduction of In^{3+} ions led to the appearance of dark dots in the samples, which could not be found in the images of micelles (see Figure 5.2(a)). We assumed that these dark dots correspond to $In(OH)_{3s}$ nanoparticles. After 2 min of reaction, the majority of indium precipitates (yellow

arrows) were still outside the micelles (red circles). When the reaction reached 10 min, the indium aggregation outside the micelles decreased (Figure S5.4(c)), and the dark dots started to appear inside the micelles (see Figure 5.2(c)) with most of the micelles still being empty. After 30 mins, clear dark dots could be observed in the majority of the micelles (Figure 5.3 (d)). The encapsulated In nanoparticles (Figure 5.2(c) and (d)) had at that point various morphologies, like nano-rod and nano-circles structures, different than the ones in Figure 5.2(b) where mostly spherical nanoparticles were found. It has to be noted that these experiments are performed at higher In concentration (0.137 mM) than typically used for the radiolabeling studies, in order to be able to observe the In precipitates.

To get a better insight behind this mechanism, we employed the free software CHEAQs to determine the speciation of indium species at different pH values and concentrations. HEPES buffer is known to have limited coordination ability with metal ions, therefore, the influence of HEPES in this case was neglected.[17] First, the influence of pH values on the metal speciation was evaluated as shown in Figure 5.3(a). Under acidic conditions, i.e. pH lower than 4, the free In^{3+} ions are the dominant species; between pH 5 to 10, the indium species existed as aqueous $In(OH)_3$ which has no charge; for pH higher than 9, the $In(OH)_4^-$ with negative charge is the main species in the system. The CHEAQs speciation results in Figure 5.3(a) indicate that the ^{111}In mainly existed as $In(OH)_{3aq}$ in the aqueous system during the radiolabeling process when the pH value was 7.4. At higher concentration, the aqueous $In(OH)_{3aq}$ converted to $In(OH)_{3s}$ solids (Figure 5.3(b)).

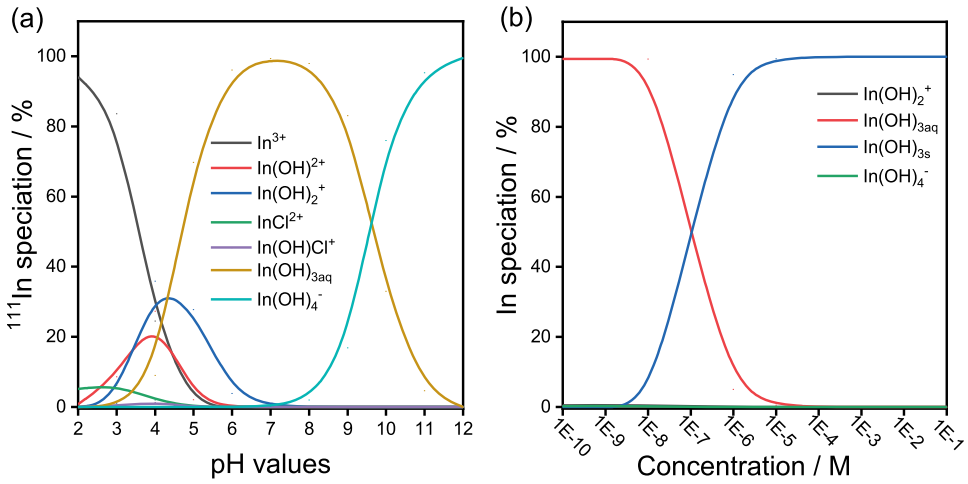

Figure 5.3. The speciation of (a) Indium at equilibrium in water as a function of pH (In concentration: $2.9*10^{-11}$ M (50 kBq as the initial activity), Cl^- concentration: 0.1 mM) and (b) ^{111}In in water at equilibrium as a function of the concentration (pH: 7, Cl^- concentration: 0.1 mM). These figures are based on data calculated by CHEAQS. For more details see Table S5.1 and S5.2)

4.3 Loading of micelles with other metal ions

To broaden the application of the chelator-free method, we explored the possibility for PCL-10000 interacting with other metals. In this case, for sake of simplification and to avoid unnecessary radiation dose exposure, we used the following non-radioactive metal ions Lu^{3+}, Zr^{4+}, Ho^{3+}, and Y^{3+} to interact with PCL-10000 micelles. All of the selected metal ions have radioisotopes already applied in the clinic. ^{89}Zr is a typical β^+ emitter and widely used as radioactive tracers in PET imaging. ^{177}Lu, ^{90}Y and ^{166}Ho are β^- emitters which are used in radionuclide cancer therapy. The addition of these metal ions did not pose significant influence on the morphology of the PCL-10000 micelles (Figure S5.2). As summarized in Table 5.1, the PCL-10000 micelles appeared capable of interacting with different metal ions when applying initial metal concentration of around 0.1 mM. The loading efficiency of Ho^{3+} ions was up to 31.21 ± 4.49 %, indicating a strong interaction between the Ho species and PCL-10000 micelles. In contrast, the interaction with Lu^{3+} and Zr^{4+} species was relatively weaker, achieving loading efficiency of 2.33 ± 0.22 % and 7.41 ± 0.22 %, respectively.

Table 5.1. Loading efficiency of metal ions in PCL-10000 micelles.

Samples	Loading efficiency (%)
Lu-PCL-10000	2.33 ± 0.22
Zr-PCL-10000	7.41 ± 0.22
Ho-PCL-10000	31.21 ± 4.49
Y-PCL-10000	13.70 ± 0.82

* The standard deviation is based on experimental uncertainty of three samples.

The results in Figure 5.1 suggested that PCL and PLA based micelles had much better loading capacity as well as stability. Both polymers have a carbonyl group which is known to be able to have weak coordination with metal ions.[12] To investigate whether this is the cause for the higher loading capacity, FT-IR was applied to detect whether certain functional groups of the polymers change upon addition of the different metal ions. In Figure 5.4(a), the peak at 1100 cm^{-1} corresponds to the -C-O-C- stretch in the PEO segment, while the peak at approximately 1722 cm^{-1} is due to the C=O stretch in the PCL block.[13, 14] The peaks around 2864 cm^{-1} and 1943 cm^{-1} are due to the existence of the symmetric and asymmetric CH_2 moiety, while the peak at 1294 cm^{-1} is due to the C-O and C-C stretch in the crystalline phase of the PCL block polymer.[15,16] No noticeable shifts could be observed by inspecting the spectra of the -C=O group (see Figure 5.4(b)). Similarly, no changes could be observed from the enlarged spectra of the -C-O-C- group. (Figure 5.4(c)). The FT-IR results indicated that there was no interaction between these metal ions and carbonyl groups or the interactions were too weak to be detected.

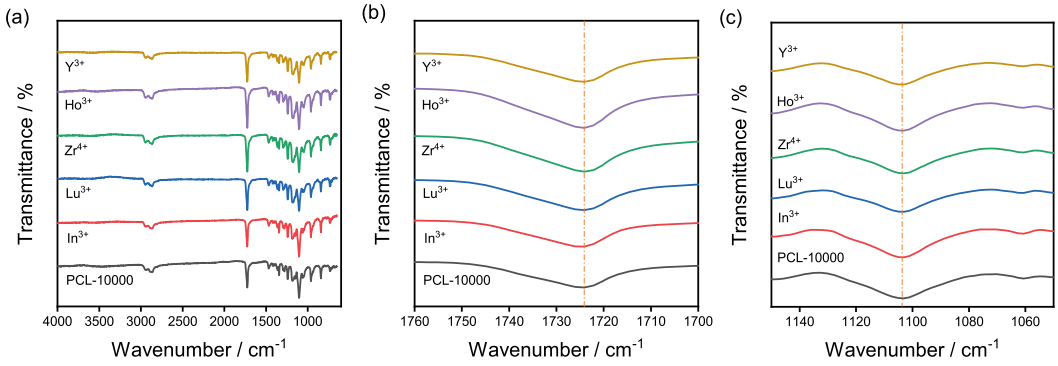

Figure 5.4. (a) The full FT-IR spectra of PCL-10000 micelles loaded with metal ions (In^{3+}, Lu^{3+}, Zr^{4+}, Ho^{3+} and Y^{3+}); (b) the enlarged FT-IR spectra of -C=O; (c) The enlarged FT-IR spectra of -C-O-C.

4.4 Radiolabeling with other radioisotopes

So far we have radiolabeled micelles with SPECT radioisotopes. Here, we have attempted to radiolabel the micelles with PET radioisotope (^{89}Zr) as well as with a therapeutic radioisotope, i.e. ^{177}Lu. Figure 5.5(a) shows that PCL-6500 micelles had excellent radiolabeling efficiency for all radioisotopes used (i.e. ^{111}In, ^{89}Zr and ^{177}Lu). The radiolabeling efficiency for ^{177}Lu and ^{89}Zr is 94.21± 0.54 % and 84.75 ± 1.83%, which was comparable to that of ^{111}In. However, the radiolabeling stability differed per radioisotope. The ^{111}In radiolabeled micelles showed the best stability in which only 7.28 ± 1.35% and 3.48 ± 1.16 % of ^{111}In was removed by DTPA and FBS after one day of incubation. Contrarily, the poor stability of ^{177}Lu radiolabeled samples resulted in 78.35 ± 0.28% and 63.33± 2.27 % of ^{177}Lu loss from the PCL-micelles under DTPA and serum challenge, respectively. The ^{89}Zr radiolabeled micelles, were slightly more stable with 58.03 ± 0.93% and 26.74 ± 0.73% of the encapsulated ^{89}Zr lost when challenged with DTPA and serum, respectively.

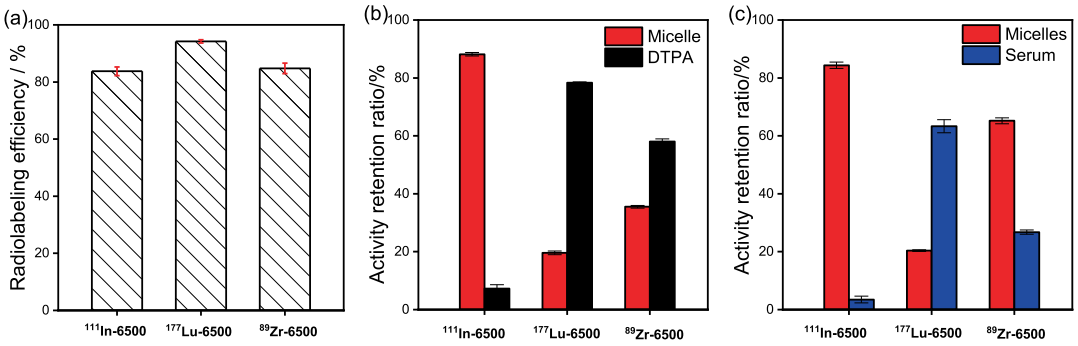

Figure 5.5. (a) The radiolabeling efficiency of PCL-6500 micelles radiolabeled with ^{111}In/^{177}Lu/^{89}Zr. Radiolabeling stability using (b) DTPA (incubation time 24h, room temperature) and (c) Serum (incubation time 24h, 37°C). (Polymer concentration was 4.35 mg/mL for PCL-6500 micelle; ~0.79 mg/mL in the DTPA challenge study and ~0.44 mg/mL in the serum stability test).

The high radiolabeling efficiency proved that the PCL-6500 micelles could interact with ^{177}Lu and ^{89}Zr, while the poor stability indicated that the interaction was not as strong as that for ^{111}In. To determine the role of ion speciation, we used CHEAQS again. As shown in Figure S5.5 (a,b), lutetium species have quite complex metal speciation as function of pH and concentration. Free Lu^{3+} ions are the major species under acidic conditions, while $Lu(OH)_4^-$ ions are mainly formed in alkaline environment. The percentage of $Lu(OH)_{3aq}$ increases to a maximum around pH 8 but it is still not the dominant specie under these conditions. $Lu(OH)_{3s}$ only appears at concentration above $1 \cdot 10^{-6}$ M and at a pH of 8. In the case of Zr^{4+} ions, they form $Zr(OH)_{4aq}$ once the pH is higher than 3. However, it is much harder for Zr^{4+} ions to precipitate, requiring a concentration higher than $1 \cdot 10^{-4}$ M.

According to the speciation results of CHEAQs in Figure S5.5(a,b), the lutetium species with positive charges are the main species under our experimental conditions. In order to check whether precipitation is important for the stability of radiolabeling we performed several test experiments. Based on the radiolabeling of PLA micelles shown in Figure S5.6 (b), we noticed that a slight alkaline condition maybe better for the radiolabeling with ^{177}Lu. Therefore, instead of using the standard pH of 7.4, we slightly increased the pH to 8.1. Moreover, according to the CHEAQs simulation results, the addition of phosphate ions would help to form lutetium precipitations. Therefore, in this case, after preparing the ^{177}Lu-radiolabeled micelles by the standard approach, we added 10 µL of phosphate ions with

different concentrations to the micelle solution. After 1 hour of reaction, the DTPA and serum stability tests were carried out.

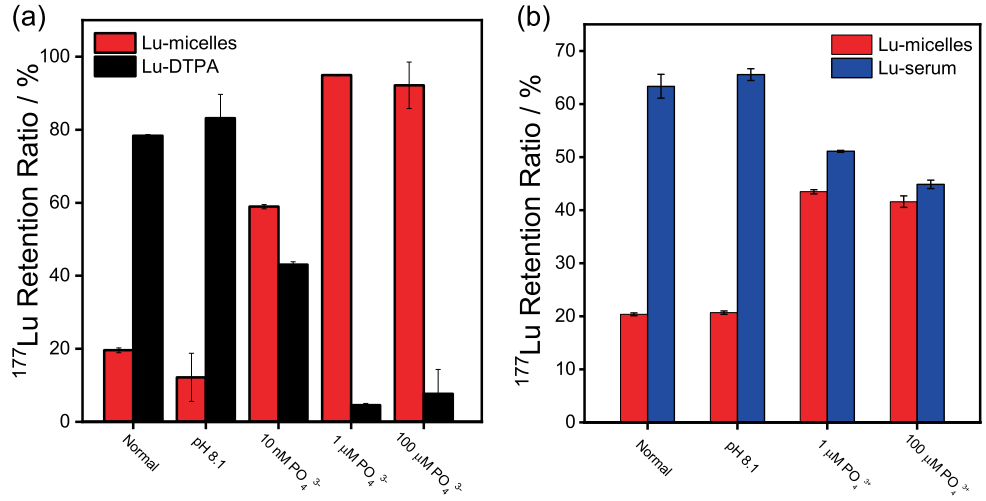

Figure 5.6. The ^{177}Lu radiolabeling stability in (a) DTPA solution and (b) serum stability test of ^{177}Lu radiolabeled PCL-6500 micelles prepared under different conditions. (Polymer concentration: ~0.79 mg/mL in DTPA test and ~0.44 mg/mL in serum stability test).

The results for the DTPA and serum stability tests of the ^{177}Lu radiolabeled samples obtained in these experiments are shown in Figure 5.6(a, b). Compared to the ^{177}Lu prepared under the "normal" approach, the samples radiolabeled at a pH of 8.1 did not show a better ^{177}Lu retention. However, the addition of PO_4^{3-} evidently improved the ^{177}Lu retention in the presence of DTPA, even at concentrations as low as 10 nM (final PO_4^{3-} concentration in the micelles solution). When increasing the concentration of PO_4^{3-} ligands to 1μM and 100 μM, more than 90% of ^{177}Lu was kept inside the micelles after one day of incubation with DTPA. However, although the ^{177}Lu stability in the serum test was evidently improved by the introduction of PO_4^{3-} ligands, still 50% of ^{177}Lu appeared in the serum fraction.

The CHEAQS speciation results (Figure S5.5(c and d)) showed that the Zr^{4+} ions could easily form $Zr(OH)_{4aq}$ regardless of pH values, but required a high concentration to form precipitated $Zr(OH)_{4s}$. Thus, to increase the zirconium concentration, 10 μL of Zr^{4+} stock solution with the concentration of 1 μM and 50 μM (in HCL, pH =2) was added during the normal ^{89}Zr radiolabeling process, which resulted in the final non-radioactive Zr^{4+} concentrations of around 10 nM and 495 nM. The initial activity 50 kBq of ^{89}Zr was equal to

~1.5 nM of radioactive Zr^{4+} under these experimental condition (specific activity was ~0.11 GBq/μg). Therefore, the presence of non-radioactive Zr^{4+} ions increased the total Zr^{4+} concentration to 11.5 nM and 496.5 nM, respectively. As summarized in Figure 5.7(a), the radiolabeling efficiency decreased with increasing Zr^{4+} concentration, and 35.28 ± 0.56% of zirconium ions reacted with PCL-6500 micelles under Zr^{4+} concentration of 496.5 nM. However, the increased concentration of Zr^{4+} did not pose any significant influence on the stability under DTPA challenge, i.e. 38.04 ± 14.53% and 51.71 ± 3.18% of the encapsulated zirconium species were captured by DTPA after 24 hour of interaction. In contrast, the presence of extra Zr^{4+} ions could evidently increase the stability in serum.

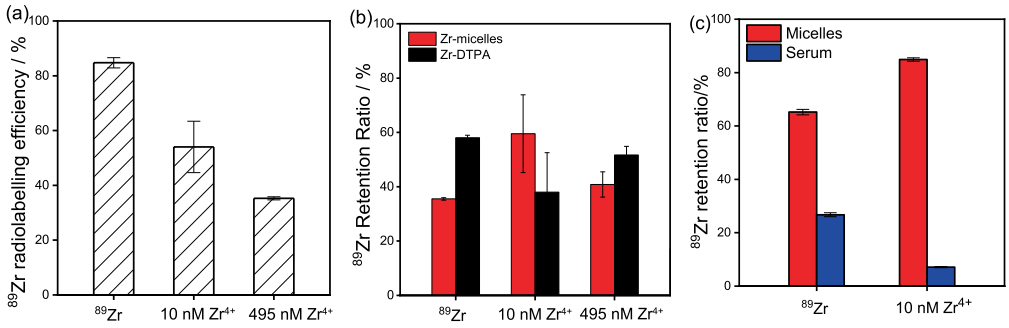

Figure 5.7.(a) The radiolabeling efficiency of ^{89}Zr-radiolabeled PCL-6500 micelles prepared at different Zr concentrations; (b) stability in the presence of DTPA and (c) serum stability at different Zr concentrations. (Polymer concentration was 4.3 mg/mL in radiolabeling process, ~0.79 mg/mL in the DTPA test and ~0.44 mg/mL in the serum stability test).

4.5 Discussion

According to the above-mentioned results, the interaction process between $^{111}In/In^{3+}$ and PCL-PEO micelles could be described as followed: once administered into the system, In species interact with the micellar core, although the nature of this interaction remains unknown. At a certain concentration inside the core, $In(OH)_{3s}$ is most likely formed. It is not clear whether Indium precipitates are already formed before entering the micelles or afterwards. Although the Cryo-EM images suggest that In precipitates could be formed outside the micelles, the non-radioactive In concentration used for these experiments was much higher than in the radiolabeling experiments. It is also possible that due to the

hydrophobic environment in the core and the increasing amount of indium species entering the micelles, precipitates were formed at a certain concentration. The appearance of Indium precipitates in the core of the micelles indicated that this method indeed radiolabeled the core, so in this way preserving the inherent surface properties of the micelles.

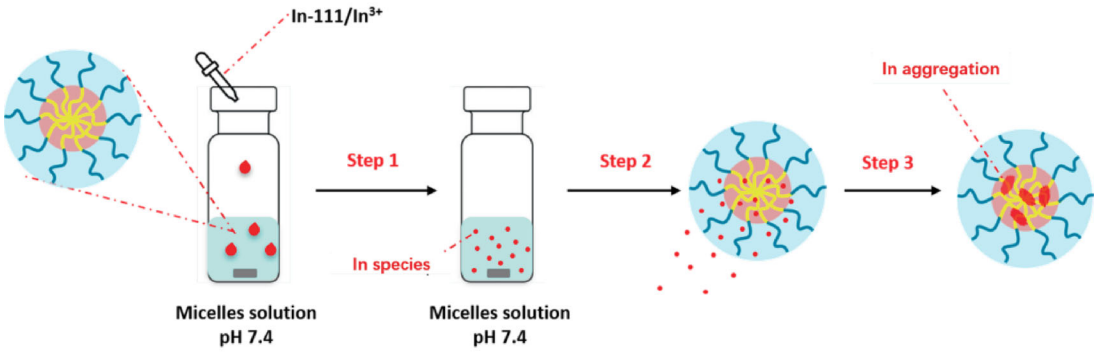

Scheme 5.1: The loading mechanism of In in PCL-PEO micelles. The interaction between In^{3+} ions and PCL-PEO micelles can be briefly divided into 3 steps. Step 1: the quick formation of $In(OH)_{3aq}$ in the aqueous system; Step 2: the migration of $In(OH)_3$ into the micelles; Step 3: the formation of $In(OH)_{3s}$ in the core of the micelles.

According to CHEAQS, during the radiolabeling Indium ions exist as $In(OH)_{3aq}$ in the absence of micelles. However, the presence of micelles in the system might influence the indium speciation. To check this, a small experiment was done by adding 10 µL of the In^{3+} stock solution (concentration is 13.87 mM) to 1 mL of HEPES buffer (10 mM, pH 7.4) with and without micelles. Clear precipitation could be observed on the wall of the vial within 5 min after adding In^{3+} ions to the vial without micelles, while no visible aggregation could be found in the micelle solution (Figure S5.7). The observed phenomenon suggested that $In(OH)_{3aq}$ appeared in the aqueous system quickly and that it could cluster into $In(OH)_{3s}$ precipitates within 5 mins. In the presence of micelles, the $In(OH)_3$ species might prefer to interact with PCL-10000 micelles rather than form large $In(OH)_3$ precipitates. Additionally, if micelles were added to the precipitated In solution, the precipitates were still observed on the wall of the container, suggesting that if $In(OH)_{3s}$ reach a certain size they were certainly not incorporated in the micelles. Taking these experiments into account, we can speculate that the interaction of $In(OH)_3$ with the micelles was faster than the formation of sufficiently

large In precipitates. However, our experiment could not reveal which species of In interacted with the PCL-PEO micelles, $In(OH)_{3aq}$ complexes or small $In(OH)_{3s}$ precipitates.

By comparing the radiolabeling behavior of various different polymeric micelles, it is clear that the block copolymer type also played a role in the radiolabeling process. The block copolymers having carbonyl groups, i.e. PCL and PLA micelles, appeared to have better interaction with the ^{111}In species, although the C=O groups did not show any detectable change according to the FT-IR spectra. There are quite a lot of studies focusing on the interaction between metal ions and polymers,[18, 19] but we could not find studies in similar systems as ours where ions are added after the formation of the micelles. The interaction between metal ions and polymer are categorized in five types, namely pi-complexation, abstraction, oxidative addition, electron transfer and cluster formation.[12]. In this work, we believe that cluster formation was the reason for the successful ^{111}In radiolabeling.

The radiolabeling with ^{177}Lu and ^{89}Zr indicated that the metal speciation was another significant factor for successful metal-micelle interaction. Although the PCL-PEO micelles were capable of interacting with ^{177}Lu, the bond between Lu species and the core of the micelles was weak and not sufficient to prevent DTPA from stealing away the metal ions. The addition of phosphate buffer saline (PBS) could significantly improve the loss of ^{177}Lu under DTPA challenge, indicating that the formation of precipitates, i.e. $LuPO_4$ in this case, was essential for a stable radiolabeling. The low stability in serum of the ^{177}Lu loaded micelles was unexpected and requires further studies. In the case of the loading with ^{89}Zr, $Zr(OH)_{4aq}$ was expected to be formed under these experimental conditions, according to CHEAQs calculation results. However, the low Zr concentration was not sufficient to result in $Zr(OH)_{4s}$ precipitates. By increasing the amount of Zr^{4+} metal ions, the $Zr(OH)_4$ displayed a stronger interaction with PCL-PEO micelles, though in this case we could not confirm whether $Zr(OH)_{4s}$ was formed or not. Based on the radiolabeling performance of ^{111}In, ^{177}Lu and ^{89}Zr, the formation of precipitates inside the micelles appears to be a key point for a stable radiolabeling.

Conclusion

In this chapter, the mechanism behind the chelator free method was investigated. According to the obtained results we can conclude that two important requirements need to be fulfilled for a successful radiolabeling and good radiolabeling stability. First, the metallic species need to be attracted to the block copolymer composing the core of the micelles, second a precipitate should be formed in order to have sufficient radiolabeling stability. The exact nature of the interaction between the block copolymers and the metallic species remains unknown. However, taking into account these two requirements, we showed that the radiolabeling of different type of micelles and different radioisotopes could be successfully achieved, opening new radiolabeling possibilities for different polymeric nano-carriers.

Reference

[1] Y. Li, T. Thambi, D.S. Lee, Co-Delivery of Drugs and Genes Using Polymeric Nanoparticles for Synergistic Cancer Therapeutic Effects, *Adv Healthc Mater*. **2018**, 7.

[2] D.Y. Fan, Y. Tian, Z.J. Liu, Injectable Hydrogels for Localized Cancer Therapy, *Front Chem*. **2019**, 7, 675.

[3] A. Sharma, K. Vaghasiya, P. Gupta, A.K. Singh, U.D. Gupta, R.K. Verma, Dynamic Mucus Penetrating Microspheres for Efficient Pulmonary Delivery and Enhanced Efficacy of Host Defence Peptide (HDP) in Experimental Tuberculosis, *J Control Release*. **2020**, 324, 17-33.

[4] A. Varela-Moreira, Y. Shi, M.H.A.M. Fens, T. Lammers, W.E. Hennink, R.M. Schiffelers, Clinical Application of Polymeric Micelles for the Treatment of Cancer, *Mater. Chem. Front*. **2017**, 1, 1485-1501.

[5] Y. Miura, A.B. Tsuji, A. Sugyo, H. Sudo, I. Aoki, M. Inubushi, M. Yashiro, K. Hirakawa, H. Cabral, N. Nishiyama, T. Saga, K. Kataoka, Polymeric Micelle Platform for Multimodal Tomographic Imaging to Detect Scirrhous Gastric Cancer, ACS Biomater. Sci. Eng. **2015**, 1, 1067-1076.

[6] J. Sun, L. Sun, J. Li, J. Xu, Z. Wan, Z. Ouyang, L. Liang, S. Li, D. Zeng, A Multi-Functional Polymeric Carrier for Simultaneous Positron Emission Tomography Imaging and Combination Therapy, *Acta Biomater*. **2018**, 75, 312-322.

[7] A.C. Laan, C. Santini, L. Jennings, M. de Jong, M.R. Bernsen, A.G. Denkova, Radiolabeling Polymeric Micelles for In Vivo Evaluation: A Novel, Fast, and Facile Method, *EJNMMI Res*. **2016**, 6, 12.

[8] B. Hoang, H. Lee, R.M. Reilly, C. Allen, Noninvasive Monitoring of the Fate of ^{111}In-Labeled Block Copolymer Micelles by High Resolution and High Sensitivity microSPECT/CT Imaging, *Mol Pharm*. **2009**, 6, 581-592.

[9] F. Chen, P.A. Ellison, C.M. Lewis, H. Hong, Y. Zhang, S. Shi, R. Hernandez, M.E. Meyerand, T.E. Barnhart, W. Cai, Chelator-Free Synthesis of A Dual-Modality PET/MRI Agent*, Angew Chem Int Ed Engl*. **2013**, 52, 13319-13323.

[10] S. Goel, F. Chen, E.B. Ehlerding, W. Cai, Intrinsically Radiolabeled Nanoparticles: An Emerging Paradigm, *Small.* **2014**, 10, 3825-3830.

[11] Y. Liu, G. Liu, D. Hnatowich, A Brief Review of Chelators for Radiolabeling Oligomers, *Materials.* **2010**, 3, 3204-3217.

[12] M.P. Andrew, Metallization of Polymers, Reactions of Metal Atoms with Monomers and Polymers, **1990**, pp. 242-264. DOI: 10.1021/bk-1990-0440.ch018

[13] T. Chen, C. Fan, Large-Pore Mesostructured Silicas Templated from Amphiphilic Diblock Copolymer PEO-b-PCL: Synthesis, Structure, and Methyl Orange Adsorption, *J. Porous Mater*. **2013**, 20, 927-936.

[14] A. Huang, Y. Jiang, B. Napiwocki, H. Mi, X. Peng, L.-S. Turng, Fabrication of Poly(ε-caprolactone) Tissue Engineering Scaffolds with Fibrillated and Interconnected Pores Utilizing Microcellular Injection Molding and Polymer Leaching, *RSC Adv*. **2017**, 7, 43432-43444.

[15] S. Petrova, I. Kolev, S. Miloshev, M.D. Apostolova, R. Mateva, Synthesis of Amphiphilic [PEO(PCL)$_{(2)}$] Triarm Star-Shaped Block Copolymers: A Promising System for in Cell Delivery, *J Mater Sci Mater Med*. **2012**, 23, 1225-1234.

[16] M.I.E. Gohary, B.M.A.E. Hady, A.A.A. Saeed, E. Tolba, A.M.I.E. Rashedi, S. Saleh, Electrospinning of Doxorubicin Loaded Silica/Poly(ε-caprolactone) Hybrid Fiber Mats for Sustained Drug Release, *Advances in Natural Sciences: Nanoscience and Nanotechnology*. **2018**, 9.

[17] Hopax Fine Chemicals, Biological Buffers and Their Interactions with Metal Ions, **2018** Oct, Retrieved from URL: https://www.hopaxfc.com/en/blog/biological-buffers-and-their-interactions-with-metal-ions

[18] J. Wang, On the Stability and Imaging Applications of Metal-containing Coacervate Micelles, PhD dissertation, Wageningen University, **2012**.

[19] J. Wang, M.A. Cohen Stuart, A.T.M. Marcelis, M. Colomb-Delsuc, S. Otto, J. van der Gucht, Stable Polymer Micelles Formed by Metal Coordination, *Macromolecules*. **2012**, 45 7179-7185.

Appendix

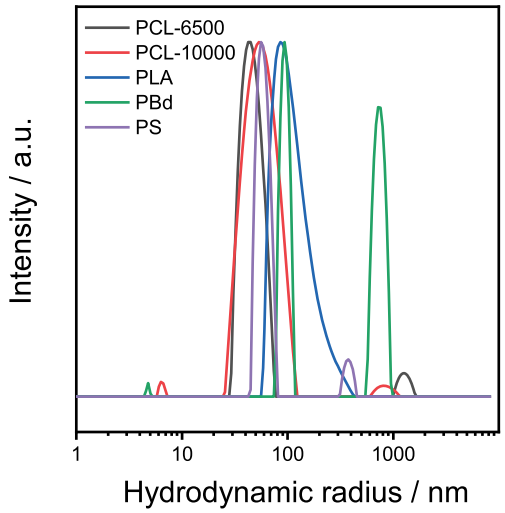

Figure S5.1. The size distribution of the different polymeric micelles before filtration. (Polymer concentration was 0.435 mg/mL for DLS measurement.)

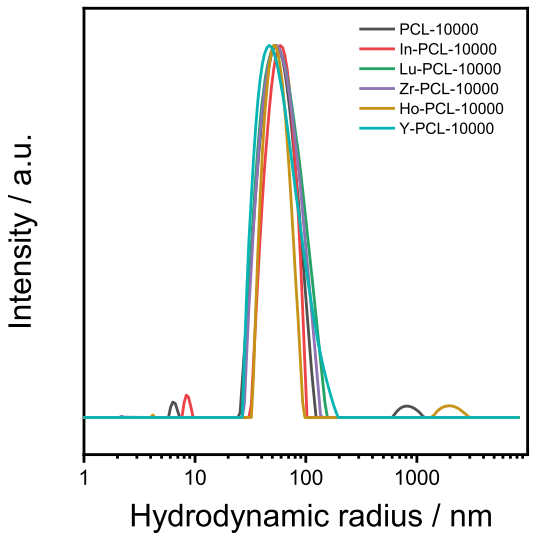

Figure S5.2. The size distribution of the metal loaded PCL-10000 micelles. (Polymer concentration was 4.35 mg/mL for the reaction, and 0.435 mg/mL for DLS measurement.)

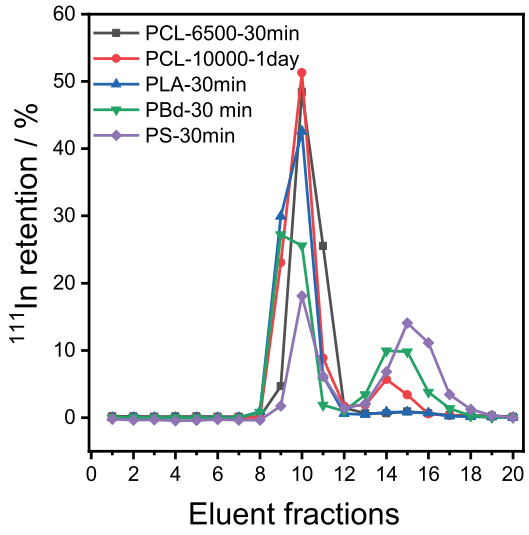

Figure S5.3. The ^{111}In ratio in every eluent fraction collected after SEC of radiolabeled micelles under DTPA challenge. (DTPA concentration: 1mM, polymer concentration: ~0.79 mg/mL for PCL/PBd/ PS micelles and ~0.45 mg/mL for PLA micelles).

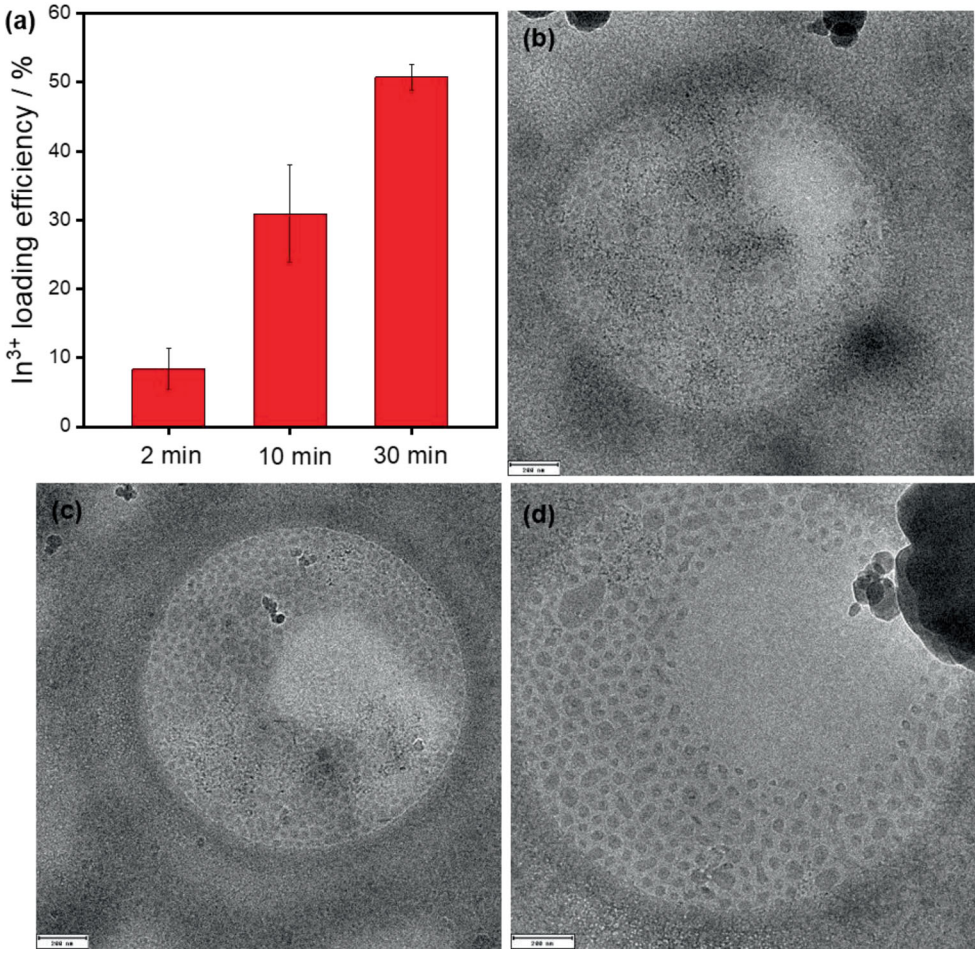

Figure S5.4. The In^{3+} loading efficiency of PCL-10000 micelles after interacting with ^{111}In radiolabeled In^{3+} ions for different times: 2 min, 10 min and 30 min. Cryo-EM of PCL-10000 micelles after reacting with In^{3+} ions for (b) 2 min; (c) 10 min and (d) 30 min. (For sample preparation: the concentration of polymers were 4.3 mg/mL in HEPES buffer; the In^{3+} concentration was 0.137 mM.)

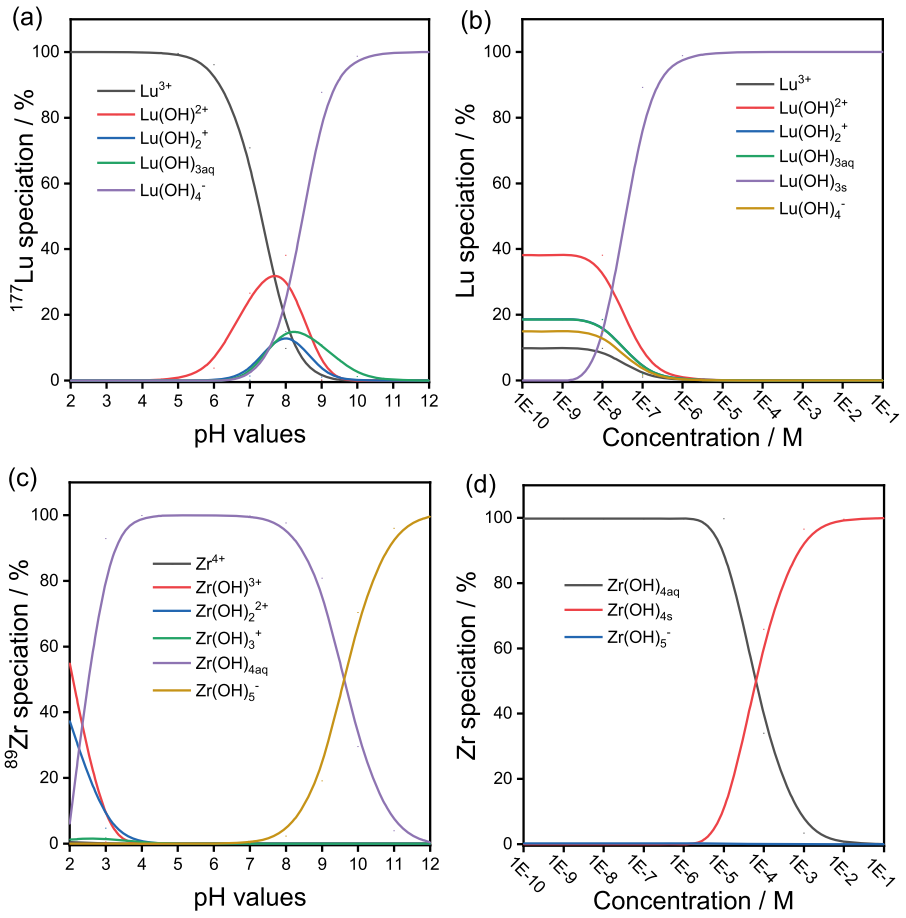

Figure S5.5. The speciation of (a) ^{177}Lu and (c) ^{89}Zr at equilibrium as a function of different pH values (50 kBq was used as the initial activity, Cl^- concentration: 0.1 mM). The speciation of (b) ^{177}Lu and (d) ^{89}Zr at equilibrium as a function of different concentrations (the pH for zirconium is 7, for lutetium the pH is 8; Cl^- concentration: 0.1 mM). These figures are based on plotted CHEAQS data points, see Table S5.1 and Table S5.2).

We also investigated the influence of pH on the interaction between the micelles and ^{177}Lu. Rather than using PCL-6500 micelles, PLA micelles were also applied for the loading with ^{177}Lu. As shown in Figure S5.6(b), the loading of ^{177}Lu in PLA micelles was influenced by the pH. The ^{177}Lu radiolabeling efficiency of PLA micelles was 19.90 ± 3.27% at a pH of 7.4, which increased to 56.07 ± 5.85% at a pH of 8.5 and decreased to 4.10 ± 0.31% at a pH of 10. Lutetium ions would mainly be present as charged species at a higher or lower pH. The fact that PLA micelles showed poor loading ability at a lower or higher pH indicated that these charged complexes did not interact well with PLA When the aqueous solution was set

a pH of 8, 18.54% of the Lu^{3+} ions formed $Lu(OH)_{3aq}$, which could play an essential role for the radiolabeling process.

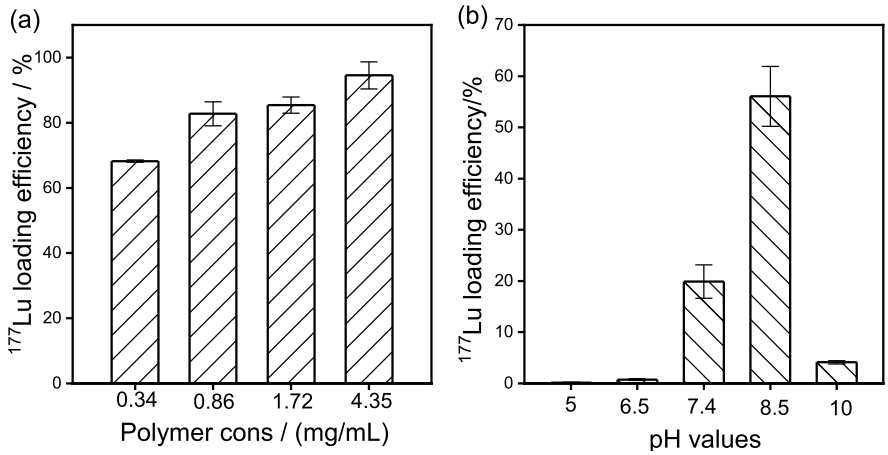

Figure S5.6. The ^{177}Lu loading efficiency of (a)PCL-6500 micelles as a function of polymer concentration and (b) PLA micelles as a function of pH (Polymer concentration is 2.5 mg/mL for PLA micelles).

10 μL of In^{3+} ions stock solution was added to HEPES buffer without the presence of micelles, evident aggregation could be observed within 5 min which attached to the walls of vials. These precipitates were not observed when adding In^{3+} ions to the PCL-10000 micelles. (Figure S5.7). The absence of Indium aggregates in micelle solution suggested that the micelles strongly interact with the indiums species preventing the formation of $InOH_{(3)s}$. To test the stability of the In aggregates, we first added the 10 μL of Indium stock solution (13.87 mM, in HCl with pH 2) to 1 mL of HEPES buffer (10 mM, pH 7.4). 30 min was given to allow the indium to fully aggregate. Later on, 100 μL of DTPA solution (11 mM, in HEPES buffer) was added to the above mixture. After ~2 min, all the In aggregates disappeared, revealing the bonding between the In aggerates was not as strong as the coordination bond between In^{3+} and DTPA under these experimental conditions.

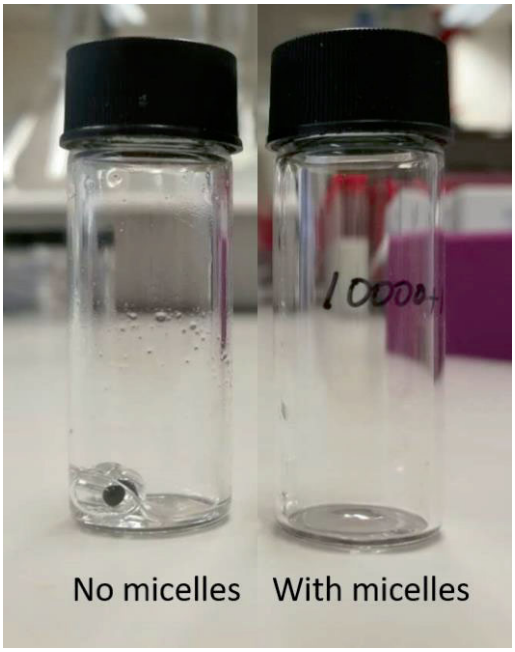

Figure S5.7. Left) The empty vial in which In^{3+} ions were added to HEPEs buffer at pH 7.4. Right) the empty vial after adding In^{3+} ions in HEPEs buffer with pH 7.4 to PCL-1000 micelles. The concentration for In^{3+} was 0.137 mM.

Using CHEAQs to speculate the metal speciations

Assumption: the specific activity (SA) of the activity was as followed (according to the supplier):

^{111}In SA 15.5 GBq/μg

^{177}Lu SA 0.5 GBq/μg

^{89}Zr SA 0.11 GBq/μg

So for 50 kBq activity in 1 mL solutions (without micelles):

Mass In ions = 50 kBq/(15.5 GBq/ug) = $3.2*10^{-6}$ ug ; Con In ions = ($3.2*10^{-6}$ ug / 111 g/mol)/($1*10^{-3}$ L) = $2.88*10^{-11}$ M

Mass Lu ions = 50 kBq/(0.5GBq/ug) = $1*10^{-4}$ ug ; Con Lu ions = ($1*10^{-4}$ ug / 177 g/mol)/($1*10^{-3}$ L) = $5.71*10^{-10}$ M

Mass Zr ions = 50 kBq/(0.11 GBq/ug) = $4.55*10^{-4}$ ug ; Con Zr ions = ($4.55*10^{-4}$ ug / 89 g/mol)/($1*10^{-3}$ L) = $1.48*10^{-9}$ M

Table S5.1. Metal species and their distribution with 50 kBq of $^{111}In/^{177}Lu/^{89}Zr$ as a function of varying pH values.

Indium	Parameters: Con(In) = 2.88E-011 M; Con(Cl)1E-004 M;										
Species	pH 2	pH 3	pH 4	pH 5	pH 6	pH 7	pH 8	pH 9	pH 10	pH 11	pH 12
Free In^{3+}	94.09*	83.65	24.50	0.19							
$In(OH)^{2+}$	0.75	8.65	27.35	2.10							
$In(OH)_2^{+}$		1.08	35.89	27.82	3.83	0.4					
$InCl^{2+}$	5.11	6.19	1.99	0.1							
$In(OH)Cl^{+}$		0.39	1.3								
$In(OH)_{3\ aq}$			8.97	69.77	96.12	99.40	97.98	83.15	32.97	4.62	0.46
$In(OH)_4^{-}$						0.20	1.98	16.85	76.02	95.38	99.54
Lutetium	Parameters: Con(Lu) =5.71E-010 M; Con(Cl)1E-004;										
Free Lu^{3+}	100*	100	99.96	99.61	96.24	70.91	9.80	0.01			
$Lu(OH)^{2+}$				0.39	3.75	27.61	38.15	0.22			
$Lu(OH)_2^{+}$						1.34	18.56	1.09			
$Lu(OH)_{3\ aq}$						0.13	18.54	10.88	1.22	0.12	
$Lu(OH)_4^{-}$							14.95	87.80	98.76	99.88	99.99
Zirconium	Parameters: Con(Zr) = 1.48E-009M; Con(Cl) = 1E-004										
Free Zr^{4+}	0.47										
$Zr(OH)^{3+}$	55.00	0.54									
$Zr(OH)_2^{2+}$	37.40	4.76									
$Zr(OH)_3^{+}$	1.18	1.76	0.19								
$Zr(OH)_{4\ aq}$	5.94	92.94	99.77	99.98	99.97	99.76	97.68	80.83	29.59	3.97	0.39
$Zr(OH)_5^{-}$						0.24	2.32	19.17	70.41	96.02	99.61

* The percentage of certain species in all.

Table S5.2. Metal species and their distribution under optimized pH as a function of varying concentrations.

Indium	Parameters: Con(H) 1E-007 M; Con(Cl)1E-004 M										
Species	1E-10	1E-9	1E-8	1E-7	1E-6	1E-5	1E-4	1E-3	1E-2	1E-1	1E-0
$In(OH)_2^+$	0.40	0.40	0.40	0.20							
$In(OH)_{3\ aq}$	99.40	99.40	99.40	50.17	5.01	0.5					
$In(OH)_{3\ s}$				49.58	94.96	99.50	99.95	99.99	100	100	100
$In(OH)_4^-$	0.20	0.20	0.20								
Lutetium	Parameters: Con(H) 1E-008 M; Con(Cl)1E-004 M;										
Free Lu^{3+}	9.80	9.80	9.80	1.05	0.11	0.01					
$Lu(OH)^{2+}$	38.15	38.15	38.15	4.11	0.41						
$Lu(OH)_2^+$	18.56	18.56	18.56	2.00	0.20						
$Lu(OH)_{3\ aq}$	18.54	18.54	18.54	2.00	0.20						
$Lu(OH)_{3\ s}$				89.24	98.92	99.89	99.99	99.99	100	100	100
$Lu(OH)_4^-$	14.95	14.95	14.95	1.61	0.16						
Zirconium	Parameters: Con(H) 1E-007 M; Con(Cl)1E-004 M;										
$Zr(OH)_{4\ aq}$	99.76	99.76	99.76	99.76	99.76	99.76	34.01	3.40	0.34		
$Zr(OH)_{4\ s}$							65.91	96.59	99.66	99.97	100
$Zr(OH)_5^-$	0.24	0.24	0.24	0.24	0.24	0.24					

* The percentage of certain species in all.

6

Exploring the potential of combined chemotherapy and radionuclide therapy by using poly(ε-caprolactone-b-ethylene oxide) micelles co-loaded with Paclitaxel and ^{177}Lu

Abstract

Combination of therapies is rather common in cancer treatment. For instance, external beam therapy is often combined with chemotherapy. Such combined therapies are desirable provided superior therapeutic outcome without additional adverse side effects. In this work, we explored the possibility to combine chemotherapy with radionuclide therapy using polymeric micelles. For this purpose, we prepared poly(ε-caprolactone-b-ethylene oxide) (PCL-PEO) micelles and loaded them simultaneously with Paclitaxel(PTX) and ^{177}Lu. We chose 3D tumour spheroid composed of glioblastoma cells (U87) as in vitro model to evaluate the combined treatment. First, we optimized the experimental parameters for preparing PTX-loaded PCL-PEO micelles. Next, we determined tumor uptake of the micelles by radiolabeling them with ^{111}In, The diffusion of the micelles in the tumour spheroid was then investigated by labeling them with FTIC and using light sheet imaging. The results showed that the micelles were able to penetrate the spheroid within 24 hours of incubation. Subsequently, we evaluated the cell killing efficiency of single treatment (PTX or ^{177}Lu) versus combined treatment (PTX+^{177}Lu) by measuring the growth of the spheroids as well as by performing a cell-viability assay. The results indicated that the combined therapy achieved a superior therapeutic outcome with higher cell growth inhibition and better cell killing efficiency compared to the single treatments.

Introduction

Currently, the three main approaches for cancer treatment are surgery, radiotherapy and chemotherapy. Combined therapies are also often applied, for instance, external radiation therapy and adjuvant chemotherapy have in many cases been shown to result in better treatment efficacy.[1] Some of the explanations for the enhanced therapeutic outcome of radio-chemotherapy are: the synergistic excessive oxidative loading at the tumor sites;[2] the arrest of tumor cells in the G2/M phase of the cell cycle by chemotherapeutics making them more sensitive to radiation;[3] improved uptake of chemotherapeutics as result of radiation exposure;[4] and reduced ability of tumour cells to repair DNA damage caused by radiation[5] and so on. Although the exact mechanism behind radio-chemotherapy is still not fully understood, this therapy has already become the standard treatment for certain cancer types, e.g. non-small cell lung cancer.[6]

In clinical practice, radio-chemotherapy is usually carried out by simply applying external radiation beam therapy with chemotherapy according to different operation protocols, for instance, irradiating the patient after chemotherapy. [7, 8] One of the main issues of this combined therapy is the severity of the side effects. For instance, in the case of oesophagus cancer, the patients treated with radio-chemotherapy indeed achieved higher survival than the groups treated with radiotherapy alone, but they also experienced considerably more side-effects due to the toxicity of the drugs.[9] Clearly, reduction of side effects would lead to much better therapy and better quality of life. Ionizing radiation is also applied in radionuclide therapy, which is typically used to treat metastasized tumours. Radionuclide therapy and chemotherapy are currently not combined in the clinic although studies suggest that such a combination would lead to much better treatment efficiency.[10-12] Here again, such a combination should be applied only if additional adverse side effects can be kept to a minimum.

One way to diminish side effects of chemotherapeutic drugs is to use nano-carriers such as polymeric micelles. [13] Polymeric micelles are composed of block copolymers and typically have a hydrophobic core in which drugs can be encapsulated, and hydrophilic shell meant to

increase bloodstream circulation and hence tumour uptake. Polymeric micelles are already applied in the clinic in different chemotherapeutic treatments.[14] In this chapter, we investigated the possibility to combine chemotherapy and radionuclide therapy in one vehicle and we investigated the combined therapeutic effect using 3D tumor models. Moreover, we also studied the diffusion of the micelles in these 3D tumor models as function of time. Poly(ε-caprolactone-b-ethylene oxide) (PCL-PEO) micelles were chosen as the nano-carriers, Paclitaxel (PTX) as the chemotherapeutic drug and ^{177}Lu as the therapeutic radionuclide, aiming to build up a multifunctional drug delivery system for combined radionuclide therapy and chemotherapy.

Materials and methods

2.1 Materials

Poly (ε-caprolactone-b-ethylene oxide) block copolymers PCL-PEO (2800-2000), PCL-PEO (6500-5500) were bought from Polymer Source (Quebec, Canada). Paclitaxel (PTX), 4-(2-hydroxyethyl)-1-piperazineethanesulfonic acid (HEPES), chloroform and Sephadex G-25 resins were bought from Sigma Aldrich (Zwijndrecht, the Netherlands). ^{111}In and ^{177}Lu (in 0.01 M HCl solution, the specific activity is 15.5 GBq/μg and 0.5 GBq/μg for ^{111}In and ^{177}Lu, respectively) were a kind gift of Erasmus Medical Centre (Rotterdam, the Netherlands). The Dulbecco's Modified Eagle's Medium High Glucose (DMEM) culture medium, Fetal Bovine Serum, Penicillin-Streptomycin Solution 100X, Dulbecco's Phosphate Buffered Saline (PBS), and Trypsin-Ethylenediaminetetraacetic acid 1X (Trypsin-EDTA) were purchased from Biowest (Amsterdam, the Netherlands). The Human U87 glioblastoma cells were obtained from VU Medical Centre Cancer Centre Amsterdam (Amsterdam, the Netherlands). The U shaped 96-wells plates were purchased from Greiner Bio-One (Alphen aan den Rijn, the Netherlands). The CellTiter-Glo®3D Cell Viability Assay reagent was obtained from Promega (Leiden, the Netherlands). Plasma membrane marker (MemBrite™ Fix 568/580, Biotium) was utilized to label the membrane of the spheroids for imaging purpose.

2.2 Synthesis

2.2.1 Synthesis of PCL-PEO micelles and PTX-loaded micelles

The PCL-PEO micelles were prepared by the solvent evaporation method described in our previous work.[15] The drug-loaded micelles were also prepared using the same method. Typically, 0.1 mL of polymer stock solution (200 mg/mL, in chloroform) was mixed with 0.1 mL of PTX solution (in chloroform, with different PTX concentrations of 5, 7.5, 10, 20 mg/mL) under sonication. The mixture was added dropwise to 2.3 mL of MQ water and stirred overnight to evaporate the chloroform. Syringe filters with 220 nm cut-off were applied to remove large structures in the micelles and PTX-loaded micelles. Subsequently, the unencapsulated drugs were removed by size exclusion chromatography (SEC). MQ water was used as the eluent for SEC. Every 1 mL of eluent was collected as one fraction. The PTX-loaded micelles appeared in the 9th to 12th fractions, therefore 4 mL of samples were eventually collected. After the above process, the polymer concentration for empty micelles sample and PTX-loaded micelles sample was around 8.7 mg/mL and 2.2 mg/mL (assuming that the polymer loss during the filtration was negligible).

2.2.2 Synthesis of ^{111}In radiolabeled micelles

First, a centrifugation filter was used to concentrate the micelle sample which yielded a final solution with polymer concentration of 17.4 mg/mL. Then, the concentrated micelle solution was mixed with HEPES buffer (20 mM, pH 7.4) in a volume ratio of 1:1. To radiolabel the micelles with ^{111}In, 15 MBq of ^{111}In was added to 0.4 mL of the micelle solution (8.7 mg/mL, in 10 mM HEPES) and stirred for 0.5 hour. The obtained samples were passed through SEC to remove the free ^{111}In ions, during which HEPES buffer (10 mM, pH = 7.4) was used as the eluent. Similarly, the radiolabeled micelles eluted in the 9th to 12th fractions, therefore 4 mL of samples were eventually collected and the final concentration of the samples was 0.87 mg/mL.

The centrifugation filters were also applied in later-on experiments to concentrate or replace the solvent of the sample. The exact polymer concentration and solvent would be specified for the samples treated with centrifugation filters.

2.2.3 Synthesis of FITC-labeled PCL-PEO micelles

The FITC-loaded PCL micelles were prepared by adding 0.1 mL of FITC stock solution (5 mg/mL in ethanol) during the self-assembly process of the block copolymers. After being stirred overnight, the obtained mixture was passed through SEC to remove the un-encapsulated FITC. MQ water was used as the eluent, and five fractions from 8^{th} to 12^{th} were collected as the FITC-labelled micelles (5 mL).

2.2.4 Synthesis of ^{177}Lu loaded PCL-PEO micelles

To make the ^{177}Lu loaded micelles, 20 MBq of ^{177}Lu was added to 1 mL of micelles (8.7 mg/mL, in HEPES) and stirred for half an hour. SEC was utilized again to separate the free ^{177}Lu ions and 4 fractions were collected as the ^{177}Lu radiolabeled samples (4 mL).

2.2.5 Synthesis of ^{177}Lu&PTX co-loaded PCL-PEO micelles

To prepare the co-loaded micelles, the PTX-loaded micelles were first prepared with the PTX/polymer mass ratio of 0.05:20 (mg). Then, a 220 nm cut-off filter was applied to remove the large clusters presented in the solution, and SEC was used to remove the un-encapsulated PTX. Four milliliters of PTX-loaded micelles were collected after the SEC, which was concentrated to 1 mL and mixed with HEPES buffer with volume ratio of 1:1. Next, 10 MBq of ^{177}Lu was added to 1 mL of PTX-loaded micelles (in HEPES buffer, polymer concentration is 4.3 mg/mL), followed by being stirred for 1h. Then SEC columns were used to remove the unencapsulated ^{177}Lu, and 9^{th} – 12^{th} fractions of the eluent were collected as the ^{177}Lu&PTX co-loaded micelles for further use.

Characterization

3.1 Instruments

A dynamic light scatting (DLS) instrument consisting of a JDS uniphase 633 nm 35 mW laser, an ALV sp 125 s/w 93 goniometer, a fibre detector and a Perkin Elmer photo counter

was employed to determine the size distributions of the obtained micelles. A Cryogenic electron microscope (Cyro-EM, Jeol JEM 1400) was used to image the morphology of the micelles. A high-performance liquid chromatography (HPLC) coupled to a UV detector set at 227 nm was applied to determine the drug concentration. The mobile phase was a mixture of acetonitrile and aqueous formic acid solution (10 mM) having volume ratio of 45:55 respectively. Automatic Gamma counter (Wallac WIZARD2 2480, Perkin Elmer Technologies) was used to determine the radiolabeling efficiency. A 12MP camera connected to the binocular microscope using automated imaging software (SampleScan) was utilized to record the images of the tumour spheroids. A fluorescence spectrophotometer (Agilent Cary Eclipse) was utilized to measure the luminescence by choosing Bio/chemiluminescence data mode.

3.2 Characterization

Drug loading efficiency

THF was added to the micelle solutions in a volume ratio of 1:1 and left until a homogeneous solution was formed, resulting in disintegration of the micelles. Subsequently the HPLC setup was used to detect the PTX concentration in each sample.

LE(%) of drugs (PTX) = (The concentration of drugs in final samples)/(The initial drug concentration)×100%

Drug release profile

The PBS buffer solution with pH 7.4 and 5.4 were utilized to determine the drug release profile. The solution with pH 5.4 was obtained by using HCl to adjust the commercial PBS butter (pH 7.4) to this lower value. Next, 1.1 mL of the drug-loaded micelles was mixed with 1.1 mL of PBS buffer. The solution was transferred to a dialysis bag with a cut-off of 2000-5000. The dialysis bag was placed in a beaker containing 800 mL of PBS buffer under gentle

stirring. 0.2 mL of the samples were taken out at various timepoints to determine the drug amount left in the micelles.

Residual drug ratio = (The concentration of drugs at different timepoints)/(The initial drug concentration)×100%

3.3 In vitro evaluation

Cell line

Human U87 glioblastoma cells were utilized as 3D model for in vitro experiment. The cells were maintained in DMEM culture medium supplemented with 10% mL fetal bovine serum and 1% Penicillin/Streptomycin under humidified normoxic (95% air, 5% CO_2) at 37°C. For preparation of the 3D cell models, 2000 cells (suspended in 200 μL cell culture medium) were seeded in each well in a U shape 96-well plate and incubated for five days before use.

Cell uptake

The cell uptake was evaluated by using ^{111}In radiolabeled micelles. Centrifuge filter tubes were applied to replace the solvent (HEPES) with PBS (pH 7.4) before adding the radiolabeled micelles to the cells. Then, 20 μL of ^{111}In labelled micelles were added to each tumour spheroid to achieve a final micelle concentration of 0.079 mg/mL. The spheroids were harvested and washed by 4 mL of PBS (4*1 mL) at certain time points (5h, 1d, 2d, 3d). The final activity in each spheroid was measured using the Wallac gamma counter.

Cell distribution in tumour spheroid

The diffusion of the PCL-PEO micelles within the tumor spheroids was followed by a home-made light-sheet imaging setup. Two channels were applied, the parameters are as following: blue laser channel 1 mW, absorbed light 488 nm, emitted light = 525 nm; green laser channel 1 mW, absorbed light 561 nm, emitted light = 620 nm. First, a centrifuge filter tube was applied to prepare the final FITC-labelled samples with a polymer concentration of 3.48 mg/mL. Then 0.2 mL of FITC-labelled micelles was mixed with 1.5 mL of culture medium

resulting in a solution with polymer concentration of 0.41 mg/mL. Finally, 150 uL of the obtained samples was added to each spheroid (6 day culture) and incubated for 30 minutes and 24h. Prior to imaging, spheroids were washed with PBS (twice) and stained with plasma membrane dye for 20 minutes. The distribution of the micelles within the spheroids was followed using the FITC whereas the membrane dye outlined each cell within the spheroid.

Cell growth inhibition

The cell growth inhibition caused by the empty micelles, PTX-loaded micelles, ^{177}Lu-loaded micelles and ^{177}Lu& PTX co-loaded micelles was first checked. Briefly, the centrifuge filters were applied to replace the solvent of the obtained micelles samples from HEPES to PBS buffer (pH 7.4). Then the micelles dispersed in PBS buffer were sterilized by exposure to a UV light source for 30 seconds, then 20 μL of the sample solution was added to each U87 spheroid. After 1 day of incubation, the old culture medium was removed carefully, the spheroid was washed with PBS for 3 times followed by adding 200 μL of fresh culture medium. The morphology of the spheroids was recorded at different timepoints using the binocular microscope. And the ImageJ software was used to analyse the obtained graphs.

CellTiter-Glo® 3D Cell Viability Assays

CellTiter-Glo® 3D Cell Viability Assay (ATP-based viability assay) was performed to determine the therapeutic effect of the micelles loaded with different anticancer substances. The drug administration process was exactly the same as that in the evaluation of cell growth inhibition. Rather than recording the morphology at different timepoints, the spheroids were sacrificed at day 1 and day 5 for checking the cell viability. For this purpose, all of the medium was carefully removed from the spheroid containing wells, then 200 μl of a mixture composed by CellTiter-Glo®3D reagent and culture medium with a volume ratio of 1:1 was added to each spheroid and reacted for around 1 hour. The medium in each counting well was pipetted gently to destroy the spheroids during the reaction. Finally, 190 μl of the medium of each well was transferred to a non-transparent plate for subsequent luminescence measurements. The setup parameters of fluorescence spectrophotometer were as followed:

Bio/chemiluminescence data mode; emission wavelength of 600 nm, emission slit of 20 nm, open emission filter, gate time of 200 ms.

The cell viability was determined according to the following formula.

Cell Viability = (The luminescent intensity of each sample)/(The luminescent intensity of the control group)×100%

Results and analysis

4.1 The formation of PTX-loaded PCL-PEO micelles and their drug release profile

Paclitaxel, a typical taxane medicine, was utilized in this work as a model chemotherapeutic drug.[16, 17]. The PTX-loaded micelles were prepared by adding PTX during the self-assembly process of the block copolymer. According to previous publications, the presence of PTX may alter the morphology of the micelles.[18, 19] Therefore, a Cryo-EM was applied to observe the morphology of the PTX-loaded micelles obtained at different PTX to polymer mass ratios. As shown in Figure 6.1, at a drug/polymer mass ratio of 2:20 mg, rod-like crystals composed of PTX were formed with lengths up to several micrometers.[20] No micelles could be observed. As the drug to polymer ratio was decreased to 1:20, some micelles (red arrows) appeared but long nanorods were still presented. By further decreasing the drug amount to a mass ratio of 0.75:20, the rod-like structure disappeared, but instead, some dense clusters (yellow arrows) were observed which most likely were composed of PTX. Only at a PTX:polymer mass ratio of 0.5:20, no PTX crystals could be detected indicating that the majority of PTX molecules were encapsulated in the micelles.

Therefore, we chose the drug/polymer mass ratio of 0.5:20 for further experiments. Two block-copolymers, i.e. PCL-PEO (2800-2000) and PCL-PEO (6500-5500) were utilized to encapsulate PTX. The drug loading efficiency was 86.39 ± 6.28%, 75.72 ± 6.75% for PTX-2800 and PTX-6500 respectively. The DLS results in Figure S6.1 showed that the PTX-6500 micelles with mean hydrodynamic radius of 50 nm were larger than that of PTX-2800 micelles having mean radius of 16 nm radius. The release profile of PTX in the drug-loaded

micelles was evaluated by dialysis, i.e., 2.2 mL of the obtained samples were dialyzed against 800 mL of PBS buffer with pH values 5.2 and 7.4. All the PTX-loaded micelles behaved similarly under these experimental conditions regardless of the pH values and polymer used. Around 30% of the PTX still remained inside the micelles after 10 days of incubation (Figure S6.2).

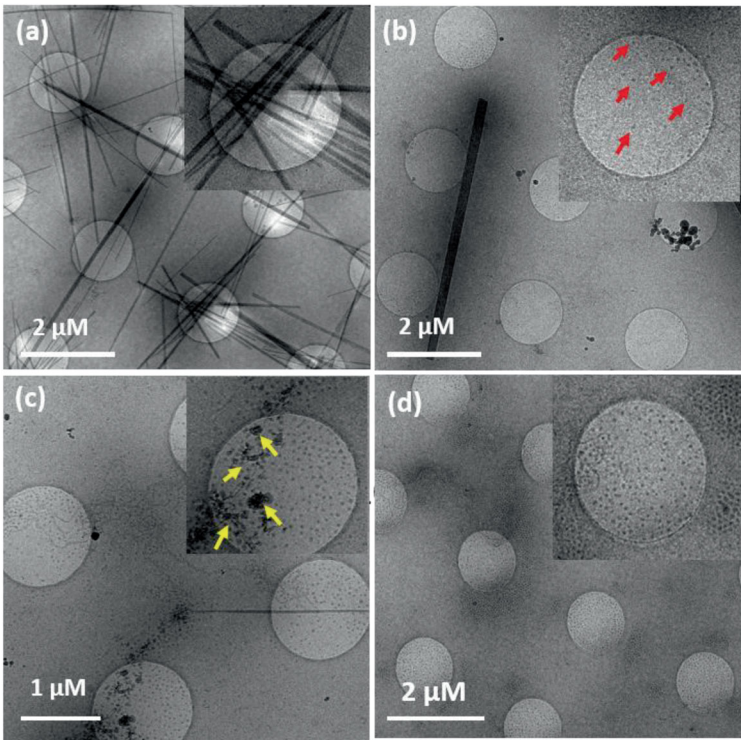

Figure 6.1. Cryo-EM images of PTX-loaded PCL-2800 micelles prepared at PTX to polymer mass ratio of (a) 2:20; (b) 1:20; (c) 0.75:20 and (d) 0.5:20. (Polymer concentration: 8.7 mg/mL, without filtration process).

4.2 Cell uptake and diffusion of the micelles in the spheroid

A 3D cell model (U87) was utilized to evaluate the in vitro cell uptake of PCL-PEO micelles radiolabeled with ^{111}In. As shown in Figure 6.2(a), the spheroid uptake was found to be 0.19±0.06 % and 0.21±0.08 % for PCL-2800 and PCL-6500 micelles after 24 hours of incubation, which increased to 2.2±0.44 % and 1.45±0.23% after 72 hours. To further observe the diffusion of the micelles within the 3D spheroid, we labeled the micelles with a

fluorescein isothiocyanate, FITC, and used a light sheet imaging technique to follow the distribution of the micelles in time. The FITC micelles are represented by green color, while the membrane is represented by pink color. As shown in Figure 6.2(b), after being incubated for 30 min, small amount of the micelles were diffused into the spheroid with slight green color. After 24 hours of incubation, evident green color could be observed inside the cells, both at the membrane and inside of the cells, indicating that the micelles managed to penetrate deeper and actually were distributed through the whole spheroid.

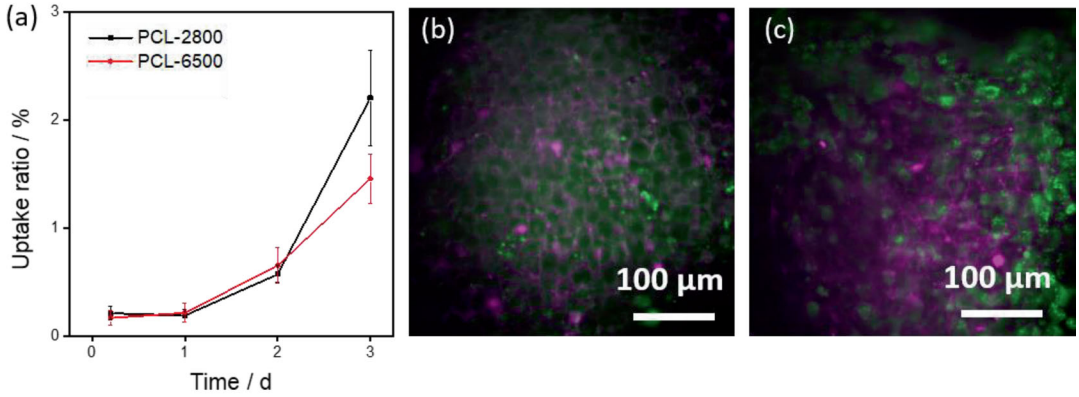

Figure 6.2 (a) Tumour uptake of ^{111}In-radiolabeled micelles as a function of time and distribution of FITC-labeled micelles within a U87 spheroid after (b) 30 min and (c) 24 hour. (Polymer concentration in the tumour uptake was 0.079 mg/mL, the error bar represents the experimental uncertainty of n=4; the polymer concentration in the light sheet imaging experiments was 0.41 mg/mL).

4.3 Cell killing efficiency

We first used PTX-6500 micelles prepared with a PTX to polymer mass ratio of 0.5:20(mg) to evaluate the influence of the drug alone on the growth of U87 spheroid. The applied PTX-loaded micelles appeared to be very toxic to the tumor cells, and the spheroids displayed an evident shrinkage (the results are not shown in this work). Therefore, we decreased the encapsulated amount of PTX by preparing PTX-6500 micelles (denoted as PTX-con-1X, i.e. samples without dilution) with a PTX to polymer mass ratio of 0.05:20(mg). We obtained in this way a PTX-6500 micelles solution dispersed in PBS with PTX concentration of 39.9 µg/mL and polymer concentration of 17.4 mg/mL. After adding 20 µL of the PTX-6500 micelles to the spheroid with 200 uL of culture medium, the final PTX concentration was 3.6 µg/mL. Apart from PTX-con-1X sample, we also prepared PTX-containing samples with lower concentrations by diluting PTX-con-1X sample with PBS 5, 10 and 20 times before

adding them to the spheroids. Therefore, four PTX-loaded micelles, namely PTX-con-1X, PTX-con-5X, PTX-con-10X and PTX-con-20X were added to the spheroid, which resulted in the final PTX concentrations in each counting well of 3.6, 0.7, 0.25 and 0.18 μg/mL, respectively.

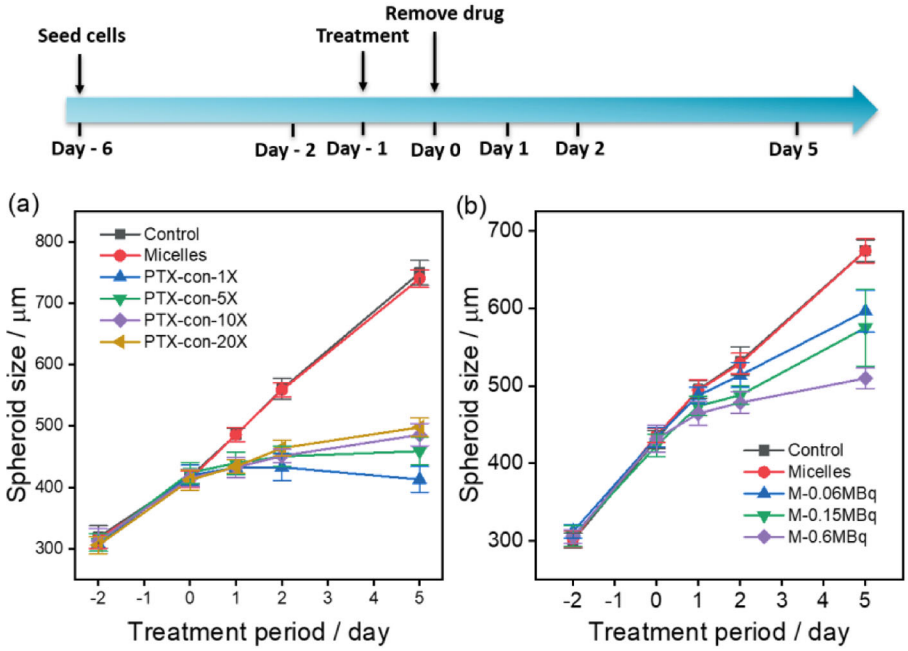

Figure 6.3 (a) The size of spheroids when exposed to different PTX concentrations as function of time (Control: treated with 20 μL of PBS; Micelles: polymer concentration 1.58 mg/mL; PTX-con-1X: polymer concentration 1.58 mg/mL, drug concentration 3.6 μg/mL; PTX-con-5X: polymer concentration 0.32 mg/mL, drug concentration 0.7 μg/mL; PTX-con-10X: polymer concentration 0.16 mg/mL, drug concentration 0.35 μg/mL. PTX-con-20X: polymer concentration 0.08 mg/mL, drug concentration 0.18 μg/mL); (b) The size of the spheroid as function of time at different activities of ^{177}Lu (Control: treated with 20 μL of PBS; Micelles: polymer concentration 1.32 mg/mL; M-0.06MBq: polymer concentration 0.132 mg/mL and 0.06 MBq per spheroid; M-0.15 MBq: polymer concentration 0.33 mg/mL and 0.15 MBq per spheroid; M-0.15 MBq: polymer concentration 1.32 mg/mL and 0.6 MBq per spheroid. The error bar represents the experimental uncertainty of n=3).

The images of the spheroids treated with chemotherapy are shown in Figure S6.3(a), which indicates that the micelles themselves had negligible influence on the tumor growth, comparable to the PBS control group. Contrarily, the PTX-loaded micelles posed significant influence on the spheroid growth and smaller spheroids could clearly be observed after being treated with PTX. Interestingly, no noticeable effect could be seen on day 0 (24 h after drug

administration). On day 1, all spheroids treated with drugs appeared to have a similar size. The influence of PTX as function of concentration was to show from day 2 on. The spheroids treated with the highest concentration (3.6 μg/mL) had a much smaller size than the ones treated with lower amount of PTX (Figure S6.3). On day 5 the spheroids that were given the highest PTX concentration already showed an evident shrinkage, while the ones treated with less PTX kept on growing although at much lower rate than the control group.

Subsequently we investigated the influence of the activity of ^{177}Lu on the growth of spheroids. For this purpose, we added 10 MBq of ^{177}Lu to radiolabel the PCL-6500 micelles and achieved final samples with ^{177}Lu concentration of 30 MBq/mL and polymer concentration of 14.5 mg/mL. In these experiments the ^{177}Lu-loaded micelles were further diluted to 5 and 10 times. After adding 20 uL of the ^{177}Lu-loaded micelles samples to the spheroid, the final activity added to each spheroid was 0.06, 0.15 and 0.6 MBq/well, which was denoted as M-0.06 MBq, M-0.15MBq and M-0.6 MBq. Figure 6.3(b) shows the results of the radionuclide treatment suggesting no evident size difference at day 0, similar to the PTX experiments. The spheroids treated with activities had much smaller size than the control group on Day 5 and the ones given 0.6 MBq even started to visibly fall apart (Figure S6.4).

The combined radionuclide and chemotherapy treatment was carried out using ^{177}Lu&PTX co-loaded PCL-6500 micelles. To properly evaluate the therapeutic effects of the combined therapy, 5 samples were prepared, namely PTX-M, Lu-M, P&Lu-1X, P&Lu-2X and P&Lu-5X. Among them, PTX-M and Lu-M denoted the single treatment with PTX and ^{177}Lu respectively, the former had the same PTX concentration as P&Lu-1X with a PTX concentration of 0.48 μg/mL, while the latter had the same activity as P&Lu-1X, i.e. 30 kBq of ^{177}Lu. The P&Lu-2X and P&Lu-5X samples were 2 and 5 time dilutions of the P&Lu-1X samples.

As shown in Figure 6.4(a), the single treatment with PTX and ^{177}Lu could inhibit the spheroid growth, although the Lu-M with 30 kBq of ^{177}Lu given to each spheroid showed lower growth inhibition than the PTX-M sample with PTX concentration of 0.48 μg/mL. The combined therapy already showed its potential on the second day after drug and radionuclide administration resulting in an evidently less spheroid growth than the control group and the

spheroids receiving single treatment. Typical images of the spheroids treated in this study can be seen in Figure 6.4(a). The spheroid of the control group continued to grow during the whole observation period and had a smooth surface on day 5. Although the spheroids that received single treatment had a smaller size on day 5 compared to the control group, their surface still remained smooth, while the combined treatment clearly led to fuzzy surface indicating that the cells were coming loose. Cells typically become loose if they died.

Due to the fuzzy surface, it was very hard to determine the size of the spheroid in a precise way. Therefore, an ATP test was carried out to evaluate the viability of the spheroids when exposed to the different treatments. The viability on Day 0 and Day 5 was measured and shown in Figure S6.5 and Figure 6.4(c). The single treatment with PTX or ^{177}Lu did not show to be toxic on Day 0 with similar viability as the control group. However, the PTX treatment showed higher toxicity at Day 5, with only 80.52 ± 10.55 % cell being alive. The ^{177}Lu treated spheroid had viability of around 100% when compared to the control group, indicating that 30 kBq of ^{177}Lu was insufficient to cause cell damage under these experimental conditions.

In terms of the combined treatment, an interesting phenomenon occurred, that is, the addition of P&Lu-2X and P&Lu-5X with low dose of both PTX and ^{177}Lu initially led to better growth of the spheroid on Day 0 (more viable cells than the control group, Figure S6.5). We cannot find the exact reason for this phenomenon since this was rarely reported in the literature. One possible reason is that at low concentrations the drug may activate certain growth-related factors of the tumour.[21] However, it is also possible that these results are simply due to uncertainties in the viability assay such as the penetration of the viability test reagents in the spheroid. On Day 5, the co-loaded samples had a better therapeutic outcome than the single treatment, that is, 57.37 ± 1.32%, 63.15 ± 2.64% and 51.58 ± 13.05% for P&Lu-1X with 0.48 μg/mL of PTX and 30 kBq of ^{177}Lu, P&Lu-2X with 0.24 μg/mL of PTX and 15 kBq of ^{177}Lu, and P&Lu-5X with 0.096 μg/mL of PTX and 6 kBq of ^{177}Lu, indicating that the combined treatment was more efficient. Moreover, we also checked the viability of the empty micelles, which confirmed that the nano-carriers were not toxic to the U87 cells and had a comparable number of living cells to the control group on both Day 0 and Day 5.

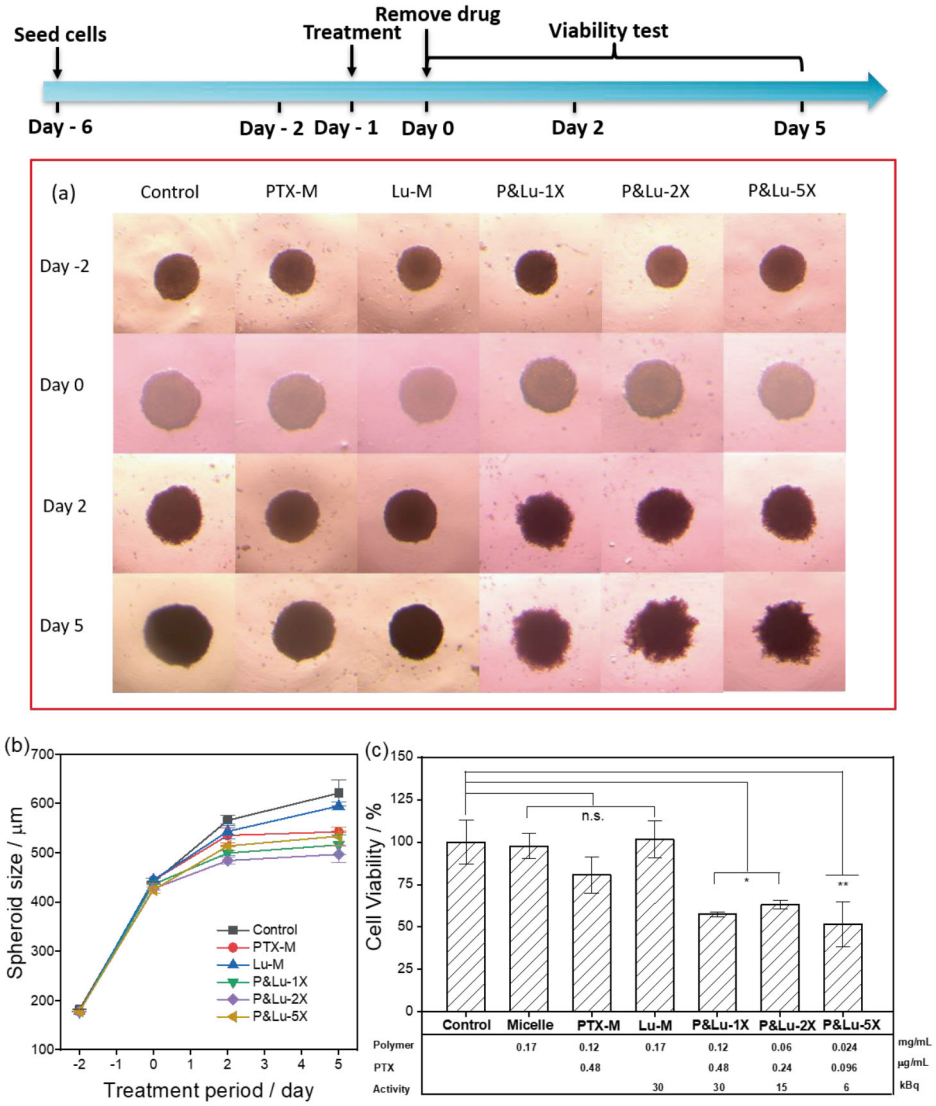

Figure 6.4 (a) Representative images of the spheroids for the various treatments and at different time points (b) the size of the spheroids exposed to PTX or ^{177}Lu loaded micelles and PTX&^{177}Lu co-loaded micelles as a function time (c) percentage of viable cells on Day 5 of the spheroids when exposed to the different treatments. (Control: add 20 µL of PBS; Micelles: polymer concentration 0.17 mg/mL. PTX-M: polymer concentration 0.12 mg/mL, PTX concentration 0.48 µg/mL; Lu-M: polymer concentration 0.17 mg/mL, 30kBq of ^{177}Lu; P&Lu-1X: polymer concentration 0.12 mg/mL, PTX concentration 0.48 µg/mL, 30kBq of ^{177}Lu; P&Lu-2X: polymer concentration 0.06 mg/mL, PTX concentration 0.24 µg/mL, 15 kBq of ^{177}Lu; P&Lu-5X: polymer concentration 0.024 mg/mL, PTX concentration 0.096 µg/mL, 6 kBq of ^{177}Lu. The error bars represent the experimental uncertainty of n=3. * = $p<0.05$, ** = $p<0.01$, *** = $p<0.001$, **** = $p<0.0001$).

Conclusion

In this chapter, PTX-loaded micelles, ^{177}Lu-radiolabeled micelles and PTX&^{177}Lu co-loaded micelles were synthesized for chemotherapy, radionuclide therapy and combined treatment (radionuclide therapy + chemotherapy). In order to encapsulate PTX in the micelles a mass ratio of 0.5:20 (mg) (PTX: block copolymer) was used. Higher ratios led to PTX crystal formation which influenced the self-assembly process of the micelles. The micelles could also be readily radiolabeled with ^{177}Lu yielding a radiolabeling efficiency higher than 90%. 3D tumour spheroid composed of U87 was used to evaluate the potential of the combined treatment. First, we showed that the micelles were able to penetrate to the spheroids within 24 hours. We then measured the size of the spheroid as function of time upon exposure of micelles containing PTX, ^{177}Lu and both ^{177}Lu+PTX. The results showed that the combined treatments was the most effective and cell viability studies further confirmed this observation. The results showed that at low activity of ^{177}Lu as well as low amounts of PTX, high killing efficiency could be obtained if combined, which is beneficial in reducing side effects to healthy tissue. Nevertheless, more studies need to be conducted to further optimize such a combined treatment.

Reference

[1] M. Zak, J. Drobnik, Effect of Cis-Dichlorodiamine Platinum (II) on the Post-Irradiation Lethality in Mice after Irradiation with X-rays, *Strahlentherapie*. **1971**, 142, 112-115.

[2] S. Nagasawa, J. Takahashi, G. Suzuki, Y. Hideya, K. Yamada, Why Concurrent CDDP and Radiotherapy Has Synergistic Antitumor Effects: A Review of In Vitro Experimental and Clinical-Based Studies, *Int J Mol Sci*. **2021**, 22 .

[3] E.B. Golden, S.C. Formenti, P.B. Schiff, Taxanes as Radiosensitizers, *Anticancer Drugs*. **2014**, 25, 502-511.

[4] X. Yi, L. Chen, J. Chen, D. Maiti, Z. Chai, Z. Liu, K. Yang, Biomimetic Copper Sulfide for Chemo-Radiotherapy: Enhanced Uptake and Reduced Efflux of Nanoparticles for Tumor Cells under Ionizing Radiation, *Adv. Funct. Mater*. **2018**, 28.

[5] G.D. Wilson, S.M. Bentzen, P.M. Harari, Biologic basis for combining drugs with radiation, *Semin Radiat Oncol*. **2006**, 16, 2-9.

[6] M. Zwitter, V. Kovac, U. Smrdel, P. Strojan, Gemcitabine, Cisplatin, and Hyperfractionated Accelerated Radiotherapy for Locally Advanced Non-small Cell Lung Cancer, *J. Thorac. Oncol*. **2006**, 1, 662-666.

[7] S. Kranjc Brezar, A. Prevc, M. Niksic Zakelj, A. Brozic, M. Cemazar, P. Strojan, G. Sersa, Synergistic Effect of Cisplatin Chemotherapy Combined with Fractionated Radiotherapy Regimen in HPV-Positive and HPV-Negative Experimental Pharyngeal Squamous Cell Carcinoma, *Sci Rep*. **2020**, 10, 1563.

[8] K. Mortezaee, A. Narmani, M. Salehi, H. Bagheri, B. Farhood, H. Haghi-Aminjan, M. Najafi, Synergic Effects of Nanoparticles-mediated Hyperthermia in Radiotherapy/Chemotherapy of Cancer, *Life Sci*. **2021**, 269, 119020.

[9] A. Herskovic, K. Martz, M. al-Sarraf, L. Leichman, J. Brindle, V. Vaitkevicius, J. Cooper, R. Byhardt, L. Davis, B. Emami, Combined Chemotherapy and Radiotherapy Compared with Radiotherapy Alone in Patients with Cancer of the Esophagus, *N Engl J Med*. **1992**, 326, 1593-1598.

[10] L. Tian, Q. Chen, X. Yi, G. Wang, J. Chen, P. Ning, K. Yang, Z. Liu, Radionuclide I-131 Labeled Albumin-Paclitaxel Nanoparticles for Synergistic Combined Chemo-radioisotope Therapy of Cancer, *Theranostics*. **2017**, 7, 614-623.

[11] X. Zhong, K. Yang, Z. Dong, X. Yi, Y. Wang, C. Ge, Y. Zhao, Z. Liu, Polydopamine as a Biocompatible Multifunctional Nanocarrier for Combined Radioisotope Therapy and Chemotherapy of Cancer, *Adv. Funct. Mater*. **2015**, 25, 7327-7336.

[12] K. Liu, D. Zheng, J. Zhao, Y. Tao, Y. Wang, J. He, J. Lei, X. Xi, pH-Sensitive Nanogels Based on the Electrostatic Self-assembly of Radionuclide $^{(131)}$I Labeled Albumin and Carboxymethyl Cellulose for Synergistic Combined Chemo-Radioisotope Therapy of Cancer, *J Mater Chem B*. **2018**, 6, 4738-4746.

[13] A.G. Denkova, H. Liu, Y. Men, R. Eelkema, Enhanced Cancer Therapy by Combining Radiation and Chemical Effects Mediated by Nanocarriers, *Adv. Ther*. **2020**, 3.

[14] A. Varela-Moreira, Y. Shi, M.H.A.M. Fens, T. Lammers, W.E. Hennink, R.M. Schiffelers, Clinical application of polymeric micelles for the treatment of cancer, *Mater. Chem. Front*. **2017**, 1, 1485-1501.

[15] H. Liu, A.C. Laan, J. Plomp, S.R. Parnell, Y. Men, R.M. Dalgliesh, R. Eelkema, A.G. Denkova, Ionizing Radiation-Induced Release from Poly(ε-caprolactone-b-ethylene glycol) Micelles, *ACS Appl. Poly. Mater*. **2020**, 3, 968-975.

[16] M. Shahin, A. Lavasanifar, Novel Self-Associating Poly(ethylene oxide)-b-Poly(epsilon-caprolactone) Based Drug Conjugates and Nano-Containers for Paclitaxel Delivery, *Int J Pharm*. **2010**, 389 213-222.

[17] E.K. Rowinsky, R.C. Donehower, Paclitaxel (taxol), *N Engl J Med*. **1995**, 332, 1004-1014.

[18] A. Schulz, S. Jaksch, R. Schubel, E. Wegener, Z. Di, Y. Han, A. Meister, J. Kressler, A.V. Kabanov, R. Luxenhofer, C.M. Papadakis, R. Jordan, Drug-Induced Morphology Switch in Drug Delivery Systems Based on Poly(2-oxazoline)s, *ACS Nano* **2014**, 8, 2686-2696.

[19] C. Cao, J. Zhao, F. Chen, M. Lu, Y.Y. Khine, A. Macmillan, C.J. Garvey, M.H. Stenzel, Drug-Induced Morphology Transition of Self-Assembled Glycopolymers: Insight into the Drug–Polymer Interaction, *Chem. Mater*. **2018**, 30, 5227-5236.

[20] S. Farah, A.J. Domb, Crystalline Paclitaxel Coated DES with Bioactive Protective Layer Development, *J Control Release* **2018**, 271, 107-117.

[21] B. Liu, S. Pan, X. Dong, H. Qiao, H. Jiang, G.W. Krissansen, X. Sun, Opposing Effects of Arsenic Trioxide on Hepatocellular Carcinomas in Mice, *Cancer Sci*. **2006**, 97, 675-681.

Appendix

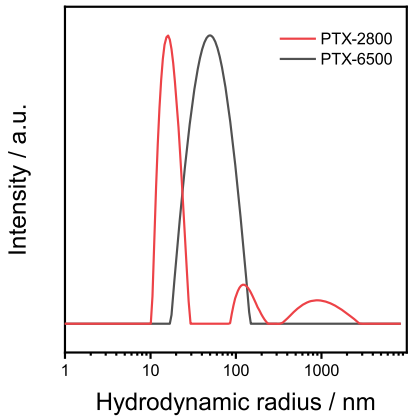

Figure S6.1 The size distribution PTX-loaded micelles with drug to polymer mass ratio of 0.5:20. (Polymer concentration: 0.435 mg/mL)

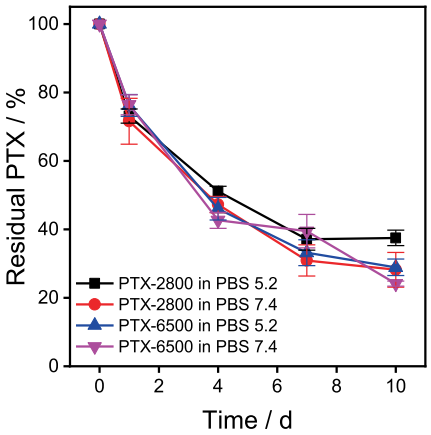

Figure S6.2 The drug release profile of PTX-loaded micelles when being dialysed against PBS buffer at different pH values. (Polymer concentration was 4.3 mg/mL inside the dialysis tube)

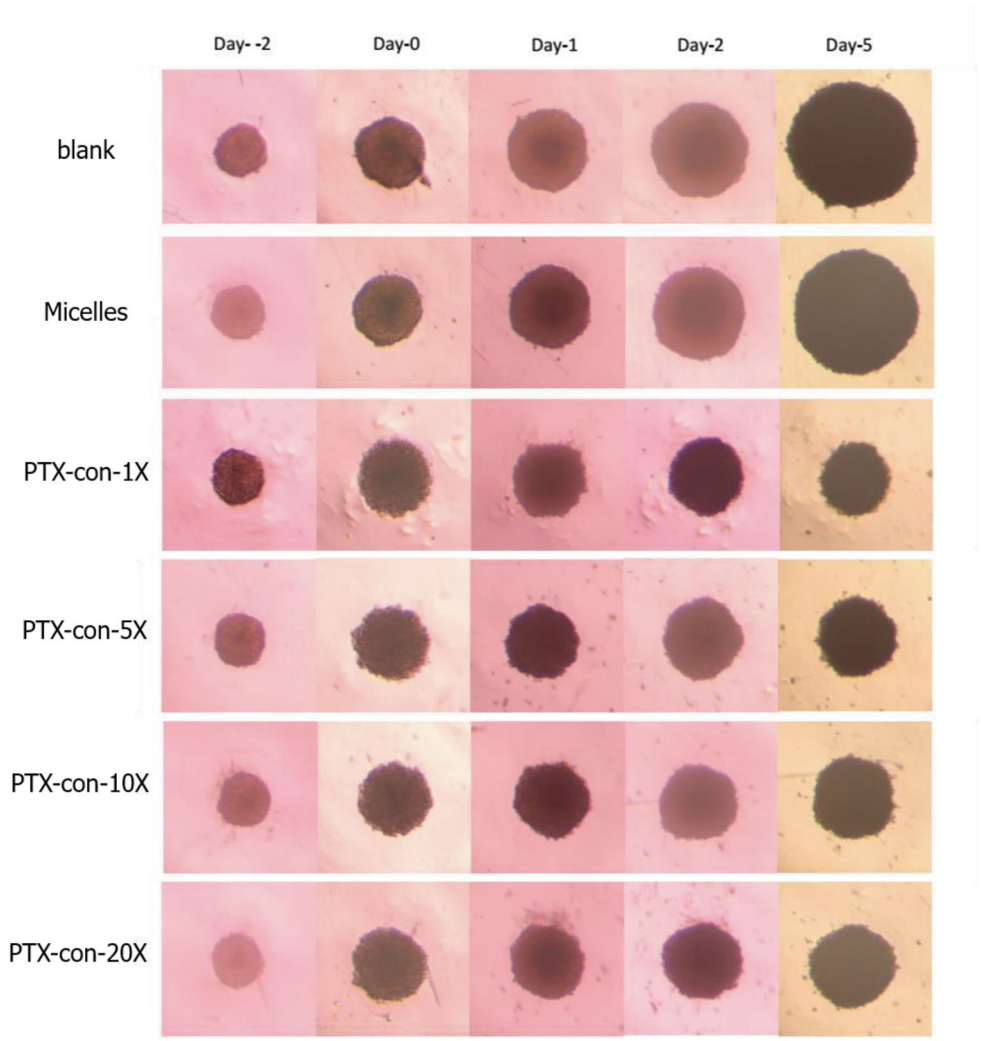

Figure S6.3 Light microscopy images of spheroids when exposed to different PTX amounts and at different time points. (Blank: add 20 μL of PBS; Micelles: polymer concentration 1.58 mg/mL; PTX-con-1X: polymer concentration 1.58 mg/mL, drug concentration 3.6 μg/mL; PTX-con-5X: polymer concentration 0.32 mg/mL, drug concentration 0.7 μg/mL; PTX-con-10X: polymer concentration 0.16 mg/mL, drug concentration 0.35 μg/mL. PTX-con-20X: polymer concentration 0.08 mg/mL, drug concentration 0.18 μg/mL)

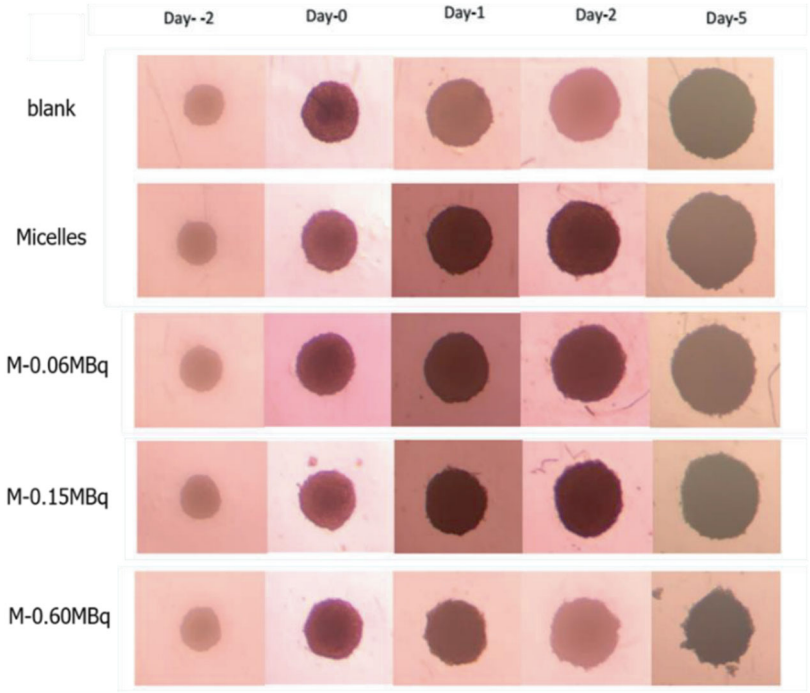

Figure S6.4 Light microscopy images of spheroid when exposed to different ^{177}Lu activity and different time points. (Blank: add 20 µL of PBS; Micelles: polymer concentration 1.32 mg/mL; M-0.06MBq: polymer concentration 0.132 mg/mL and 0.06 MBq per spheroid; M-0.15 MBq: polymer concentration 0.33 mg/mL and 0.15 MBq per spheroid; M-0.15 MBq: polymer concentration 1.32 mg/mL and 0.6 MBq per spheroid).

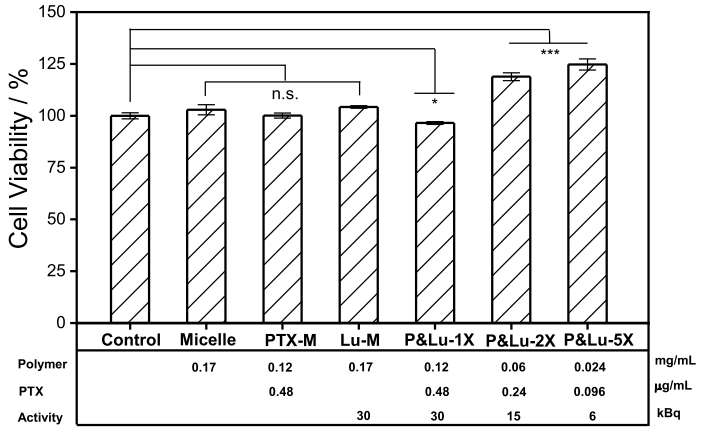

Figure S6.5 Percentage of viable cells on Day 0 of the spheroids when exposed to the different treatments. (Control: add 20 µL of PBS; Micelles: polymer concentration 0.17 mg/mL. PTX-M: polymer concentration 0.12 mg/mL, PTX concentration 0.48 µg/mL; Lu-M: polymer concentration 0.17 mg/mL, 30kBq of 177Lu; P&Lu-1X: polymer concentration 0.12 mg/mL, PTX concentration 0.48 µg/mL, 30kBq of 177Lu; P&Lu-2X: polymer concentration 0.06 mg/mL, PTX concentration 0.24 µg/mL, 15 kBq of 177Lu; P&Lu-5X: polymer concentration 0.024 mg/mL, PTX concentration 0.096 µg/mL, 6 kBq of 177Lu. The error bars represent the experimental uncertainty of n=3. * = $p<0.05$, ** = $p<0.01$, *** = $p<0.001$, **** = $p<0.0001$).

Conclusion

7

The research in this thesis mainly focused on the combination of polymeric micelles and ionizing radiation for therapeutic or imaging purpose in cancer treatment. As the by-product of ionizing radiation, the reactive oxygen species play important role in the interaction between ionizing radiation and matters. Therefore, in Chapter 2, we first attempted to detect the ROS produced due to radiation exposure by using some commercial probes. The results showed that the fluorescent probe Singlet Oxygen Sensor Green (SOSG) could somehow be excited upon radiation exposure and the excitation phenomenon still existed even when the irradiation was terminated. The SOSG was claimed to be specifically sensitive to singlet oxygen ($^1O_2$) under circumstances without ionizing radiation. Therefore, we evaluated the influence of $^1O_2$ on the SOSG fluorescence, as well as other ROS including H_2O_2 and OH•, produced directly or indirectly. The results indicated that $^1O_2$ and H_2O_2 did not influence the photochemical properties of SOSG under our experimental conditions. The scavenging of OH• was found to significantly decrease the fluorescence signal. However, considering the many different species formed during water radiolysis, it is hard to draw a solid conclusion that OH• was the only specie that affected the fluorescence performance of SOSG. Apart from SOSG, other three probes, including 1,3-diphenylisobenzofuran (DPBF), 9,10-antherachenediyl-bis(methylene) dimalonic acid (ABDA) and aminophenyl fluorescein(APF), were also studied, and they all showed to be influenced by ionizing radiation.

In last chapter, we by chance observed that the photosensitizer Ce6 can slightly improve the florescence signal of SOSG under radiation exposure, thus, in Chapter 3 attempted to prepare a radiation-sensitive drug delivery system by combing PCL-PEO micelles with Ce6. The Ce6 molecules could be released from the Ce6-loaded micelles once being exposed to ionizing radiation, and the amount released increased with increasing radiation dose irrespective whether X-rays of low energy or gamma rays of high energy were used. Additionally, ionizing radiation (up to 50 Gy) appeared not to damage the micelles or the Ce6 alone, but affected the interaction between the two. The fact that Ce6 release disappeared when the micelles were irradiated in HEPES, which acts as radical scavenger, showed that the release was mainly induced indirectly by interaction with species formed by water radiolysis. By using different scavengers, we showed that hydrated electrons (e_{aq}^-) might play an important

role in this release. The PCL-PEO micelles were also loaded with therapeutic drugs, i.e. Dox, PTX and DTX, with and without the presence of Ce6. The micelles single loaded with drugs displayed no detectable drug release upon radiation exposure, while the Ce6&Dox co-loaded micelles showed that only 56.1±1.8% of Dox remained inside the micelles after being irradiated by gamma-rays of 50 Gy. In contrast, the co-loaded micelles with PTX and DTX exhibited no drug release. The DSC data analysis indicated that the drugs which were more hydrophobic interacted with the micelles in a different way than Ce6 and Dox, which might be the reason for the observed Dox release.

The micelles have shown its potential as the nanoplatform for radiation-sensitive drug delivery system. Therefore, to have more understanding of the in vivo behaviours of the PCL-PEO micelles is of great important. In Chapter 4, we developed a chelator-free method to radiolabel the core of PCL-PEO micelles with ^{111}In, without disturbing the inherent properties of the micelles. The micelles showed excellent radiolabeling efficiency (above 80%) as well as good stability under DTPA challenge and in serum. Furthermore, the micelles behavior was investigated in vivo using SPECT/CT scan revealing that the majority of activity appeared in the liver and spleen, which are the typical organs for mononuclear phagocyte system (MPS). 48 hours later, the majority of activity was still found in the liver, proving that the radiolabel remained in the micelles. No ^{111}In was detected in the bones. We also showed that the same method could be applied to radiolabel PTX-loaded micelles, and the presence of PTX did not have a significant influence on the radiolabeling efficiency or stability.

The work described in Chapter 5 further looked into the mechanism of the chelator-free radiolabeling process. Firstly, we compared the ^{111}In radiolabeling efficiency between five different polymeric micelles, namely, two different PCL micelles (the chain length of the block copolymers was varied), PLA micelles, PBd micelles and PS micelles. The results showed that the PCL and PLA micelles had better interaction with ^{111}In reaching higher radiolabeling efficiency and better radiolabeling stability than the other micelles. A cryo-EM study showed that Indium clusters were initially formed outside of the micelles but appeared within 30 minutes in the core of the PCL based micelles. However, FT-IR study of the micelles in the presence of In ions did not reveal a chemical bond between the block

copolymer and In species. We also radiolabeled the PCL micelles with other radioisotopes, i.e. ^{89}Zr and ^{177}Lu. Also here high radiolabeling efficiency was achieved, but the radiolabeling stability of ^{89}Zr and ^{177}Lu was not as good as that of ^{111}In. According to the speciation results using the program CHEAQs, the In^{3+} ions tended to form $In(OH)_{3aq}$ under our experimental conditions, which would eventually precipitate to $In(OH)_{3s}$ above a concentration of 1 μM. Contrarily, the Lu^{3+} remained as free metal ions having positive charge under our experimental conditions, and Zr^{4+} could form $Zr(OH)_{4aq}$ which would only have $Zr(OH)_{4s}$ precipitate as the dominant species above a concentration of 1 mM. Taking the speciation into account, we were able to improve the radiolabeling stability by adding phosphate ions to stabilize ^{177}Lu as $LuPO_4$ and adding more Zr^{4+} ions to facilitate the precipitation of $Zr(OH)_4$.

Encouraged by the interaction between PCL-PEO micelles and radionuclides, in Chapter 6, we extended the application of PCL-PEO micelles to combined radionuclide therapy and chemotherapy by co-loading the micelles with ^{177}Lu and PTX. The PTX-loaded micelles could only be prepared at a mass ratio 0.5:20 (mg) (PTX to block copolymer), since larger amount of PTX led to the formation of rod-like structures. The distribution of the micelles in 3D tumour spheroids composed of U87 tumour cells was studied using light sheet imaging, which showed that after 1 day of incubation the micelles could penetrate deeply to the spheroid. Subsequently, the cell killing potential of the co-loaded micelles was studied versus single treatment (^{177}Lu or PTX). The empty PCL-PEO micelles were not toxic at all, while the micelles loaded with PTX/^{177}Lu showed significant cell growth inhibition 5 days after drug administration. The combined therapy exhibited a superior therapeutic outcome than the single treatments, leading to much smaller spheroids as well as disintegration of the 3D structures, indicating cell death.

In this thesis, we showed that polymeric micelles, especially PCL-PEO micelles, have the potential to be used in cancer treatment in combination with ionizing radiation. At the same time, many challenges still remain. Due to the difficulties of ROS measuring under radiation exposure, such as the short lift-time, it is very hard to determine the exact mechanism for probes excitation and also Ce6 release. The current approaches we applied in this work were static, which means we can only be aware of the situations after the reaction, the further effects could be turned to dynamic characterization. Also, the probes were easily affected by

ionizing radiation, maybe more roust technique, such as electron spin resonance (ESR) spectroscopy, could work better. In terms of the micelles, they could be further incorporated with more functions, such as adding some targeted reagents on the surface of the micelles which would result in better tumor accumulation. We believe that gaining fundamental understanding of the interaction between photosensitizers and ionizing radiation and the interaction between radionuclide and micelles would create exciting opportunities in cancer treatment.

Summary

Ionizing radiation is widely utilized in cancer treatment for therapeutic or diagnostic purposes. The therapeutic function of ionizing radiation in cancer treatment relies on difference of radiation sensitivity between tumor and healthy tissue, that is, the tumor cells are more sensitive to radiation and can less easily repair DNA damage caused by this exposure, than healthy tissue. Ionizing radiation can induce DNA damage directly or indirectly. Generally speaking, the indirect effect, through the formation of different reactive species upon water radiolysis, is the main mode of action. The detection of these reactive species is of great importance for understanding the damage mechanism induced by ionizing radiation to DNA but also to other systems of interest. Therefore, in Chapter 2, we checked whether commonly used commercial probes could work properly to detect reactive oxygen species (ROS) under exposure to ionizing radiation. The fluorescent probe Singlet Oxygen Senser Green (SOSG) is widely applied due to its claimed specific response to singlet oxygen ($^1O_2$) which is one of the most reactive oxygen species. To evaluate the performance of SOSG, we irradiated the SOSG probe with both X-rays and gamma-rays. The results indicated that the SOSG probe could somehow be activated when exposed to ionizing radiation even in the absence of singlet oxygen. The influence of different radiolysis species on the activation of SOSG by ionizing radiation was systematically studied. Additionally, we also checked the reliability of other commercial probes, including aminophenyl fluorescein (APF), 1,3-diphenylisobenzofuran (DPBF) and 9,10-antherachenediyl-bis(methylene) dimalonic acid (ABDA), upon radiation exposure. We showed that in all cases careful design of control experiments was absolutely essential due to the strong influence of ionizing radiation on the probes.

In the following chapters, we focused on the combination of polymeric micelles, in particular poly(ε-caprolactone-b-ethylene oxide) (PCL-PEO) micelles with ionizing radiation. In Chapter 3, a radiation-sensitive drug delivery system was developed by the combination of PCL-PEO micelles and Chlorin e6 (Ce6) which is a typical photosensitizer used in photodynamic therapy. The Ce6-loaded micelles exhibited evident cargo release when irradiated by X-rays or gamma-rays. Further exploration on the mechanism behind this release suggested that hydrated electrons, formed by water radiolysis, may play a role that influence the interaction between Ce6 and the micelles. The exact mechanism, however,

remains unknown. We also prepared co-loaded micelles encapsulating Ce6 and anticancer drugs and attempted to achieve further drug release. Interestingly, the hydrophobic drugs, i.e. Paclitaxel (PTX) and Docetaxel (DTX), were not influenced by the Ce6 release at all and remained inside the co-loaded micelles upon radiation exposure. On the other hand Dox showed evident release from the co-loaded micelles, which was not observed for the micelles that were single loaded with Dox.

SPECT and PET are nuclear imaging techniques that are essential in drug development and that can also play an important role in determining the efficacy of micelles as drug carriers in chemotherapy. In order to use these techniques, the micelles need to be radiolabeled without changing their inherent properties. In Chapter 4, a chelator-free method was developed to radiolabel the PCL-PEO micelles with ^{111}In. The radiolabeling efficiency and stability were evaluated, and an in vivo test was performed using SPECT/CT. The results showed that high radiolabeling efficiency can be easily achieved with negligible loss of radiolabel, indicating that this radiolabeling method has great potential to be used in clinic. Furthermore, we also applied the chelator free method to radiolabel micelles encapsulating the anticancer drug PTX, which showed that the presence of the hydrophobic drug inside the micelles hardly influenced the radiolabeling process. Additionally, the chelator-free method was also applied to other radioisotopes and polymeric micelles.

In Chapter 5, the mechanism of the chelator-free labelling process was further explored. We first started by radiolabeling micelles composed of different block copolymers (PCL-PEO, PLA-PEO, PBd-PEO and PS-PEO) with ^{111}In. PCL-PEO micelles showed the most outstanding radiolabeling ability and stability compared to the other micelle candidates. A Cryo-EM was used to get more insight in the radiolabeling process by taking images at different times of the loading process. These results suggested that initially In-precipitates were formed on the outside of the micelles but eventually entered the core of the micelles. Next, we checked the possibility to use PCL-PEO micelles as carriers for other radioisotopes, i.e. ^{89}Zr and ^{177}Lu, via this chelator-free method. Interestingly, although the micelles exhibited quite a high radiolabeling efficiency for these two radioisotopes, the loss of radiolabel was much higher. The speciation program CHEAQs was applied to get more insight in the radiolabeling process and to improve stability. We speculated that the metal

precipitation in the core should improve the radiolabeling stability and indeed we showed that to be the case.

Chapter 6 focuses on the utilization of the PCL-PEO micelles as nanocarriers for combined radionuclide therapy and chemotherapy. We first optimized the experimental parameters for the preparation of PTX-loaded micelles, and subsequently radiolabeled them with ^{177}Lu. Then in vitro experiments were carried out to evaluate the cell uptake and biodistribution of the obtained micelles by using 3D tumour spheroids composed of U87 glioblastoma cells. The results proved that the micelles were able to penetrate to the inside of the 3D structures within 24 hours. The therapeutic effect of the PTX-loaded micelles, ^{177}Lu-radiolabeled micelles and ^{177}Lu&PTX co-loaded micelles were evaluated by observing the spheroid growth inhibition and measuring the cell viability at different time points. The results indicated that the combined radionuclide therapy and chemotherapy exhibited superior cell killing performance than the single treatments.

Finally, the thesis finishes by providing general conclusions, illustrating the potential of using polymeric micelles in nuclear medicine but also the challenges that lay ahead.

Samenvatting

Ioniserende straling wordt veel gebruikt bij de behandeling van kanker voor therapeutische of diagnostische doeleinden. De therapeutische functie van ioniserende straling bij de behandeling van kanker is afhankelijk van het verschil in stralingsgevoeligheid tussen tumor en gezond weefsel, dat wil zeggen dat de tumorcellen gevoeliger zijn voor straling en minder gemakkelijk DNA-schade kunnen herstellen die door de straling wordt veroorzaakt dan gezond weefsel. Ioniserende straling kan direct of indirect DNA-schade veroorzaken. Over het algemeen komt het indirecte effect vaker voor, waarbij verschillende reactieve zuurstofcomponenten door radiolyse van water worden gevormd. De detectie van deze reactieve componenten is van groot belang voor het begrijpen van het mechanisme achter het veroorzaken van schade door ioniserende straling. Daarom hebben we in Hoofdstuk 2 gecontroleerd of veelgebruikte commerciële sondes kunnen worden gebruikt om verschillende reactieve zuurstofcomponenten (Reactive Oxygen Species, ROS) te detecteren tijdens blootstelling aan ioniserende straling. De fluorescerende sonde Singlet Oxygen Senser Green (SOSG) wordt veel toegepast vanwege de geclaimde specifieke respons op singlet-zuurstof ($^1O_2$), de meest reactieve zuurstofcomponent. Hiervoor hebben we de SOSG-sonde bestraald met zowel Röntgen- als gammastraling. De resultaten gaven aan dat de SOSG-sonde een vals positief signaal zou kunnen geven bij blootstelling aan ioniserende straling, zelfs in afwezigheid van singlet-zuurstof. De invloed van verschillende soorten radiolyse op de activering van SOSG door ioniserende straling is systematisch bestudeerd. Daarnaast hebben we ook de betrouwbaarheid gecontroleerd van andere commerciële sondes, waaronder aminofenylfluoresceïne (APF), 1,3-difenylisobenzofuran (DPBF) en 9,10-antherachenediyl-bis(methyleen)dimalonzuur (ABDA), tijdens blootstelling aan straling. We toonden aan dat in alle gevallen een zorgvuldige opzet van controle-experimenten absoluut essentieel is vanwege de grote invloed van ioniserende straling op de sondes.

In de daaropvolgende hoofdstukken hebben we ons gericht op de combinatie van polymere micellen, in het bijzonder poly(ε-caprolacton-b-ethyleenglycol) (PCL-PEO) micellen. In Hoofdstuk 3 werd een stralingsgevoelig medicijnafgiftesysteem ontwikkeld door de combinatie van PCL-PEO-micellen en chlorine e6 (Ce6), een typische fotosensibilisator die

wordt gebruikt in fotodynamische therapie. De Ce6-geladen micellen vertoonden een duidelijke afgifte van de medicijnen wanneer ze werden bestraald met Röntgen- of gammastraling. Verder onderzoek naar het mechanisme achter deze afgifte suggereerde dat gehydrateerde elektronen, gevormd door radiolyse van water, een rol kunnen spelen en de interactie tussen Ce6 en de micellen kunnen beïnvloeden. Het exacte mechanisme blijft echter onbekend. We hebben ook co-geladen micellen bereid die Ce6 en geneesmiddelen tegen kanker inkapselen en probeerden verdere geneesmiddelafgifte te bereiken. Interessant is dat de zeer hydrofobe geneesmiddelen, d.w.z. Paclitaxel (PTX) en Docetaxel (DTX), helemaal niet werden beïnvloed door de Ce6-afgifte en in de co-geladen micellen bleven tijdens blootstelling aan straling, terwijl Doxorubicine een duidelijke afgifte uit de co-geladen micellen vertoonde.

SPECT en PET zijn nucleaire beeldvormingstechnieken die essentieel zijn bij de ontwikkeling van geneesmiddelen en die ook een belangrijke rol kunnen spelen bij het bepalen van de werkzaamheid van micellen als geneesmiddeldragers bij chemotherapie. Om deze technieken te kunnen gebruiken, moeten de micellen radioactief worden gelabeld zonder hun inherente eigenschappen te veranderen. In Hoofdstuk 4 is een chelatorvrije methode ontwikkeld om de PCL-PEO-micellen te labelen met ^{111}In. De efficiëntie en stabiliteit van de radiolabeling werden geëvalueerd en er werd een in vivo-test uitgevoerd met SPECT/CT. De resultaten tonen aan dat een hoge efficiëntie van radiolabeling gemakkelijk kan worden bereikt met weinig verlies van radiolabel, wat aantoont dat deze methode van radiolabeling een groot potentieel heeft om ook voor andere polymere micellen te worden gebruikt. Verder hebben we ook de chelatorvrije methode toegepast om de micellen die het antikankergeneesmiddel PTX inkapselen, radioactief te labelen, wat aantoonde dat de aanwezigheid van de hydrofobe geneesmiddelen in de micellen het radiolabelingsproces nauwelijks beïnvloedde. Daarnaast werd de chelatorvrije methode ook toegepast op andere isotopen en polymere micellen.

In Hoofdstuk 5 werd het mechanisme van het chelatorvrije labelingproces verder onderzocht. We zijn eerst begonnen met het radioactief labelen van micellen bestaande uit verschillende blokcopolymeren (PCL-PEO, PLA-PEO, PBd-PEO en PS-PEO) met ^{111}In. PCL-PEO-micellen vertoonden het meest opmerkelijke vermogen en stabiliteit om radioactief te labelen

in vergelijking met de andere micelkandidaten. Een Cryo-TEM werd gebruikt om meer inzicht te krijgen in het radiolabelingproces door op verschillende momenten van het laadproces beelden te maken. Deze resultaten suggereren dat aanvankelijk indiumprecipitaten worden gevormd aan de buitenkant van de micellen, die uiteindelijk de kern van de micellen binnendringen. Vervolgens hebben we de mogelijkheid gecontroleerd om PCL-PEO-micellen te gebruiken als dragers voor andere radio-isotopen, namelijk ^{89}Zr en ^{177}Lu, via deze chelatorvrije methode. Interessant is dat, hoewel de micellen een vrij hoge radiolabelingsefficiëntie vertoonden voor deze twee radio-isotopen, het verlies van radiolabel veel groter was. Het speciatieprogramma CHEAQs werd toegepast om meer inzicht te krijgen in het radiolabelingproces en om de stabiliteit te verbeteren. We speculeerden dat de metaalionprecipitatie in de kern de stabiliteit van radiolabeling zou moeten verbeteren en we hebben aangetoond dat dit inderdaad het geval is.

Hoofdstuk 6 richt zich op het gebruik van de PCL-PEO-micellen als nanodragers voor gecombineerde radionuclidetherapie en chemotherapie. We hebben eerst de experimentele parameters geoptimaliseerd voor de bereiding van met PTX geladen micellen, en deze vervolgens radioactief gelabeld met ^{177}Lu. Vervolgens werden in vitro experimenten uitgevoerd om de celopname en cellulaire biodistributie van de verkregen micellen te evalueren met behulp van 3D-tumorsferoïden samengesteld uit U87-glioblastomacellen, wat aantoonde dat de micellen in staat waren om tot de binnenkant van de 3D-structuren te dringen. Het therapeutische effect van de PTX-geladen micellen, ^{177}Lu-radioactief gelabelde micellen en ^{177}Lu&PTX co-geladen micellen werden geëvalueerd door de sferoïde groeiremming te observeren en de levensvatbaarheid van de cellen op verschillende tijdstippen te meten. De resultaten gaven aan dat de gecombineerde radionuclidetherapie en chemotherapie superieure celdodingsprestaties vertoonden vergeleken met de afzonderlijke behandelingen.

Ten slotte wordt het proefschrift afgesloten met algemene conclusies, die het potentieel illustreren van het gebruik van polymere micellen in de nucleaire geneeskunde, maar ook de uitdagingen die voor ons liggen.

List of publications

Publications

Related to this thesis

1. H. Liu, A.C. Laan, J. Plomp, S.R. Parnell, Y. Men, R.M. Dalgliesh, R. Eelkema, A. G. Denkova. Ionizing Radiation-Induced Release from Poly(ε-caprolactone-b-ethylene glycol) Micelles, *ACS Appl. Poly. Mater*. **2021**, 3, 2, 968–975.
2. A.G. Denkova, H. Liu, Y. Men, R. Eelkema, Enhanced cancer therapy by combining radiation and chemical effects mediated by nanocarriers. *Adv. Therap*., **2020**, 3, 1900177.
3. H. Liu, P.J.H. Carter, A.C. Laan, R. Eelkema, A.G. Denkova, Singlet oxygen sensor green is not a suitable probe for $^1O_2$ in the presence of ionizing radiation, *Sci. Rep*. **2019**, 9, 8393.
4. H. Liu, R. Eelkema, A. G. Denkova, Core precipitation of radiometal salts as a simple and efficient method to radiolabel polymer micelles for theragnostic applications, in preparation.
5. H. Liu, R. Eelkema, A. G. Denkova, Combining chemotherapy and radionuclide therapy by using by poly(ε-caprolactone-b-ethylene oxide) micelles co-loaded with Paclitaxel and ^{177}Lu, in preparation.

Others

6. Y. Men, T. G. Brevé, H. Liu, A. G. Denkova, R. Eelkema, Photo cleavable thioacetal block copolymers for controlled release. *Polym. Chem*. **2021**, 12, 3612.
7. T. G. Brevé, H. Liu, A. G. Denkova, R. Eelkema, Gamma Radiation Induced Contraction of Alkyne Modified Polymer Hydrogels, **2021**, submitted.
8. W. Zhang, H. Liu, M.M.C.H. van Schie, P. L. Hagedoorn, M. Alcalde, A.G.Denkova, K. Djanashvili, F.Hollmann, Nuclear Waste and Biocatalysis: A Sustainable Liaison? : *ACS Catal*. **2020**, 10, 14195−14200.
9. H. Liu, D. Chen, Z. Wang, H. Jing, R.Zhang, Microwave-assisted molten-salt rapid synthesis of isotype triazine-/heptazine based g-C_3N_4 heterojunctions with highly

enhanced photocatalytic hydrogen evolution performance. *Appl. Catal. B: Environ*. **2017**, 203, 300–313

10. M. Hu, X. Wang, H. Liu, N. Li, T. Li, R. Zhang, D. Chen, Visible-light-driven photodegradation of aqueous organic pollutants by Ag/AgCl@$Zn_3V_2O_8$ nanocomposites. Desalin. *Water Treat*. **2017**, 86:102-114.

Oral presentations

Huanhuan Liu, Polymeric micelles in the fight against cancer, Chemical Engineering colloquium, Delft University of Technology, 2021-4-26.

Posters

1. Huanhuan Liu, Philippe Carter, Antonia Denkova, Rienk Eelkema. Is SOSG a suitable probe in radio-involved therapy? European symposium on controlled drug delivery, Egmond aan Zee, Netherlands, 2018. (Poster presentation)

2. Huanhuan Liu, Adrie Laan, Rienk Eelkema, Antonia Denkova. Radiation-induced drug release from PEO-PCL micelles. The seventh international conference on radiation in various fields of research, Herceg Novi, Montenegro, 2018. (Poster presentation)

Acknowledgements

The past four years spent in the Netherlands is a remarkable period in my life, and all the people I meet here make my life more colorful and enjoyable. At this moment, I would like to express my gratitude to all of you.

Firstly, I want to thank Antonia, my perfect promoter. We first saw each other through a skype interview. I was so nervous since that's my first time to speak to foreigners for so long. But your warm smile encouraged me a lot. On 19th Sep, 2017, we met each other in real life, you gave me a very deep impression by the warm welcome. In the four years, you offer endless patience and help to me and my research. You are super kind and always be there to share your time and knowledge with all students, including me. You are open mind to research and always try your best to help deal with the difficulties in my project. I have learned a lot from you during the four years, not only academic attitude and professional knowledge, but also how to be a kind supervisor. Honestly, when I almost lose temper during the lab-supervision of students, I always think about you and imagine what you will do if facing these situations, and then I could calm down and be patient again. You are really one of these persons change my life. I feel super lucky to be your student.

I would like to thank my promoter Rienk for giving me the opportunity to do my PhD work. In 2016, I first contacted Dr. Michiel Makkee for the PhD position but got a negative result since I am not a chemistry student. But luckily, you contacted me! We had very happy conversations and then I arrived TUD. Thanks a lot for your tolerance of my limited knowledge of chemistry, I have to admit that sometimes my question on chemistry was stupid. Thank you for the rigorous scientific spirit and insightful suggestion which help correct my project and develop my research in a better way. I can really feel your encouragement from every discussion and your kindness when you emailed to congratulate the first citation of my first paper. It is an honor to work with you.

I also want to thank Bert Wolterbeek. Though you are not my promoter anymore, you still share your time with me to discuss my research and give advice to the existing problems. I always surprised by the way you thinking, which always reminds me something I never think of. You remind me that as a scientific worker, we cannot confine our thought in a certain area and we have to explore the broad world of science.

A lot thanks to the technicians who help to make my research work out. Adrie, thank you for training me on the operation with the majority of equipment in our lab and teaching me how to prepare micelles and work with radioactive things. Astrid, thank you for training me the cell skill and the endless help with isotopes ordering. Baukje, thanks for the training of ICP and the help with ordering lab stuff. I will never forget your help with "$InCl_3$" which is super essential for my project. Thank you Folkert for training me with Wallac and helping with computer problems. Eline, though you come to ARI not as long as other technicians, you still give me a lot of support and fun, thanks a lot! I also thank Anton in Fame group who helps me with DSC. Also a lot thanks to Anouk, our excellent secretary, who always gives support that makes my work smooth. I also appreciate Melmet and Dalia for the help with Freeze-drying. I could never finish my thesis without the help and kindness from all of you. I also need to thank the teaching group who taught the basic knowledge about ionizing radiation and protection in the first beginning of PhD, which made me feel quite safe as a fresher step into a new field.

Furthermore, I would like to thank all colleagues in SBD, Hank, Coos, Maris, Radboud, Misja, Erwin, Josette. Coos and Radboud gave me very detailed training for Co-60 and X-ray sources, which are essential for my research. During the four years, I did endless wipe tests and borrowed the keys so many times, thanks for your tolerance! Besides, I also thank you for running the Koepeltje bar, where we hold pub quiz and from which I learned a lot of cultural knowledge about the Netherlands and Europe. Rene, thanks a lot for the transportation of radioisotope delivery. Elco, thanks a lot for arranging the lab access for me!

Retna, Chao, Runze, Rogier, Alexcandra, Robin(both!), Hu, Tiantian… thanks for all these happy lunch time and warm working atmosphere in ARI group. It is my honor to work with you and make friends with all you guys. Special thanks to Retna, we started PhD at same

time and we help each other to use the blackboard which now named brightspace for registering courses. Besides, we also faced the same PhD stage during the four years. It was not easy for us as totally new students to start here, super thanks for your support and all the conversations. Thanks Chao and Runze for the dinner party for each Chinese festival, before you coming, I usually spent these time alone, your presence gives me so many unforgettable moment, thanks. Robin de Kruijff helped me a lot with the cryo-TEM which is super important for my research, and Robin Nadar helped me with the cell experiment which modified my project a lot, many thanks to both of you. It is also my pleasure to work with Juncheng, Yongjun, Bowen, Tobias, Guotai, Irene in ASM group and Wuyuan in BOC group, you are very nice people and provide me lots of valuable advice. And I also thank for my Chinese colleagues in RID for the happy lunch time.

For all the students I supervised in the lab, Kirsten, Britt, Max, Emma, Jana, Calvin, Cato, Charley, Joep, Robin, Matthijs and Willem, thank you for allowing me to work with you. I really treasure the time we spend together. We are not only lab-partners, but also friends. You helped me a lot with the lab work and also generously gave your personal suggestion to make my work better. By supervising you guys, I learned how to be a patient and nice supervisor.

To all my Chinese friends met here, Changrang, Yifan, Wenting, Qi, Kailun, Meiqi, Xinmin, Bei, Lihua, Na, Bing, Kailan, Yueer, Shengnan, Fengqi&Ziying, Hongpeng and Chao, thanks for coming to my life. How lucky I meet you here and become friends. It is never easy for us to live in a foreign country. The dinner party and reading club help to form my comfortable lifestyle here and could even influence my whole life. Here, I want to show my special gratitude to Yaya, my remote-roommate, for your accompany and supporting in the four years. Though we live in different countries, we spent so many time for our night talking. We talked about the homesick, the future plan and also decided to be lifelong friends. I really look forward to our reunion in China.

I would like to express my gratitude for my family for their endless understanding and supporting. When I was in blue mind, my parents always told me not to be so worried and even failure is also part of life, and they are always here no matter who I will become. Thanks for my brother Chao, a good boy, who helped to take care of my parents during my absence,

which makes me feel more comfortable. Great thanks to my grandfather, my life mentor, he really influences me by his dedication and positive attitude to life. He always reminds me to work hard and responsible to what I am doing, he always reminds me that money and fame is not as important as to be a warm person. Thank you for providing me a such warm home. And I also need to thank my boyfriend, Zhiqiang, who accompanies and supports me for such long time and distance. You never know how lucky I feel for finding a boyfriend like you.

Finally, I would like to give my biggest thanks to my great country, China. Though you are still not that rich and well-developed, I really appreciate all the things you did for your people. You are a huge mother, who would donate all you have to keep your people in a safe situation. You also give me, a girl comes from the countryside, the opportunity to study abroad, which I can never imagine before. 5000 years is a pretty long time for a country, but this doesn't mean you are old. I would like to donate myself to your development and I wish you to be prosperous, forever.

Best wishes!

Huanhuan Liu
刘欢欢

Curriculum Vitae

Huanhuan Liu was born on 24th May 1991 in Cangzhou, Hebei province, China. She had her bachelor study at Zhengzhou University from September 2010 to July 2014, and got the bachelor degree in Materials Science and Technology. Later on, she started her master' degree in the same college at Zhengzhou University. Her research topic was on the synthesis of novel photocatalysts for photocatalytic hydrogen generation. After 3 years' study, she received the master degree in July 2017.

Subsequently, she started her PhD study in the faculty of Applied Sciences at Delft University of Technology on 19th September 2017 under the supervision of Dr ir. A. G. Denkova and Dr. Rienk Eelkema. Her research focuses on the synthesis of nano-sized drug delivery system. Besides, she is also interested in the influence of radiation on chemical reactions. During the PhD, she supervised several Bachelor students and Master students, and she also took part in international conferences and presented her result orally or using poster presentation.